DISSERTATIONES PHYSICAE UNIVERSITATIS TARTUENSIS

35

DISSERTATIONES PHYSICAE UNIVERSITATIS TARTUENSIS
35

POSITIVE CORONA AT COMBINED DC AND AC VOLTAGE

Toomas Plank

TARTU UNIVERSITY
PRESS

The study was carried out at the Institute of Experimental Physics and Technology, University of Tartu.

The dissertation was admitted on November 28, 2001, in partial fulfilment of the requirements for the degree of Doctor of Philosophy in physics (optics and spectroscopy), and allowed for defence by the Council of the Department of Physics, University of Tartu.

Supervisor: Dr. Ants Haljaste, Institute of Experimental Physics and Technology, University of Tartu

Opponents: Prof. Reidar Svein Sigmond, Norwegian University of Science and Technology, Trondheim, Norway

Dr. Jaan Salm, Institute of Environmental Physics, University of Tartu

Defence: January 28, 2002 at University of Tartu, Estonia

Tartu Ülikooli Kirjastus
Tiigi 78, 50410 Tartu
Tellimus nr. 912

The study was carried out at the Institute of Experimental Physics and Technology, University of Tartu.

The dissertation was admitted on November 28, 2001, in partial fulfilment of the requirements for the degree of Doctor of Philosophy in physics (optics and spectroscopy), and allowed for defence by the Council of the Department of Physics, University of Tartu.

Supervisor: Dr. Ants Haljaste, Institute of Experimental Physics and Technology, University of Tartu

Opponents: Prof. Reidar Svein Sigmond, Norwegian University of Science and Technology, Trondheim, Norway

Dr. Jaan Salm, Institute of Environmental Physics, University of Tartu

Defence: January 28, 2002 at University of Tartu, Estonia

Tartu Ülikooli Kirjastus
Tiigi 78, 50410 Tartu
Tellimus nr. 912

CONTENTS

LIST OF ORIGINAL PUBLICATIONS INCLUDED IN THE THESIS

I Aints M Haljaste A Kudu K and Plank T 1997 Repetition rate of streamers as a measure of content of electronegative additives in the air *J. Phys. D: Appl. Phys*. **30** 210-20

II Plank T Haljaste A and Aints M 2000 The after-effect of streamers of positive corona under combined voltage *J. Phys. D: Appl. Phys*. **33** 2791-7

III Aints M Kudu K Haljaste A and Plank T 2001 Origin of photoionizing radiation in corona discharges in air *J. Phys. D: Appl. Phys*. **34** 905-8

IV Aints M Haljaste A Kudu K and Plank T 2001 Corona based detector of electronegative trace gases *Meas. Sci. Technol.* **12** 557-65

V Plank T Aints M and Haljaste A 1999 Investigation of rise probability of positive corona initiated by negative ions *Proc. 24th Int. Conf. on Phenomena in Ionized Gases* (Warsaw) **II** 145-6

VI Aints M Haljaste A Kudu K and Plank T 1996 Dependence of streamer corona characteristics on the concentration of electronegative trace gases in air *Proc. 5th Int. Symp. on High Pressure Low Temperature Plasma Chem.* (Milovy) 117-21

VII Plank T Aints M Haljaste A ja Kudu K 2001 Segapinge koroonalahendus saastegaaside detektorina *EFS aastaraamat 2000* **XI** 40-50

MAIN RESULTS PROPOSED FOR DEFENCE

The main defensible results are the following.

1. The statistical model for calculation of the repetition rate of streamers under conditions of combined DC and AC voltage.
2. The method for quantitative estimation of the after-effect of the preceding streamers on the formation probability of the following discharge.
3. The method for quantitative estimation of the after-effect of the preceding glow corona on the formation probability of the following discharge.
4. The gas photoionization caused by glow corona and streamer is the main reason for the existence of that after-effect of the discharge, provided that the photoeffect at solid surfaces is eliminated by constructional means.
5. Electron bombardment of the anode surface is in general not the source of photoionizing radiation in corona discharges.
6. The method for quantitative estimation of mean initiation probability of burst pulses by a single negative ion.
7. Positive corona at combined voltage can be used for detection of admixtures such as H_2O, CO_2, O_3, O_3+NO_x, SF_6, HNO_3, HCl, H_2SO_4, H_3PO_4, $CHCl_3$, C_6H_6, NH_4OH, CH_3COOH, $C_{10}H_{16}O$, HCHO, I_2, Cl_2 in air.
8. Ability of streamer counter to distinguish between different admixtures can be obtained

- using simultaneously several discharge gaps with point electrodes of different diameter;
- measuring the repetition rate and amplitude distribution of streamers at the same time.

1 INTRODUCTION

The present investigation is dedicated to some actual problems of the corona physics that are arisen during development of certain type of corona-based devices such as streamer counters and detectors of trace gases. The initiation mechanism of the positive corona under conditions of the combined (DC + AC) voltage in atmospheric air, and the influence of electronegative admixtures on the corona characteristics are under investigation. An overview of the basic corona physics and literature devoted to the present subject is given in chapter 2. Open problems and main goals of the present investigation are presented at the end of that chapter. The experimental set-up used is described in chapter 3. The results of visual examination of the discharge and the discharge oscillograms are presented in chapter 4. The mathematical description of discharge initiation under the conditions of the combined voltage is presented in chapter 5.

The preceding streamer or glow corona may affect the formation probability of the following one. Although different manifestations of the after-effect of corona pulses are widely investigated, special methods for their detection are poorly developed. Very few attempts have been made with the aim of quantifying these phenomena under controlled conditions. In chapter 6, we propose methods for measurement of the after-effect of both the glow corona and the streamer in conditions of the combined voltage. In addition, we will discuss which mechanism can be responsible for that after-effect. We are of the opinion that the photoionization in gas is the primary cause of that after-effect. In general, it is assumed that in corona the photoionizing radiation is emitted by gas atoms and molecules excited via electron collision. However, the recent results of Akishev *et al* [1999a, 1999b, 1999c] indicate that the soft x-ray radiation, produced by collisions of electrons against the anode surface, may act as a photoionizing agent in positive corona. In chapter 7, we will express our opinion about these two very different mechanisms of generation of photoionizing radiation.

It is well known that corona discharges show high sensitivity to many electronegative trace gases and aerosols [Loeb, 1965; Sigmond and Goldman 1983]. In recent years, a number of papers is devoted to detectors of trace gases, based on corona discharges and suitable for the environmental monitoring. Applicability of both the positive and negative corona is investigated. In chapter 8, we discuss the possibilities to use the positive corona discharge under conditions of combined voltage as a detector of electronegative trace gases.

Main results of the present work are summarised in chapter 9 (conclusions).

2 GENERAL

2.1 Gas discharges

Most of gases are in normal conditions good insulators and mainly consist of neutral atoms and molecules. If one heats the gas to high temperature, exposes it to UV radiation or X-rays or influents it with radioactive source, the charged particles will be produced in gas. Under the influence of an electric field, these charged particles start to move and cause an electrical current in gas. The phenomenon, called non self-sustained gas discharge, will appear.

Increasing the voltage leads to the development of a self-sustained gas discharge. The behaviour of a discharge depends on many factors: temperature, pressure and chemical composition of the gas; geometrical configuration, dimensions and placement of electrodes, applied voltage, current density etc. As a result, different manifestations of gas discharge are very diverse; they can be accompanied by luminosity- and sound effects.

Sigmond and Goldman divide the self-sustained DC gas discharges into three groups based on the difference in discharge mechanism [Sigmond and Goldman, 1983]:

- **Townsend discharge.** The electric field distribution is essentially Laplacian and has only small perturbations caused by the space charges. The applied voltage is much higher than the gas ionization potential. Photons, positive ions and particles in metastable exited states (metastables) are responsible for the feedback to the cathode.
- **Glow discharge.** The electric field distribution is dominantly determined by positive space charges. The applied voltage is by an order of magnitude higher than the gas ionization potential. Photons, positive ions and metastables are responsible for the feedback to the cathode.
- **Arc discharge.** The electric field distribution is dominated by positive space charges. The applied voltage is close to the gas ionization potential. The feedback to cathode is arranged mainly via thermal or field electron emission [Sigmond and Goldman, 1983].

2.2 Fundamental processes in gas discharges

Electron avalanches, first studied by Townsend, play important role in most gas discharges. Let us suppose that $N_e(0)$ electrons are released in a gas at distance $r = 0$ from the cathode and they will drift under the influence of an electric field $E(r)$ with velocity $v = \mu_e E(r)$. Here μ_e denotes the mobility of an electron. An electron produces α new electron-ion pairs and suffers η attachments per unit drift length on average. The coefficient α is called the primary ionization coefficient, the coefficient η - the attachment coefficient. For the number of

electrons dN_e produced along the elementary drift length dr, we can write

$$\mathrm{d}N_e = (\alpha - \eta) N_e(r)\mathrm{d}r = \alpha' N_e(r)\mathrm{d}r\,, \qquad (2.1)$$

where $\alpha' \equiv \alpha - \eta$ denotes the effective ionization coefficient. After integration, we will get from this equation the number of new electrons produced at distance r

$$N_e(r) = N_e(0)\exp\left(\int_0^r \alpha' \mathrm{d}x\right). \qquad (2.2)$$

In the case of discharges in strongly nonuniform electric field, the space between discharge electrodes is divided into ionization region and drift region. In ionization region $\alpha' > 0$ and free charges are produced. In drift region, $\alpha' \leq 0$ and attachment processes prevail the ionization processes. Here charged particles drift and react. In equations (2.1) and (2.2), the possible detachment of electrons from negative ions is neglected. However, in air and electron attaching gases, the detachment and ion conversion processes might cause an apparent increase of the effective ionization coefficient [Wetzer and Wen, 1991]. The exponential in equation (2.2) is often called "electron multiplication" of the gap and it can reach the values $10^3 - 10^8$ across the ionization region [Sigmond and Goldman, 1983]. The integral $I = \int_0^r \alpha' \mathrm{d}x$ is known as ionization integral.

The self-sustainment of a discharge requires that each electron leaving the place of avalanche initiation must be replaced with a new one. This feedback mechanism can be summarised by γ-processes. The secondary ionization coefficient γ is defined as the number of secondary electrons in the place of avalanche initiation per ionizing collision in the ionization region. The γ-processes can be divided into cathode processes and gas processes [Sigmond and Goldman, 1983]. From the cathode, the secondary electrons can be liberated due to influence of cathode material by positive ions (positive ion feedback γ_{ic}), by particles in metastable excited states (metastables feedback γ_{mc}) or by photons (photon feedback γ_{pc} due to photoeffect). In the gas, the secondary electrons can be produced due to photon feedback γ_{pg} while photons from exited gas molecules may ionize other gas molecules (photoionization) or detach electrons due to photodetachment.

The self-sustainment of a discharge can be characterized by a reproduction factor, which is defined as

$$\mu_r = \gamma \int_0^d \alpha \exp\left(\int_0^r \alpha' \mathrm{d}x\right)\mathrm{d}r\,.$$

Here the secondary ionization coefficient $\gamma = \gamma_{ic} + \gamma_{mc} + \gamma_{pc} + \gamma_{pg}$ and d denotes the length of the corresponding field line of the electric field. The Townsend's criterion for self-sustained discharge is that $\mu_r = 1$. If $\mu_r < 1$, the discharge

without external ionization will die soon. If $\mu_r > 1$, the discharge current grows exponentially and soon the breakdown will occur.

2.3 Corona discharges

The name corona comes from the French word *couronne* (crown). Sigmond and Goldman [1983] define corona discharge as "a self-sustained electrical gas discharge where the Laplacian (geometrically determined) electric field confines the primary ionization processes to regions close to high-field electrodes or insulators". Corona discharges are divided according to the applied voltage frequency into: direct current (DC) corona, alternating current (AC) corona, high frequency (HF) corona and the combinations of the above types. DC coronas are divided according to the polarity of the high-field electrode(s), into negative-, positive- and bipolar corona. The feedback processes in positive and negative coronas must be very different. In the case of negative corona, the cathode borders directly to the ionization region. Therefore, the cathode γ-processes (γ_{ic}, γ_{mc}, γ_{pc}) are fast and efficient. In the case of positive corona, the cathode is separated from the ionization region by the drift region, in which the photons can be absorbed and secondary electrons originating from the cathode can be attached to atoms and molecules. Thus in positive coronas, processes at cathode play the minor role and photoionization as a γ-process (γ_{pg}) often predominates [Sigmond and Goldman 1983].

2.3.1 Negative corona in air

In air, the negative corona can appear depending on electrode configuration and applied voltage in several forms: as Trichel pulses, negative glow, negative or positive streamers, or spark breakdown. Below the onset voltage of Trichel pulses U_{Tr}, only a non-self-sustained Townsend discharge can exist at the point electrode. As $\mu_r < 1$, the discharge needs for its existence an external source of electrons. An increase in voltage U above U_{Tr} results in appearance of regular light pulses on the point. Visually, one can see negative glow, positive column and dark spaces between them (figure 2.1). This phenomenon was first studied by G. W. Trichel [1938] and is called now after his name – Trichel pulses.

The electric field near the point is high enough to accelerate the positive ions to energies that enable them during collisions with the cathode to liberate electrons. Emission due to photon impact is another possible secondary electron generation mechanism. Electric field pushes electrons away from the cathode. In collisions with gas atoms and molecules, they produce avalanches of electrons and positive ions. In addition, a big amount of excited molecules and atoms will be created. In the drift region where the electric field is weak, the

electrons attach to oxygen molecules and form negative ions. The space charge of those accumulates within time and reduces the electric field strength in the ionization region. In reduced field, $\mu_r < 1$ and the discharge extinguishes. New discharge pulse can arise after the negative space charge is removed far enough to restore the initial field strength near the cathode so that $\mu_r \geq 1$ again.

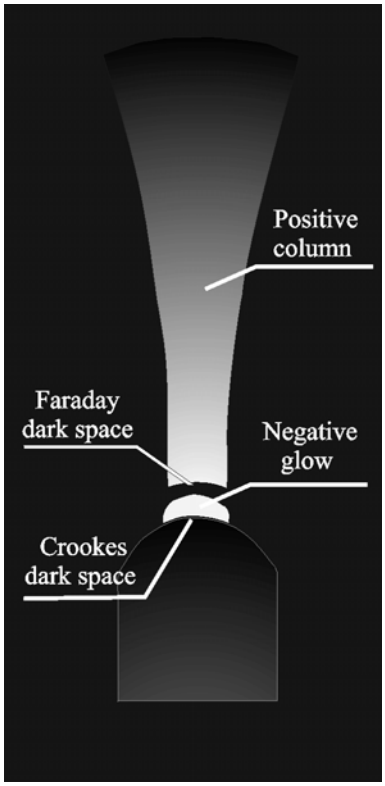

Figure 2.1. Visual appearance of a Trichel pulse.

If one increases the applied voltage, the duration of the Trichel pulses increases and the time interval between them decreases. Using the oscilloscope, one can see pulses with long and steady plateau. A further little increase in voltage gives that all pulses join in one continuous plateau – the continuous glow [Sigmond and Goldman, 1983]. Visually one can see that the volume of luminous space decreases, and will accumulate in one, usually central, space region. In spite of that, the microscopic luminous films and dark spaces between them (like in figure 2.1) remain [Nasser, 1971].

In long rod-to-plane gaps, there exists another corona form – negative streamer. It develops in transition stage from the negative glow to the spark breakdown. The positive column diminishes and filamentary negative streamer develops from glow region into discharge gap. The filaments of the streamer are diffuse and crooked. Visually, they resemble a whisk. The positive streamers can appear from luminous nuclei formerly belonging to the negative streamers and locating in the vicinity of the cathode [Reess *et al*, 1995]. Those nuclei often coincide with branching points of negative streamers and are called space stems.

2.3.2 Positive corona in air

Most investigations of positive corona are made in point-to-plane discharge gaps. The appearance of positive corona in point-to-cylinder discharge gaps is similar to the corona in point-to-plane gaps.

In the air, the positive corona can appear depending on applied voltage in several forms: as burst pulses, onset streamers, steady glow corona, breakdown

streamers or spark breakdown. Below the onset voltage of burst pulses U_{bp}, there is no self-sustained discharge in the discharge gap. An increase in voltage above U_{bp} results in generation of series of electron avalanches, which consist of a great number of electrons. Molecules and atoms excited by electrons emit photons during the transition into stable state. The photons of high energy cause photoionization of gas atoms and molecules giving rise to the new secondary avalanches. The discharge spreads rapidly over the point surface. Visually, one can see around the point tip a weak luminous layer (see figure 2.2a). Trichel [1939] called those discharge pulses as "bursts". In newer literature, the common name for this phenomenon is "burst pulse". Secondary burst pulses follow primary burst pulses. They are weaker and shorter than the primary ones. Burning of the discharge produces a positive space charge near the point (see figure 2.3a). This space charge reduces the electric field strength near the point and the sequence of burst pulses will extinguish. Formation of the next discharge requires some time because the space charge must be removed from the vicinity of the point before the new discharge can start.

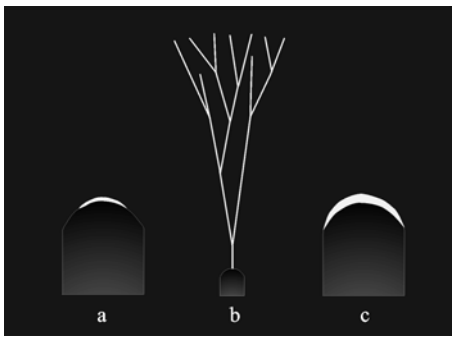

Figure 2.2. Visual appearance of forms of positive corona: (a) burst pulse; (b) onset streamer; (c) glow corona.

Within increase in voltage, the burst pulses will be more powerful and there will be more secondary burst pulses in the sequence. When the voltage reaches the onset voltage of streamers U_{str}, the stochastic current density rise in some part of the discharge cross section might increase the efficiency of the ionization processes in just that part (see figure 2.3b). The positive ions will concentrate in a spot just outside the anode surface [Kudu *et al*, 1998]. The electric field strength between this spot and the anode can be close to zero; the field strength outside the spot is high and an ionization region is created in the front of that spot. New avalanches and plasma will be formed in front of the spot. A plasma channel will grow as long as plasma is formed faster than it can be recombined or absorbed at the anode [Kudu *et al*, 1998] – the onset streamer (below called streamer) will form (see figure 2.3c). The formation time of a streamer is approximately 5 - 25 ns [Kudu, 1960]. Visually, the streamer is a luminous plasma ball, which is moving within speed approximately 10^5 - 10^6 m s^{-1} towards the cathode. The streamer radial dimensions increase linearly with the applied voltage [Babaeva and Naidis, 1996a; Georghiou *et al*, 1999].

The streamer head is considered to be a positively charged sphere [Dawson and Winn, 1965], the diameter of it is approximately from 20 [Sigmond and Goldman, 1983] to 200 μm [Kulikovsky, 2000a]. The streamer heads visible

radius can increase with streamer advancement [Aints *et al*, 1977]. The actual diameter of the plasma channel is several times larger than the visible head of streamer [Kulikovsky, 1997]. The streamer head contains a positive charge with density $n_+ \approx 10^{18}$- 10^{20} m^{-3} [Raizer, 1987; Grangé *et al*, 1995]. The electric field at the streamer tip is equivalent to the field of a charged ball of radius of the space charge front [Kulikovsky, 1997]. The width of the space charge layer at streamer tip is approximately equal to the visible radius of the streamer head and coincides with the characteristic length of absorption of ionizing radiation [Kulikovsky, 2000a]. The local field allows for electrons generated in front of the streamer head to trigger new avalanches. Those electrons are either the background ones but mainly photoelectrons created through photoionization [Pancheshnyi *et al*, 2001]. Just before the recombination with positive ions of the streamer head, the electron density n_e in the avalanche head equals approximately with the positive charge density n_+ in the streamer head [Raizer, 1987]. Behind the head, the conductive plasma channel is formed.

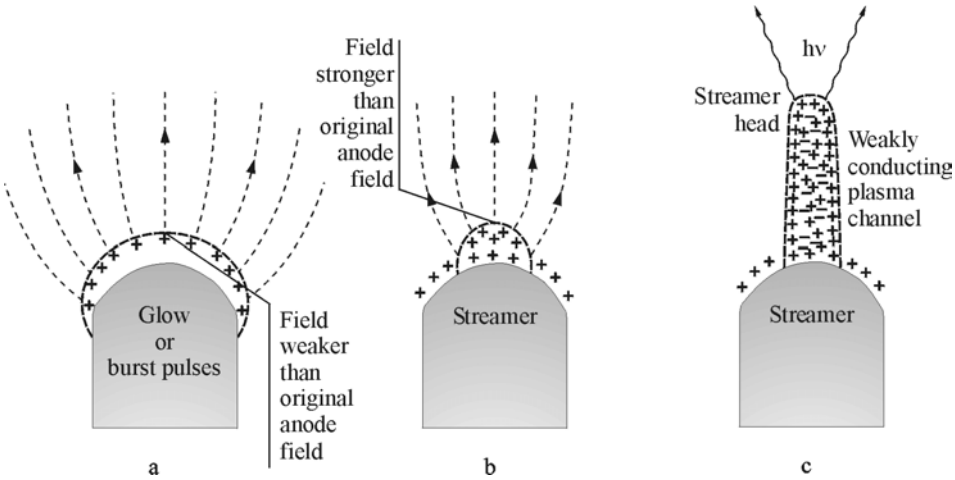

Figure 2.3. Inception of a streamer. After [Sigmond and Goldman, 1983].

Streamer can branch, that is, it can look like a luminous tree (see figure 2.2b), or to develop straightforward away from the point. Based on computer simulations, Kulikovsky [2000b] assumes that streamer branching occurs in high field when the width of the space charge layer at streamer tip exceeds the characteristic length of absorption of ionizing radiation.

Streamer needs for stable propagation a minimum external electric field [Andersson, 1958], which varies between 4 and 5.5 kV cm^{-1} in atmospheric air [Sigmond and Goldman, 1983]. His own space-charge field is much higher – approximately 150 – 300 kV cm^{-1} [Sigmond and Goldman, 1983] and is almost independent of the applied voltage [Babaeva and Naidis, 1996a]. The total field, that is the space-charge field plus the Laplacian one, allows the propagation of the ionized region towards the cathode. Depending on point's radius of

curvature and applied voltage, the development of the streamer stops at a certain distance. The length of streamer depends primarily on the shape of the high field region [Kip, 1939].

In the literature, to the electron multiplication necessary for the streamer formation is generally given the value 10^8 [Raether, 1964]. However, in inhomogeneous fields, the streamer formation is possible even when the mean number of electrons of a single avalanche is less than 10^8. In that case, the streamer is associated with the avalanche possessing the largest number of electrons [Pedersen, 1989], or there are several avalanches going at the same time. McAllister *et al* [1979] state that "... at onset, the corona discharge does not result from the formation of a single critical avalanche but from the accumulative effects of an intrinsic multiple avalanche process". Laan and Paris [1994] experimentally confirmed that multi-avalanche nature of a streamer formation in inhomogeneous fields. According to Loeb [1965], the avalanche size required for launching the onset streamers is about 10^5 ions.

When the streamer propagation stops, the discharge gap is filled with space charge of positive ions. New streamer can arise, if the space charge is removed far enough from the point electrode and the initial field strength is recovered. Secondary burst pulses may follow the streamer [Kip, 1939] just as they follow the primary burst pulse. The number of those burst pulses increases with applied voltage.

The streamers can be suppressed by α-particles, which create a big number of seed electrons so that the plasma layer will be more homogeneous than it would be in the case of single electron initiation. Thus, the occurrence of an instability, which leads to development of a streamer, is less probable.

Starting from voltage U_g, the burst pulses are not separable from each other any more – they join into a steady glow corona [Loeb, 1965] (see figure 2.2c). The streamers disappear completely. Thus, the repetition rate of streamers first increases within applied voltage and then decreases until zero at $U = U_g$. The width of voltage interval of onset streamers and that of glow corona depend on the degree of homogeneity of the electric field and on the concentration of humidity. The voltage interval of streamers is the wider and the voltage interval of glow corona is the narrower the more homogeneous the electric field is [Kudu and Veimer, 1970]. The voltage interval of streamers increases with increase in humidity content of the air [Bogdanova and Popkov, 1973].

In discharge regime of glow corona, the discharge will no longer extinguish; Sigmond and Goldman [1983] consider this regime "perfectly stabilized". The electric field strength at the surface of the corona electrode will remain constant independent of overvoltage [Waters *et al*, 1972; Bogdanova *et al*, 1976; Bogdanova *et al*, 1978]. The remarkable stability of the positive glow is due to the existence of the inactive low field drift region where a great number of positive ions will drift to the cathode. They drift in successive shells which can

merge due to mutual repulsion of positive ions [Morrow, 1997]. If local ionization increases for a moment, the corresponding rise in positive ion charge density will decrease the electric field and as a result stop the further growth in local ionization [Beattie, 1975]. However, this field can not be considered completely static – the anode field oscillates at some average value with frequency higher than 10^5 Hz [Beattie, 1975].

Electrons and negative ions produced near the anode are swept rapidly into the anode. As a result, their number density is by an order of magnitude smaller than that of positive ions [Morrow, 1997] and most of the current is caused by the movement of the positive ions.

The streamers can arise again after the voltage has reached the onset voltage of breakdown streamers U_{bs} [Loeb, 1965]. Those streamers, called breakdown streamers, are similar to the onset streamers but much longer and much more powerful than the onset streamers. The physical mechanisms of onset- and breakdown streamers seem to be identical [Sigmond, 1978]. At $U_g < U < U_{bs}$, the streamers can be induced inside the glow, if the voltage is raised at a rate greater than 10^9 V s^{-1} [Laan and Paris, 1992; Morrow, 1997] or by laser radiation [Paris, 1994; Laan and Paris, 1994].

Space charge effects tend to make the electric field strength in the streamer column uniform at a value for which effective ionization and attachment rate are equal [Lowke, 1992]. Here the "real" swarm parameters, taking into account the temporary electron trapping by attachment and later detachment of them, should be used [Wetzer and Wen, 1991]. Allen and Mikropoulos [1999] show that "an intrinsic propagation field with an associated velocity can be defined, which determine the propagation of streamers of a limiting minimum energy". The streamer propagation velocity above that stability field is a power function of the electric field [Allen and Mikropoulos, 1999]. The threshold field for the propagation of a single streamer with minimum attainable energy is 4.4 - 5.0 kV cm^{-1} [Allen and Ghaffar, 1995a; Serdyuk *et al*, 2001]. The value of this field depends on humidity and the temperature of air. At lower field, the streamer can propagate only if its energy is larger or if branching produces a significant space charge [Allen and Ghaffar, 1995a]. In background field lower than the stability field, the streamer front velocity decreases with increase of streamer length [Serdyuk *et al*, 2001]. In background field higher than the stability field, the streamer front velocity increases with increase of streamer length [Babaeva and Naidis, 1996b].

Finally, if the applied voltage exceeds the onset voltage of spark breakdown U_{sp}, the breakdown streamer touches the cathode, conductive channel forms after the breakdown streamer and the spark breakdown may occur. At the same time when the primary streamer head reaches the cathode, the secondary streamer starts from the anode. Spark breakdown follows if and when the secondary streamer bridges the complete corona gap [Sigmond, 1983 and 1984].

The temperature of neutral gas in primary streamer is about room temperature [Sigmond, 1978]. In secondary streamer, Spyrou *et al* [1992] measured a relatively high temperature (800 K) of the neutral gas at the distance of 0.5 mm from the point. At greater distances, the temperature decreases to about 450K.

2.3.3 Corona at AC voltage

In the simplest case, when one applies the relatively slowly changing unipolar voltage, we will get the unipolar transition corona. This happens for example during the first half-period of the industrial AC voltage. The peculiarities of this corona type are that the magnitude and the distribution of space charge are changing in time; and that the displacement current exists in addition to the conduction current.

If one applies to the electrodes the alternating voltage, an AC corona will appear in the discharge gap. Traditionally one calls the discharge "AC corona", if industrial AC voltage is applied to the corona electrodes. The processes in outer region of the AC corona have common features with both the unipolar transition corona and with the bipolar DC corona [Levitov, 1975]. If the frequency of the AC voltage is low or the discharge gap is so short that electrons and ions are able to move during one half-cycle from one electrode to another, the discharge behaviour is quite similar to that under static conditions. With an increase in AC frequency there will develop a situation where the charges of one or both signs are unable to cross the gap during one half-cycle. During the next half-cycle, those ions will move in opposite direction and most of them will reach the electrode of origin. Still, due to diffusion and self-repulsion, some charges of both sign will remain in gap. Under still higher frequencies, the space charge clouds of opposite sign will be localized at the centre of the discharge gap [Loeb, 1965] and the density of space charges increases in time. If the recombination and losses at walls are not too important, the space charge can alter the initial field strength at both electrodes [Loeb, 1965]. As a result, formation of positive and negative streamers is possible at instantaneous value of the AC voltage lower than the corresponding onset voltages of DC streamers. The spark breakdown will appear under lower voltage, too [Loeb, 1965].

It is characteristic to all above mentioned corona forms that the intensity of the discharge (discharge current) is controlled by the space charge formed in the ionization zone. Moving under the influence of the electric field, this space charge fills the drift region with charged particles. The distribution of space charge is such that the potential gradient near the corona electrode is time-independent during the time interval when ionization takes place at given half-cycle (except impulse- and HF corona) and has a value quite close to that at the onset of corona of that polarity [Levitov, 1975].

2.3.4 Positive corona at combined voltage

If one applies the DC and AC voltage to the electrodes at the same time, we will get a corona of combined voltage. The corona at combined voltage is similar to the DC corona, but has some peculiarities. Here the resultant voltage U traverses one after the other the region free of discharge, region of burst pulses, that of onset streamers and glow corona. Negative ions, created by an ionizer or cosmic radiation and carried into the discharge gap by an air stream and an electric field, are the source of seed electrons [Loeb, 1965]. If an electron appears in the active zone of the point electrode when the resultant voltage traverses through the region of burst pulses $U_{bp} \leq U < U_{str}$, the burst pulse can be initiated. Secondary burst pulses like in the case of pure DC corona will follow the primary burst pulse. These burst pulses produce the space charge near the point and make impossible the formation of a streamer [Kudu, 1980]. Afterwards, when the resultant voltage reaches the onset voltage of glow corona, the burst pulses develop into steady glow, which in turn blocks the formation of a streamer as long as the resultant voltage is above U_{bp} [Kudu, 1980].

If no seed electron appears during the time interval Δt_{bp}, when the resultant voltage traverses through the DC region of burst pulses $U_{bp} \leq U < U_{str}$, the later electron can initiate a streamer. The streamer, like the burst pulses, is followed by the glow corona. Repetition rate of streamers depends on the number of seed electrons and negative ions reaching the active zone per unit of time, and on the concentration of electronegative additives in the air [Kudu, 1980].

2.4 Corona wind

Ions of corona polarity will be repelled away from the high-field electrode. Due to the collisions and friction against uncharged gas particles, the ions lose some of their kinetic energy to neutral particles, which start to move in the same direction as the ions do. This energy transfer phenomenon is known as an electric wind from the high-field electrode [Loeb, 1965] and it is responsible for mass transfer phenomenon in gas coronas [Sigmond, 1989]. In negative coronas, the ring vortex can appear and trap a significant part of the excited species formed in discharge [Sigmond and Lågstad, 1993]. In positive (repetitive) streamer corona, the formation of ring vortex is also possible [Sigmond *et al*, 1992]. In a positive glow corona, a single outward-going jet is formed [Sigmond *et al*, 1992].

2.5 After-effect of a discharge

It is well known for corona researchers that a discharge may have an after-effect on the formation and development of the next discharge. In air, that after-effect is usually associated with residual ions [Waters, 1978; M & A Goldman, 1978], chemical products (nitrous oxides) [Gosho, 1981 and 1982] and neutral excited species [M & A Goldman, 1978].

The after-effect is most directly observable in changes of length of side branches of streamers. As described in section 2.3.2, the streamers branch during developing towards the cathode. The branching diminishes with increase in repetition rate of streamers. At certain repetition rate, the streamers start to follow one and the same trajectory, which situates usually in the axis of the discharge gap; the branching disappears at all. The transition from branched form to unbranched one is investigated using the voltage pulses with very short rise time and long flat top to obtain several successive discharges [M & A Goldman, 1978]. The first streamer develops in the environment unpolluted by the previous discharges. That streamer has a branching structure. The next streamers arise in environment already affected by previous streamers and develop along the axes of discharge gap. Their current amplitude is about ten times lower than that of the first streamer. Despite of the above-mentioned facts, the evolutionary scheme of the discharges remains the same in case of branched and unbranched streamers [M & A Goldman, 1978].

The streamer propagates by photoionization-avalanche mechanism and leaves behind a trail of charged products of both polarities mixed with uncharged metastable particles [Acker and Penney, 1968]. Measurements of Berger *et al* [1972] show that the influence of negative ions produced by the discharge in small gap (electrode separation 15 mm) lasts about five milliseconds. The accumulation of those negative charges increases the probability of production of seed electrons for initiation of new discharges [M & A Goldman, 1978].

The uncharged particles will be removed slower than the charged ones, as they are not influenced by the electric field. Acker and Penney [1968] showed that the presence of metastable atoms or molecules of oxygen and nitrogen changes the buildup of a streamer and the speed of streamer development. Due to their long lifetimes, the metastables can affect the development of succeeding discharges [M & A Goldman, 1978]. First, the metastables can be ionized more easily than the molecules in ground state. Second, the metastable molecules act as a reservoir of energy. That energy is transferred to the electrons in superelastic collisions [Hartmann and Gallimberti, 1975]. The concentration of metastable nitrogen molecules in a discharge trail remains significantly high for some hundreds of microseconds [Hartmann and Gallimberti, 1975]. Thus, the after-effect due to metastable nitrogen molecules appears at repetition rate of discharges above some kilohertz. On the bases of experiments of Berger [1974], the duration of influence of metastable particles in air can be about fifty

milliseconds in discharge gap with electrode spacing of 15 mm. The increase in gap length decreases that influence [Berger, 1974].

The phenomenon of an after-effect is observed also in Geiger counters [Loeb, 1965], where the residual products of burst pulses cause the spurious counts and prolong the dead time of the counter. The same problems arise in spark counters [Raether, 1964]. Products created by previous discharges can have a significant effect on the probability of spark breakdown [Waters, 1978]. Van Brunt and Kulkarni [1989] show that the amplitude of Trichel pulses and the time interval between them affect significantly the development of next Trichel pulses.

Although different manifestations of the after-effect of corona pulses are widely investigated, special methods for their detection and for measurement of their magnitude are developed poorly. Furthermore, the investigators are not in agreement whether the excited neutral particles, chemically active species or residual negative ions cause the after-effect. Some of those particles may come from a discharge channel. The residual negative ions may be produced also by a previous corona pulse due to the photoeffect at the surface of the opposite electrode or due to the photoionization of gas molecules.

The role of the gas photoionization in gas discharges was underestimated in recent years [Pancheshnyi *et al*, 2001]. There are only few papers concerning this problem. Commonly, it is assumed that the photoionizing radiation is emitted by gas atoms and molecules excited via electron collision [Badaloni and Gallimberti, 1972]. According to the recent results published in literature, another very different generation mechanism of photoionizing radiation – the soft x-ray radiation produced by collisions of electrons against the anode surface – is possible [Akishev *et al* 1999a, 1999b, 1999c]. A satisfactory experimental confirmation in favour of one or another above mentioned generation mechanism of photoionizing radiation is missing yet.

2.6 Physical processes in corona discharges

2.6.1 Ionization

Ionization processes in nonequilibrium plasma can be divided into three groups [Rusanov and Fridman, 1984].

1. *Direct ionization.* If an electron with sufficient energy collides with an atom or a molecule in the ground state:
$$e + AB \rightarrow AB^{+} + 2e.$$
2. *Stepwise ionization.* If an electron collides with an exited particle:
$$e + A^{*} \rightarrow A^{+} + 2e.$$

3. *Ionization through the collision of two neutral particles*. It can happen if the total excitation energy of neutral particles is higher than the ionization energy. However, this process has quite small probability of occurrence because it is adiabatic and the number of particles with sufficient energy is small.

In coronas, it is important to consider also the gas photoionization due to UV light emitted by corona discharge itself. This process is represented by the reaction [Rees, 1978]

$$A + h\nu \rightarrow A^+ + e.$$

In air, the photoelectrons appear mainly in the process of direct ionization of oxygen molecules [Zheleznyak *et al*, 1982].

2.6.2 Recombination

According to Rusanov and Fridman [1984], the loss processes of charged particles can be divided into three groups: electron-ion recombination, ion-ion recombination and losses on the walls of the discharge chamber.

1. *Electron-ion recombination.* If the gas contains molecular ions and the gas temperature is not too high then the dissociative recombination of positive ions and electrons occurs:

   $$e + AB^+ \rightarrow A + B^*.$$

   The energy released when the electron combines with ion to form a neutral molecule will be expended in dissociation and excitation. At high pressures, the recombination in collision of three particles can be more important:

   $$e + A^+ + B \rightarrow A + B.$$

   Here the third particle (B) will take away the excess energy. A heavy particle is unable to reduce the electron energy so quickly that the positive ion could attach the electron. Therefore, an electron plays usually most effectively the role of the third particle.

   In addition to above mentioned electron-ion recombination mechanisms, the radiative electron-ion recombination is also quite effective:

   $$e + A^+ \rightarrow A + h\nu.$$

2. *Ion-ion recombination.* The ion-ion recombination with assistance of the third body is effective at pressures higher than some mm Hg [Rusanov and Fridman, 1984]:

   $$A^- + B^+ + M \rightarrow A + B + M.$$

   At lower pressures, the ion-ion recombination occurs due to collision of two bodies [Smirnov, 1978]:

   $$A^- + B^+ \rightarrow A + B^*.$$

3. *Losses at walls.* Diffusion of charged particles to the walls of the discharge chamber and their later recombination there is important at low pressures.

2.6.3 Attachment

Attachment of electrons to atoms and molecules is an important loss factor in electronegative gases. In air, negative oxygen ions will occur [Raizer, 1987]. Also, the water molecules attach electrons effectively. Dissociative attachment, and three-body processes are important just like in the case of electron-ion recombination.

1. Dissociative attachment of fast electrons will go according to the following scheme:

   $$e + AB \rightarrow A^- + B.$$

   Attachment of electrons to halogens follows usually this scheme [Raizer, 1987]. The dissociation energy of O_2, CO_2 and H_2O is higher and the electron affinity is lower than those parameters of the halogen molecules, therefore, the dissociative attachment of O_2, CO_2 and H_2O molecules is less probable [Radsig and Smirnov, 1980].
   The reaction rate coefficient of the process

   $$e + O_2 \rightarrow O^- + O$$

   is given for the reduced field range 10×10^{-21} V m^2 < E / n < 150×10^{-21} V m^2 by the equation [Sigmond, 1983 and 1984]:

   $$\frac{\eta}{n} = 6\times10^{-23}\exp\left(-\frac{100n}{E}\right)\text{m}^2.$$

   Here E denotes the electric field strength and n is the number density of gas molecules.

2. At pressures higher than 13 kPa, the main loss process of low energy electrons is the three-body attachment:

   $$e + A + B \rightarrow A^- + B.$$

   In air, the slow electrons disappear mainly according to the reaction [Raizer, 1987]:

   $$e + O_2 + M \rightarrow O_2^- + M,$$

   where O_2, CO_2, H_2O, NH_3 or H_2S may play the role of the third body M. The rate coefficient of this reaction is given by the equation [Sigmond, 1993 and 1984]:

   $$\frac{\eta}{n^2} = 1.6\times10^{-47}\left(\frac{E}{n}\right)^{-1.1}\text{m}^5.$$

The average rate of natural production of electron-ion pairs in the air at the ground level is about 10^7 m^{-3}s^{-1} [Tammet, 1996]. The lifetime of free electrons in the air is ~10^{-8} s due to their attachment to electronegative atoms and

molecules [Bazelyan and Raizer, 1998]. This is the reason why the probability of appearance of a naturally produced free seed electron in the narrow active zone of the point electrode is negligible [M & A Goldman, 1978].

Attachment of electrons reduces the ionization rate and the effective ionization coefficient α' decreases. This will increase the onset voltages of discharges in electronegative gases.

2.6.4 Detachment

The negative ions may lose electrons in the following processes.

1. *Associative detachment*

   $$A^- + B \rightarrow AB + e.$$

   An example of this process is the reaction of oxygen ion with oxygen atom or carbon dioxide molecule:

   $$O^- + O \rightarrow O_2 + e,$$
   $$O^- + CO_2 \rightarrow CO_3 + e.$$

2. *Collisional detachment*. Electron detachment after collision of ion with neutral particle [Rees, 1978]:

   $$AB^- + M \rightarrow AB + M + e.$$

   If the neutral particle M is excited, the process is more probable.
   The example of this process is the collision of oxygen ion and excited oxygen molecule:

   $$O_2^- + O_2^* \rightarrow 2O_2 + e.$$

   Here O_2^* is molecular oxygen in a state $a^1\Delta_g$ [Lowke, 1992]. Those metastables are produced by reaction [Lowke, 1992]:

   $$e + O_2 \rightarrow O_2^* + e.$$

   At high ionization level, the electron detachment may take place due to collisions between negative ions and electrons [Rusanov and Fridman, 1984]:

   $$e + A^- \rightarrow A + 2e.$$

   Raizer [1987] considers this mechanism ineffective.

3. *Photodetachment* [Smirnov, 1978]

   $$A^- + h\nu \rightarrow A + e.$$

   Beattie [1975] considers this process as an important secondary feedback process.

It is commonly accepted that the negative ions detach electrons that can trigger the positive corona [Andersson, 1958; Loeb, 1965; Waters *et al*, 1965; Hepworth *et al*, 1972; Waters, 1978; M & A Goldman, 1978; Gallimberti, 1979; Berger, 1980; Gosho and Harada, 1982; Gosho and Saeki, 1987]. However, the mechanism of this detachment is not determined unambiguously [Morrow,

1997]. The seed electrons can be provided due to thermal detachment [Phelps and Pack, 1961]. They may appear due to ion collisions with metastable oxygen molecules [Lowke, 1992]. Those electrons can appear via collisional detachment from negative ions under the influence of the high electric field near the point electrode [Loeb, 1965]. In air under normal pressure, the ions may detach electrons if $E > 38$ kV cm^{-1} [Bogdanova *et al*, 1978]. The mean collisional detachment lifetime of these ions decreases with increase in the electric field strength and with decrease in the humidity content [Berger, 1980]. For use in computer simulations, the detachment frequency of negative (oxygen) ions as a function of the reduced electric field E / n is given by the equation [Sigmond, 1983 and 1984]:

$$\frac{\delta}{n} = 3.6 \times 10^{-18} \exp\left(-\frac{940n}{E}\right) \mathrm{m}^2 .$$

2.6.5 Formation of cluster ions

In gas, the elementary ions form the complex and cluster ions according to the equation [Smirnov, 1978]:

$$A^- + B + M \rightarrow AB^- + M.$$

Beside the formation of stable cluster ions, the formation of unstable cluster ions is possible. The lifetime of those ions is much longer than the time interval between collisions of particles in gas. The more complicated the ion is the longer lifetime it usually has [Smirnov, 1978].

In clean air, the following negative cluster ions dominate [Tammet, 1996]: $NO_3^- \cdot (HNO_3) \cdot H_2O$, $NO_2^- \cdot (H_2O)_2$, $NO_3^- \cdot H_2O$, $O_2^- \cdot (H_2O)_4$, $O_2^- \cdot (H_2O)_5$. The dominant positive cluster ions are $H_3O^+ \cdot (H_2O)_6$, $NH_4^+ \cdot (H_2O)_2$, $NH_4^+ \cdot (H_2O)$, $H_3O^+ \cdot (H_2O)_5$, $NH_4^+ \cdot NH_3$.

The annual average mobility of positive atmospheric ions is 1.36×10^{-4} m^{2}s^{-1}V^{-1} and that of negative ions is 1.56×10^{-4} m^{2}s^{-1}V^{-1} [Hõrrak *et al*, 1994; Tammet, 1996]. Nagato and Ogawa [1998] measured the mobility spectra of negative ions as a function of ion age at different temperature and humidity values. At $T = 294$ K, they obtained for $0.03 - 3$ s aged ions two peaks – one at 1.7×10^{-4} m^{2}s^{-1}V^{-1} and another at 1.9×10^{-4} m^{2}s^{-1}V^{-1}.

Luts and Salm [1994] modelled the evolution of negative ions depending on the ion age. The primary negative ions are O_2^- (95%) and O^- (5%). In the process of clustering of these ions, the ions $O_2^- \cdot (H_2O)_n$, $n \geq 1$ appear. At an age of 10^{-7} s, the ions $O_2^- \cdot (H_2O)_4$ dominate. The concentration of ions will stay practically unchanged as long as the age of ions is less than 0.1 s. The ions $O_2^- \cdot (H_2O)_n$ disappear at an age about $0.1 - 1$ s. The ions $CO_3^- \cdot (H_2O)_n$ appear in the age interval of $0.01 - 1$ s [Luts, 1995]. The ions $NO_3^- \cdot (HNO_3) \cdot (H_2O)$ start to

dominate when the ion age exceeds 0.5 s. The ions $NO_3^-\cdot(HNO_3)_m\cdot(H_2O)_n$ (85%), $NO_2^-\cdot(HNO_3)_m\cdot(H_2O)_n$ (10%) and $O_2^-\cdot(H_2O)_n$ (2.5%) are characteristic to the steady state [Luts and Salm, 1994].

Luts [1995] modelled the evolution of negative ions under the influence of the enhanced (about $4\cdot10^5$ times) ionization rate. The ions $O_2^-\cdot(H_2O)_n$ and $CO_3^-\cdot(H_2O)_n$ become dominant in the steady state due to changes in partial concentrations of the neutral constituent gases and due to shortening of ion lifetimes.

2.6.6 Production of chemically active particles in corona

Corona discharges produce chemically active particles (radicals).

The nitrogen atoms are generated in reaction

$$N_2 + e \rightarrow N + N + e.$$

The oxygen atoms are generated by dissociation of oxygen molecules

$$O_2 + e \rightarrow O + O + e,$$

or by excitation of nitrogen molecules

$$N_2 + e \rightarrow N_2\,(A^3\Sigma) + e$$

and subsequent reaction [Naidis, 1997]

$$N_2\,(A^3\Sigma) + O_2 \rightarrow N_2 + O + O.$$

The calculation by Naidis [1997] shows that N and O atoms are produced mainly in the region of high electric field (for example in the streamer head).

Those chemically active particles produce nitrous oxides (N_2O, NO, NO_2) and ozone. The production of NO_x increases with mean current intensity of the discharges [Peyrous and Lapeyre, 1982] as well as with increase in concentration of water vapour [Peyrous and Lapeyre, 1982; Martinez and Brandvold, 1996]. The production of O_3 takes place mainly in predischarge regimes [Peyrous and Lapeyre, 1982] and increases with mean current intensity. During spark regimes, the production of ozone ceases [Peyrous and Lapeyre, 1982].

2.7 Overview of earlier investigation of “streamer counter”

The first known attempt to use the repetition rate of DC corona streamers in practice was done by Andersson and Hertz [1955], who suggested to use the dependence of the repetition rate of DC streamers on humidity content for the measurement of the concentration of water vapour in ambient air. Vaska recorded the dependence of repetition rate of DC streamers on concentration of chlorine [Vaska, 1960; Kudu and Veimer, 1970]. Mohr and Weissler [1947]

report that repetition rate and amplitude of DC streamers depends on concentration of freon in air. Fouad *et al* [1978] discuss the possibility to use streamer corona for counting the alpha particles. Fouad and El-Hazek [1996] used open-air corona streamer counter with preamplification gap for detection of weakly ionizing beta rays.

The main disadvantage of those devices is the strong dependence of the counting rate on the small variation of applied voltage. A modified technique to estimate the concentration of halogens in air was suggested by Kudu [1960], who suggested a simultaneous application of a DC voltage and an AC voltage of 50 Hz frequency to the gap. Kudu [1980] called that voltage as "mixed voltage". The suggested technique enables to reduce essentially variations in the repetition rate of streamers caused by variations in applied voltage, pressure and temperature of the ambient air. Kudu suggested that this device, also called a "streamer counter", can be successfully used for measurements of the ionization level and for measurements of the amount of halogen impurities or water vapour in the air [Kudu, 1980].

Roos and Hilpus [1977] made the first extensive experimental investigation of the repetition rate of streamers under conditions of combined voltage of 50 Hz frequency. They investigated the "counting rate characteristics", that is the curves representing the dependence of repetition rate of streamers versus applied DC voltage, depending on the amplitude of AC voltage, the airflow rate, the intensity of the β-source, the concentration of water vapour and iodine admixtures. An interpretation of the experimental results of Roos and Hilpus was given by Kudu [1980]. He suggested that the appearance of a seed electron during the time interval the resultant (combined) voltage being in burst pulse region eliminates the appearance of the streamer during the same cycle of the combined voltage. On the bases of that suggestion, he deduced that decrease in preionization level decreases the formation probability of burst pulses and in that way increases the formation probability of a streamer. Last statement is true as long as the preionization level is still high enough to enable the formation of discharge during every AC cycle. The halogens influence the repetition rate of streamers in the similar way – by capturing the initial electrons they reduce the effective preionization level [Kudu, 1960]. The amplitude of AC voltage influences the repetition rate of streamers through the changing the duration of the time interval the resultant voltage being in burst pulse region. That time interval decreases if the amplitude of the AC voltage increases. Thus, the formation probability of burst pulses decreases and that of streamers increases [Kudu, 1980].

Although the possibilities to use the positive streamer corona for detection purpose of electronegative admixtures are intensively investigated during resent fifty years, there are still unsolved problems that need further investigation.

- The working principle of streamer counter needs still further investigation and a mathematical description.
- The optimal working parameters (preferable values of AC voltage amplitude and frequency, DC voltage, airflow rate, preionization level) are still unknown.
- The list of admixtures that can be detected by the streamer counter needs specification.
- As the streamer counter in its present form is unable to differentiate between different admixtures, the possibilities to make it selective to some admixtures need to be investigated in more detail than it was done so far.

2.8 The main goals of the present investigation

On the bases of cited above papers, we can bring out some actual problems and tasks for investigation.

1. Streamer counter developed by Kudu *et al* seems to be promising device for detection of electronegative trace gases. However, to estimate optimal working parameters of the device and to explain the dependence of its characteristics on conditions of operation, it is necessary to clarify the mechanism of discharge inception under conditions of combined voltage in more detail. A mathematical model of the streamer counter needs to be developed.
2. The after-effect of a discharge, having an essential effect in all types of gas discharge counters, is not taken into account in the case of the streamer counter. The reason for that is the absence of proper methods for quantitative estimation of the after-effect. Therefore, it is important to develop the method for measurement of the after-effect of a discharge under conditions of the combined voltage.
3. Photoionization plays essential role in the mechanism of corona discharges. It is a potential agent of the after-effect as well. What kind of mechanism is responsible for the generation of photoionizing radiation in corona discharge in the air – that needs further investigation because there exist at least two very different views in the literature.
4. Great disadvantage of the streamer counter as a detector of trace gases is that one can say nothing about the nature of the trace gas causing change in the repetition rate of streamers. It would be useful to find out whether it is possible to make the streamer counter capable to differentiate between some electronegative trace gases.

3 EXPERIMENTAL SETUP

Figure 3.1 shows the diagram of the experimental device, used for the investigation of positive corona discharge at combined voltage.

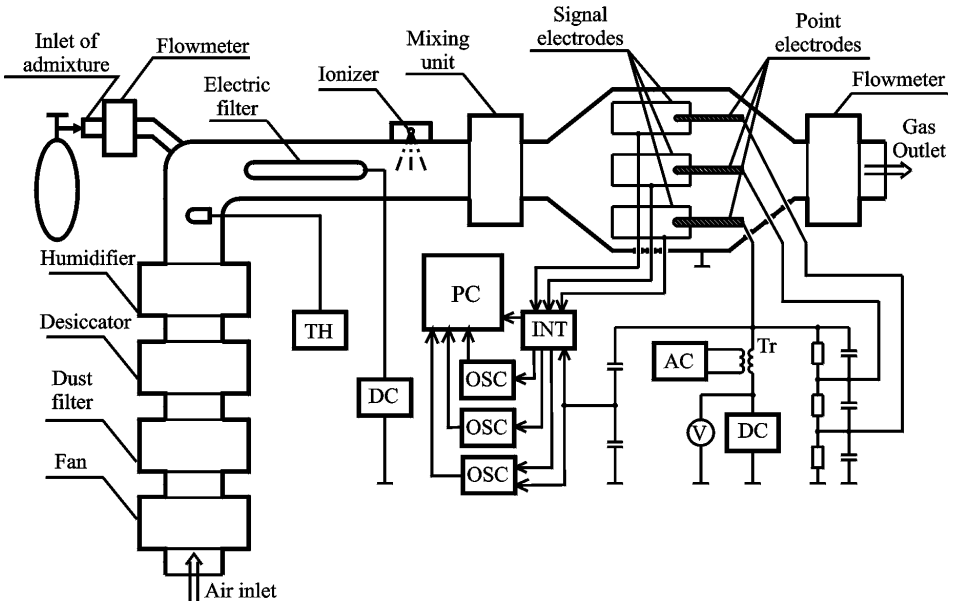

Figure 3.1. The experimental set-up.

Three hemispherically tipped platinum wires of different diameter *d* serve as point electrodes. Each of them is surrounded by a coaxial cylinder as an opposite electrode of 28 mm in inner diameter and 30 mm in length. Each point tip is placed 25 mm distant from the front edge of the corresponding opposite electrode. These opposite electrodes serve also as the signal electrodes. High DC and AC (frequency range 20–1100 Hz) voltages are applied to the point electrodes through a common RC voltage divider. Circuit arms of the voltage divider are chosen so that the combined voltage reaches the onset voltage of streamers for all gaps simultaneously. Instantaneous value of resultant voltage runs in all gaps sequentially the voltage region free of discharge, that of burst pulses, streamers and glow corona. Table I presents the onset voltages of different discharge modes. All values of voltages are reduced to the standard conditions and the reduced data are presented below in this thesis. The following relation describes the common procedure of reduction [Waters, 1978; Blair, 1978]

$$U_{\text{reduced}} = \delta^{-m} U ,$$

where power $m = 1$ and δ denotes the relative air density, which is calculated according to the equation

$$\delta = \frac{P}{101\,\mathrm{kPa}} \frac{293\,\mathrm{K}}{T}.$$

Here P denotes the pressure and T the temperature. The shift of counting-rate characteristics along the voltage axis, which occurs due to variations in air pressure and temperature, disappears as a result of application of this reduction procedure [I]. This reduction procedure is valid in the interval of δ values $0.84 < \delta < 1.16$ [Waters, 1978]. Below the value 0.85, a higher power m value should be used [Allen and Ghaffar, 1995b].

Table I. Onset voltages of burst pulses U_{bp}, streamers U_{str} and steady glow U_g [II].

Gap number	1	2	3
Point diameter, d /mm/	0.13	0.25	0.50
U_{bp} /kV/	2.46	3.08	4.10
U_{str} /kV/	2.54	3.18	4.26
U_g /kV/	2.84	3.43	4.42

The digital dual-channel 60 MHz oscilloscopes measure the amplitudes of current pulses induced on the signal electrodes. A personal computer PC stores the sequences of streamers synchronously with the AC voltage for every discharge gap. The time resolution (1 μs) and the minimal measurable time interval between subsequent streamers (10 μs for each discharge gap) are pre-set by an interface INT. The maximum duration of continuous counting (5 - 60 s) is determined by the computer program and by amount of free RAM (Random Access Memory) in PC (1MB for every second of counting time).

An electric filter neutralizes primary air ions; a subsequent ionizer (α-active source ^{239}Pu or another corona discharge) sets the preionization level to the desired value. A homogeneous mixture of ions is obtained in a mixing unit. The intensity of the ion flux Φ at the inlet of the signal electrodes is measured with an electrometer in additional experiments. Below, while discussing the preionization level, we consider just this ion flux. The volume of the pipeline between ionizer and detector gaps is 1.4×10^{-3} m^{-3}.

The experiments are carried out in laboratory air under normal pressure. A dust filter eliminates particles bigger than 10 nm in diameter. A desiccator filled with silica gel removes moisture from the air. Thereafter, the desired level of humidity is adjusted by evaporation of distilled water into air in a humidification unit. A digital thermohygrometer TH measures air temperature and humidity. A differential flowmeter measures the volumetric flow rate of the air stream.

Electronegative admixtures SF_6 and CO_2 are introduced from a cylinder. Concentration of the admixture in the discharge gaps is calculated from

readings of flowmeters. Iodine admixture is obtained by blowing air through a vessel whose inner walls are covered with crystals of iodine. Air, saturated with iodine vapour, is diluted in proportion of 1:1000 and introduced as a controlled flow into the inlet of the electronegative admixture of the experimental device. Electronegative admixtures O_3 and $O_3 + NO_x$ are produced with the help of a barrier discharge ozonizer using respectively oxygen or dry air as feeding gas. In case of $O_3 + NO_x$, the concentration of NO_x constitutes about 10% of that of O_3 [Samoilovitsh *et al*, 1989].

4 DISCHARGE PHENOMENA AT COMBINED VOLTAGE

4.1 Visual examination of discharge phenomena

A typical streamer starts in ambient air from the tip of the hemispherically capped point electrode [I]. A following glow corona will cover the remaining part of the hemisphere. Starting position of the first and subsequent streamers is the same. The stems of streamers are overlapping like it was reported by Aints *et al* [1977]. Afar from the point, the streamers may branch. In contrast, in experiments with increased concentration of carbon dioxide, the branching of streamers was reduced and the streamers covered the whole tip of the point electrode (see section 8.1 for details) [I].

We measured the length of streamers in ambient air visually and photographically using a signal electrode with a hole for that purpose. The results 2.4, 3.6 and 5.9 mm were obtained for lengths of streamers in the voltage region $[U_{str},U_g)$ in the case of point diameters $d = 0.13$ mm, $d = 0.25$ mm and $d = 0.50$ mm, respectively [II].

4.2 Oscilloscopic study of discharge pulses

4.2.1 Typical development of discharge pulses

In figure 4.1, the upper oscillogram (figure 4.1a) represents the combined voltage, which is applied to the point electrode. The AC and DC voltages are set so that instantaneous value of the resultant voltage U runs sequentially through the discharge free region and regions of different corona modes: burst pulses ($U_{bp} \le U < U_{str}$), streamers ($U_{str} \le U < U_g$) and steady glow ($U \ge U_g$). The occurrence region of burst pulses and that of DC streamers are highlighted by the dashed lines both on voltage and time scales. Δt_{bp} denotes the time during which the resultant voltage runs through the burst pulse region ($U_{bp} \le U < U_{str}$). By Δt_s we denote the time interval during which the resultant voltage stays above the onset voltage of streamers U_{str}. The time needed by the resultant voltage to traverse the region $U_{str} \le U < U_g$ is denoted by Δt_{str}. Finally, Δt_{free} denotes the time during which the resultant voltage is below the onset voltage of burst pulses U_{bp}.

Results of the oscilloscopic study of the discharge current may be summarised as follows. Normally, the discharge arises at each AC cycle either as a single streamer or as a burst pulse (figure 4.1b-e). The type of a discharge is determined by the instantaneous value of the resultant voltage U at the moment of discharge inception. A discharge starts as a burst pulse, if it is formed in the voltage region $U_{bp} \le U < U_{str}$. That discharge continues as a steady glow corona

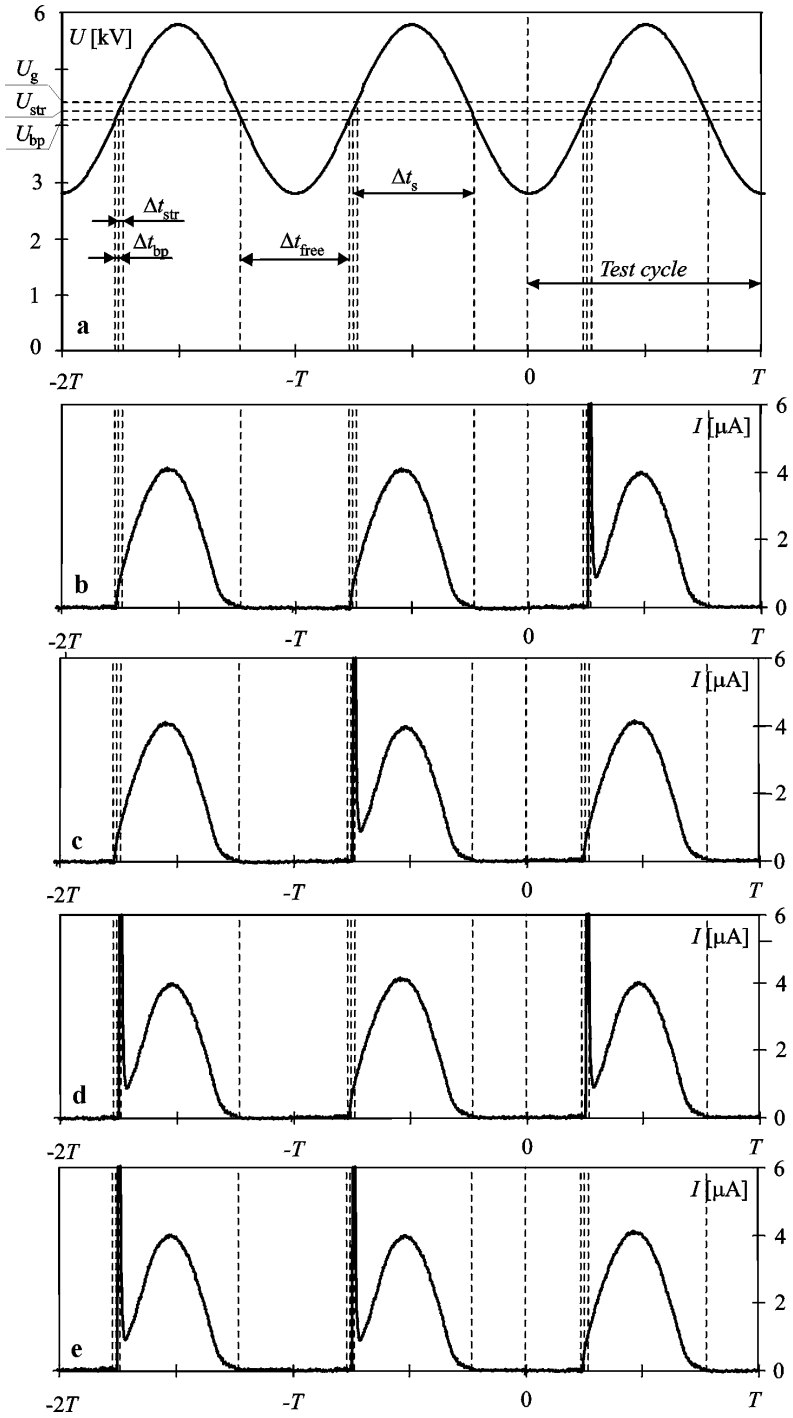

Figure 4.1. Typical oscillograms of applied voltage and discharge current: point diameter d = 0.5 mm.

as long as $U \geq U_g$, and no streamer will appear during that AC cycle. If a discharge is incepted a bit later, when U is already equal to or above the onset voltage of streamers U_{str}, the discharge starts as a streamer. Normally, the streamers arise on the positive slope of the resultant voltage like in [Kudu, 1980; I].

The streamers are followed by the glow corona, too, and the glow burns on the point electrode as long as the resultant voltage U is above U_g. The intensity of the glow corona is approximately the same, both after a burst pulse and after a streamer (figure 4.1b-e) [II].

In general, the formation of a burst pulse excludes the formation of a streamer during the same AC cycle [I]. However, the possibility of burst pulse to exclude the streamer at certain cycle does not last forever but only some hundreds of μs depending on point electrode diameter. Statistical analysis of discharge current oscillograms shows that burst pulse excludes the streamer for 150 μs in the case of gap 1 and for 700 μs in the case of gaps 2 and 3. These time intervals are called limiting ones (Δt_{lim}) for corresponding gaps below. In experiments of Miyoshi and Hosokawa [1973], the burst pulses excluded the formation of a streamer at least for 50 μs. If $\Delta t_{bp} + \Delta t_{str} > \Delta t_{lim}$, there exists a possibility that the burst pulse incepted during Δt_{bp} is followed by a streamer during the same AC cycle.

A little above the onset potential of streamers, a narrow region exists, where the formation of a burst pulse is possible instead of a streamer, although there was no discharge during Δt_{bp}. This burst pulse excludes the streamer in this cycle like a burst pulse formed during Δt_{bp} would have done. However, the effective increase in Δt_{bp} due to overlapping of regions of burst pulses and streamers remains less than 11%. We neglect that effect in the further discussion.

Under conditions of our experiments in ambient air, only a single streamer occurred during one AC cycle. The second streamer appeared sometimes during the same AC cycle in gap 1, if the time Δt_{str} was longer than 0.45 ms. In ambient air, the second streamer was never detected in gaps 2 and 3 where the maximum duration of Δt_{str} was 8.9 ms and 5.6 ms respectively. More than one streamer was detected during an AC cycle in experiments with increased concentration of carbon dioxide (see section 8.1 for details).

In principle, under condition of very low preionization level, there might be to few triggering electrons to initiate a discharge during every AC cycle. Under conditions of our experiments, the preionization level was high enough and there were no AC cycles without a discharge.

4.2.2 Amplitude analysis of discharge pulses

The amplitude of streamer pulses and the peak value of glow corona current were investigated depending on amplitude and frequency of AC voltage, DC voltage, airflow rate, preionization level and point diameter. The results can be summarized as follows.

- The minimum amplitude of streamer pulses remains independent of amplitude and frequency of AC voltage, DC voltage, airflow rate and preionization level.
- The maximum amplitude of streamer pulses increases with increase in amplitude and frequency of AC voltage. In both cases, the increase rate of resultant voltage in the streamer region increases too, and delayed streamers arise at higher instantaneous value of resultant voltage. Allen and Boutlendj [1993] report about similar increase in amplitude of pre-breakdown streamer with increase in applied voltage.
- The maximum amplitude of streamer pulses increases with airflow rate and decreases with increase in preionization level. As will be shown in section 6, both these parameters influence the total flux of ions into the active zone of the point electrode. Decrease in the number of seed ions results in later inception of streamers. Delayed streamers arise at higher instantaneous value of resultant voltage and thus have higher amplitude. The change in DC voltage in the limits $U_{str} - 0.2\ U_{AC} < U_{DC} < U_{bp} + 0.6\ U_{AC}$ has no influence on maximum amplitude of streamer pulses.
- The peak current of glow corona increases with DC voltage and amplitude of AC voltage. Change in preionization level or AC frequency has no influence on the peak current of the glow corona. The glow corona current decreases about 10% with increase in airflow rate from 0.8 m s^{-1} to 4.5 m s^{-1}.
- The peak value of the current of every streamer exceeds that of the most powerful glow corona at least 10 times.
- The amplitude of both the streamer and glow corona increases with point diameter.

5 FORMATION PROBABILITY OF A STREAMER

5.1 The statistical model for calculation of the formation probability of a streamer

We start this section with derivation of the statistical equation for formation probability of a streamer.

The dominant production process of triggering electrons for a corona discharge is the detachment of electrons from negative atmospheric ions under the influence of the applied electric field in the active zone ahead of the point electrode [Loeb, 1965]. We call this part of the active zone ahead of the point electrode where a detached electron can initiate a burst pulse at $U = U_{str}$ as the birth region of burst pulses [II]. The calculation of the lateral boundary of this region will be discussed in section 6.9. Let us assume first that the negative ions reach the birth region of burst pulses randomly and independent of each other. In this case, the probability p_m^- for m negative ions to reach the birth region of burst pulses during the time interval Δt_{bp} can be calculated proceeding from the Poisson's distribution, and it is given by equation [Anderson *et al*, 1981]

$$p_{\mathrm{m}}^{-} = \frac{\left(\Phi_{\mathrm{T}}\,\Delta t_{\mathrm{bp}}\right)^{m}}{m!}\cdot\exp\left(-\Phi_{\mathrm{T}}\,\Delta t_{\mathrm{bp}}\right). \tag{5.1}$$

Here Φ_T is a stochastic flux of negative ions reaching the birth region of burst pulses.

Two factors control the probability that an ion reaching the birth region of burst pulses initiates a burst pulse:

1) the value of applied voltage at the moment of ion arrival;
2) the entrance co-ordinates of ion on the front surface S of the birth region of burst pulses.

Let us denote by b the mean (averaged over the voltage interval $U_{bp} \le U < U_{str}$ and over the surface S) probability of initiation of a burst pulse by a single negative ion. As U depends on time in our case, we get:

$$b = \frac{\int\int_{S}\int_{\Delta t_{\mathrm{bp}}} b_{\mathrm{det}}\, b_{\mathrm{bp}}\,\mathrm{d}t\mathrm{d}s}{\Delta t_{\mathrm{bp}} S}.$$

b_{det} denotes the probability that an average single negative ion undergoes detachment of an electron and b_{bp} denotes the probability that this electron initiates a burst pulse. Thus, the probability that m negative ions will initiate the burst pulse is

$$p_{\mathrm{m}}^{\mathrm{bp}} = 1-(1-b)^{m}. \tag{5.2}$$

The formation probability of a burst pulse during the time interval Δt_{bp} can be presented as a sum

$$p_{bp} = \sum_{m=0}^{\infty} p_m^- \; p_m^{bp} \; . \tag{5.3}$$

Substituting the expressions (5.1) and (5.2) into the equation (5.3), we get

$$\begin{aligned} p_{bp} &= \sum_{m=0}^{\infty} \left(1-(1-b)^m\right) \cdot \frac{\left(\Phi_T \, \Delta t_{bp}\right)^m}{m!} \cdot \exp\left(-\Phi_T \, \Delta t_{bp}\right) = \\ &= \exp\left(-\Phi_T \, \Delta t_{bp}\right) \sum_{m=0}^{\infty} \frac{\left(\Phi_T \, \Delta t_{bp}\right)^m}{m!} - \exp\left(-\Phi_T \, \Delta t_{bp}\right) \sum_{m=0}^{\infty} \frac{\left((1-b)\,\Phi_T \, \Delta t_{bp}\right)^m}{m!} = \\ &= 1-\exp\left(-\Phi_T \, \Delta t_{bp}\right) \cdot \exp\left((1-b)\,\Phi_T \, \Delta t_{bp}\right) = \\ &= 1-\exp\left(-\Phi_T b \Delta t_{bp}\right) \end{aligned} \tag{5.4}$$

According to our results of oscilloscopic study (see section 4.2), the simplest relationship between formation of a burst pulse and a streamer can be phrased as follows. The formation of a burst pulse during Δt_{bp} eliminates the possibility that a streamer arises during the same AC cycle. The formation probability of a streamer during a particular AC cycle can be presented therefore as a product of two probabilities:

$$p = \left(1- p_{bp}\right) p_{str} \, . \tag{5.5}$$

Here p_{str} is the probability that a streamer arises during the time interval Δt_s if during Δt_{bp} there was no burst pulses.

$$p_{str} = 1-\exp\left(-\Phi_T b_{str} \Delta t_s\right), \tag{5.6}$$

where b_{str} denotes the probability that an average single negative ion undergoes detachment and initiates a streamer.

Inserting (5.4) and (5.6) into (5.5), we get

$$p = \left(1-\exp\left(-\Phi_T b_{str} \Delta t_s\right)\right) \exp\left(-\Phi_T b \Delta t_{bp}\right). \tag{5.7}$$

Δt_s is much longer than Δt_{bp} under our experimental conditions (see figure 4.1). $b_{str} > b$ as well, if peak value of U exceeds U_{str} sufficiently. In the conditions of sufficient preionization level, the first exponential in the last equation will be close to zero. As a result we get

$$p = \exp\left(-\Phi_T b \Delta t_{bp}\right). \tag{5.8}$$

The time interval Δt_{bp} is calculated from the values of DC voltage U_{DC}, peak value U_{AC} and frequency f of the AC voltage and onset voltages of different modes of the discharge by the equation

$$\Delta t_{bp} = \frac{1}{2\pi \, f} \left(\arcsin\left(\frac{U_{str} - U_{DC}}{U_{AC}} \right) - \arcsin\left(\frac{U_{bp} - U_{DC}}{U_{AC}} \right) \right). \tag{5.9}$$

The flux Φ_T is calculated from the preionization level Φ according to numerically calculated electric field lines (see section 6.9 for details).

According to oscilloscopic study, the appearance of a burst pulse will eliminate the formation of a streamer for a certain time interval. Thus, the equation (5.8) is valid only if $\Delta t_{bp} + \Delta t_{str}$ is shorter than that limiting time interval Δt_{lim}.

5.2 Experimental results

The formation probability p of a streamer can be determined when one divides the number of streamers per certain time interval by the total number of AC cycles in this time interval. The dependencies of p on DC voltage U_{DC}, peak value U_{AC} and frequency f of the AC voltage, airflow rate v and preionization level Φ are presented in figures below. The points are recorded in experiments. The black solid curves are calculated according to equation (5.8). Equation (5.8) will be called below as a rough model. In the rough model, the value of parameter b is chosen for every discharge gap individually to achieve the best agreement between the model and experimental results. In gap 1 $b = 0.21$, in gap 2 $b = 0.17$, in gap 3 $b = 0.07$.

Grey curves, presented in the same figures, represent the improved model (see equation (6.5) in section 6.3) that takes into account the after-effect of a discharge and changes in b with airflow rate and Δt_{bp}.

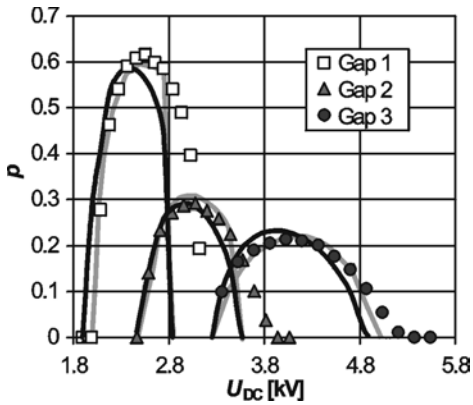

Figure 5.1. Formation probability of streamer versus the DC voltage. $f = 1000$ Hz; $v = 3.7$ m/s; $\Phi = 7.4 \cdot 10^6$ s^{-1}. Gap 1: $U_{AC} = 0.437$ kV; Gap 2: $U_{AC} = 0.578$ kV; Gap 3: $U_{AC} = 0.894$ kV.

Figure 5.1 presents the dependence of streamer formation probability on the DC voltage U_{DC}. In paper [I], this dependence is called "the counting rate characteristic". The theoretical curves of rough model fit the experimental points satisfactorily, except the region of higher values of DC voltages where the instantaneous values of the combined voltage do not drop below the onset potential of burst pulses. If $U_{AC} >> \Delta U_{bp}$ and $U_{str} - 0.6\ U_{AC} < U_{DC} < U_{bp} + 0.6\ U_{AC}$, then the time Δt_{bp} of the growth of the combined voltage through a narrow voltage interval ΔU_{bp} varies little with DC voltage. This is the reason for the appearance of a plateau (see figures 2, 3, and 14 in [I]) in "counting rate characteristics" [I].

Figure 5.2 shows the dependence of streamer formation probability on the amplitude of AC voltage. The values of DC voltage are chosen close to U_{str}. One can see that the streamer formation probability increases with AC voltage. This is in accordance with our model, as at higher AC voltages the resultant voltage traverses the region of burst pulses more swiftly than at lower AC voltages. However, the curve of the rough model fits experimental points well only in the case of gap 1. In other gaps, the curve of the rough model fits experimental points to an accuracy of 25%.

Figure 5.3 presents the influence of preionization level on the streamer formation probability. One can see that the higher is the preionization level the less is the formation probability of a streamer. Our model predicts the similar behaviour. However, the curves of the rough model fit experimental points well only at high values of the preionization level. At lower values, the experimental points are below the curves of the rough model.

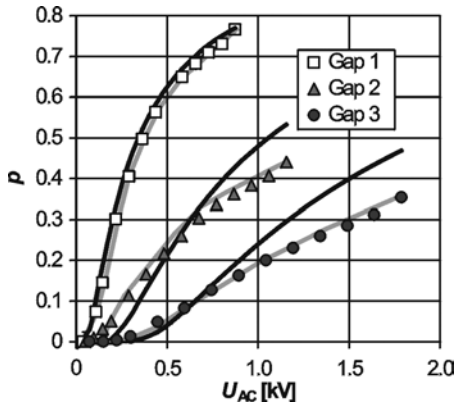

Figure 5.2. Formation probability of streamer versus the AC voltage. f = 1000 Hz; v = 3.7 m/s; $\Phi = 7.4 \cdot 10^6$ s^{-1}. Gap 1: U_{DC} = 2.43 kV; Gap 2: U_{DC} = 3.16 kV; Gap 3: U_{DC} = 4.31 kV.

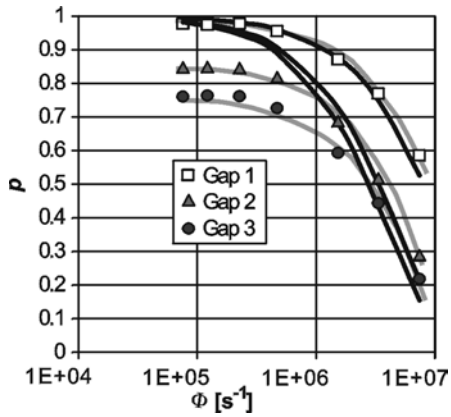

Figure 5.3. Formation probability of streamer versus the preionization level. f = 500 Hz; v = 3.7 m/s. Gap 1: U_{DC} = 2.40 kV; U_{AC} = 0.697 kV; Gap 2: U_{DC} = 3.12 kV; U_{AC} = 0.920 kV; Gap 3: U_{DC} = 4.25 kV; U_{AC} = 1.41 kV.

The influence of AC frequency is presented in figure 5.4. One can see that the streamer formation probability increases with increase in AC frequency. Our model predicts the similar behaviour because the resultant voltage traverses the voltage interval of burst pulses the faster the higher is the frequency. The curve of the rough model and experimental points are in satisfactory accordance in the case of gap 1. The accordance is much worse for gaps 2 and 3.

Figure 5.5 shows the dependence of the streamer formation probability on the airflow rate. The airflow carries the air under test into the discharge gaps. It also carries the ions produced by the ionizer into the discharge gap. The flow rate determines the number of ions reaching the birth region of burst pulses. This

number decreases with an increase in airflow rate (see the limiting trajectories of ions in figure 6.15 for more information). In figure 5.5, we can see that the formation probability of a streamer increases with the airflow rate. The curve of the rough model fits the experimental points satisfactorily in gap 1. In gaps 2 and 3, the curves of rough model lay above all experimental points.

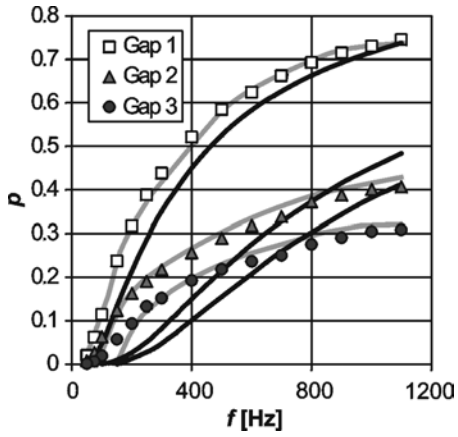

Figure 5.4. Formation probability of streamer versus the frequency of the AC voltage. v = 3.7 m/s; $\Phi = 7.4 \cdot 10^5$ s^{-1}. Gap 1: U_{DC} = 2.39 kV; U_{AC} = 0.695 kV; Gap 2: U_{DC} = 3.11 kV; U_{AC} = 0.915 kV; Gap 3: U_{DC} = 4.25 kV; U_{AC} = 1.40 kV.

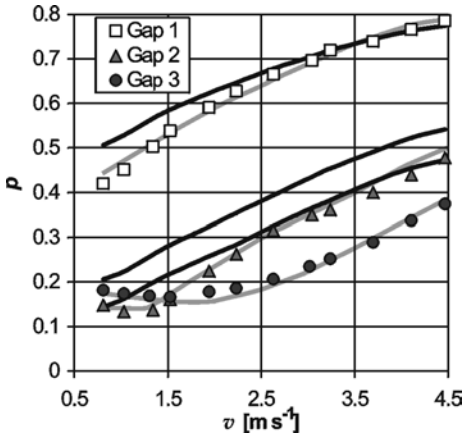

Figure 5.5. Formation probability of streamer versus the airflow rate. f = 1000 Hz; $\Phi = 4.0 \cdot 10^6$ s^{-1} – $7.4 \cdot 10^6$ s^{-1}. Gap 1: U_{DC} = 2.41 kV; U_{AC} = 0.740 kV; Gap 2: U_{DC} = 3.13 kV; U_{AC} = 0.980 kV; Gap 3: U_{DC} = 4.27 kV; U_{AC} = 1.51 kV.

5.3 Reasons for discrepancy between experimental results and theoretical calculations carried out according to the proposed statistical model

The theoretical curves of the rough model describe the dependence of the repetition rate of streamer on U_{AC}, U_{DC}, f, Φ and v satisfactorily in gap 1. In other gaps, a discrepancy exists between theoretical and experimental results such that it exceeds the experimental uncertainty. That discrepancy might be caused by an after-effect of a discharge. The after-effect increases the flux of ions reaching the birth region of burst pulses and thus reduces the formation probability of streamers. The possible presence of an after-effect can explain the discrepancy between the rough model and experiment at high frequency of the AC voltage and low rate of the airflow. However, it is difficult to explain only by the presence of an after-effect of a discharge the considerable discrepancy between theoretical and experimental results, for example in figure 5.5 or at low values of AC frequency in figure 5.4.

The consideration of the after-effect will change our choice for the concrete value of b. Furthermore, the experimental results presented in section 6.6.2

indicate that we have to revise the assumption that b is independent of airflow rate and Δt_{bp}.

The improved model, where the after-effect and the dependence of b on both Δt_{bp} and airflow rate are taken into account (see section 6.3), gives theoretical curves that fit experimental points satisfactorily in all gaps as long as $U_{DC} < U_{bp} + U_{AC}$.

Both our models predict that the counting rate diminishes to zero at $U_{DC} \approx U_{str} + U_{AC}$ but in figure 5.1 one can see that the experimental counting rate characteristics reach $U_{DC} \approx U_{str} + U_{AC} + \Delta U_{str}$. This discrepancy between the models and experimental results needs some further improvements in the statistical model.

6 THE AFTER-EFFECT OF A DISCHARGE

6.1 Definitions

Variation of experimental conditions in wide range and statistical analysis of experimental results show that the formation probability p of a streamer may be different for AC cycles with and without streamer during the foregoing AC cycles. Therefore, four formation probabilities p of a streamer will be used:

- with p_{bb} we denote the streamer formation probability for an AC cycle that is preceded by two AC cycles without any streamer (figure 4.1b);
- with p_{bs} we denote the streamer formation probability providing that there was a streamer during the foregoing cycle, but there was no streamers during the antepenultimate cycle (figure 4.1c);
- with p_{sb} we denote the streamer formation probability providing that the foregoing cycle was without any streamer, but there was a streamer during the antepenultimate cycle (figure 4.1d);
- with p_{ss} we denote the streamer formation probability providing that there was a streamer during both the foregoing and antepenultimate cycle (figure 4.1e).

These streamer formation probabilities are easy to measure using the sequences of streamers recorded in our experiments. The set of recorded AC cycles should be split into several subsets according to the type of the discharge during those two AC cycles, which precede the test cycle. Dividing the number of streamers in each subset by the number of AC cycles in the same subset, we get the formation probability of a streamer after the certain succession of discharge types at preceding AC cycles.

6.2 Experimental investigation of the after-effect

6.2.1 Experimental results

The formation probabilities of a streamer p_{bb}, p_{bs} and p_{sb} plotted against the DC voltage U_{DC} are presented for all three gaps in figure 6.1. The values of parameters are given in the caption of the figure. It can be seen that in gap 1 the probabilities coincide within the limits of experimental accuracy over the whole range of DC voltage except the beginning of the curves, where p_{bs} is much less than other two probabilities. In gap 2, the probabilities p_{sb} and p_{bb} coincide within the limits of experimental accuracy over the whole range of DC voltage. Probability p_{bs} becomes equal to p_{sb} and p_{bb} at $U_{DC} > 3.6$ kV. In gap 3, the probabilities differ markedly over the whole range of the DC voltage used.

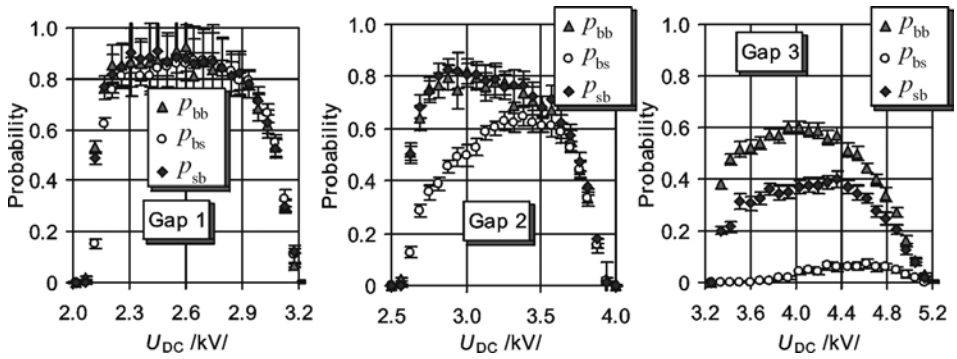

Figure 6.1. Formation probabilities of streamer versus DC voltage. f = 1000 Hz; v = 1.4 m/s; $\Phi = 3.04 \cdot 10^5$ s^{-1}. Gap 1: U_{AC} = 0.430 kV. Gap 2: U_{AC} = 0.570 kV. Gap 3: U_{AC} =0.890 kV.

According to equation (5.8), the plots $-\ln(p) = F_f(\Phi)$ (if Δt_{bp} is kept constant) and $-\ln(p) = F_t(\Delta t_{bp})$ (if Φ is kept constant) should represent straight lines. Here we consider that Φ_T is proportional to Φ. These straight lines should go through the axes origin (p = 1; Φ = 0) or (p = 1; Δt_{bp} = 0) respectively.

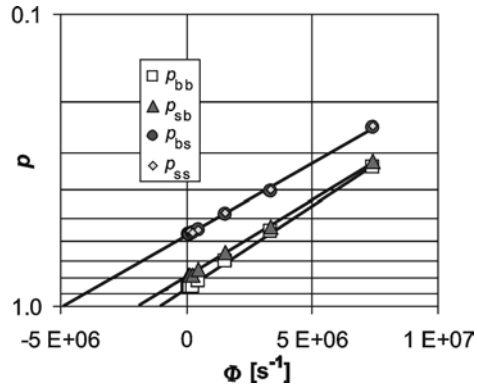

Figure 6.2. Formation probabilities of streamer versus the flux of ions Φ. v = 3.7 m/s; f = 1000 Hz.
Gap 3: U_{DC} = 4.25 kV; U_{AC} = 1.41 kV; Δt_{bp} = 16 μs.

In figure 6.2, the formation probabilities p_{bb}, p_{bs}, p_{sb} and p_{ss} of streamer in Gap 3 are plotted in the semilogarithmic scale versus the flux Φ. One can see that experimental points actually fall on straight lines, but these lines are not going through the axes origin (p = 1; Φ = 0). The intersection of trendline and Φ-axis is farther from zero if during the previous AC cycle arised a streamer. In paper [V], it is shown that the distance between that intersection point and axes origin increases with the point electrode diameter (see figure 2 in [V]) and AC frequency (see figure 3 in [V]).

In figure 6.3, the formation probabilities p_{bb}, p_{bs}, p_{sb} and p_{ss} of streamer are plotted in the semilogarithmic scale versus time interval Δt_{bp} (varied by changing the amplitude of the AC voltage; AC frequency is kept constant). One can see that experimental points fall on straight lines, but non of those lines goes through the axes origin (p = 1; Δt_{bp} = 0). The intersection points of the straight lines with abscissa are shifted about 12 μs from the axes origin.

In figure 6.4 the formation probabilities, p_{bb}, p_{bs}, p_{sb} and p_{ss}, of streamer are plotted in the semilogarithmic scale versus time interval Δt_{bp} (varied by changing the frequency of the AC voltage; U_{AC} is kept constant). One can see that the experimental values of p_{sb} and p_{ss} do not fall on straight lines at small values of Δt_{bp} which correspond to high values of AC frequency. The formation probability even decreases with decrease in Δt_{bp}.

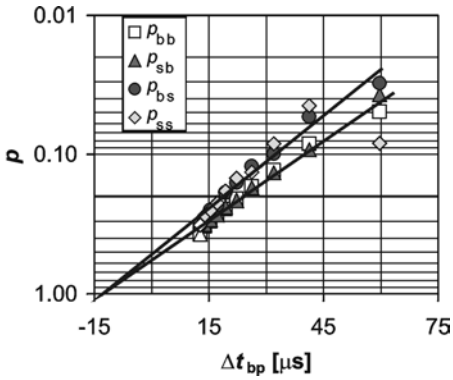

Figure 6.3. Formation probabilities of streamer versus Δt_{bp} varied by changing the amplitude of the AC voltage. f = 1000 Hz; v = 3.7 m/s; $\Phi = 7.4 \cdot 10^6$ s^{-1}. Gap 3: U_{DC} = 4.31 kV. U_{AC} = 0.45 – 1.79 kV.

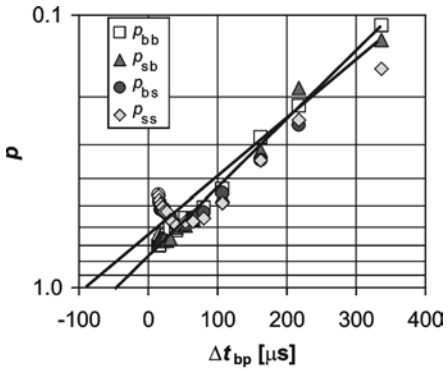

Figure 6.4. Formation probabilities of streamer versus Δt_{bp} varied by changing the frequency of the AC voltage. v = 3.7 m/s; $\Phi = 1.5 \cdot 10^6$ s^{-1}. Gap 3: U_{DC} = 4.25 kV; U_{AC} = 1.40 kV. f = 50 – 1100 Hz.

6.2.2 Discussion

Many authors have reported that a previous discharge pulse may have an after-effect on the formation and development of the next one [Berger *et al*, 1972; Berger, 1974; Waters, 1978; M & A Goldman, 1978; Gosho, 1981 and 1982]. In the case of the streamer counter, this after-effect may be caused by additional ions generated by previous streamers and/or previous glow corona. The difference between probabilities p_{bs}, p_{sb} and p_{bb} indicates, that the formation probability of a discharge depends on the type of the discharge during the previous and antepenultimate AC cycle. This fact confirms that the discharge has an after-effect.

The possible presence of the after-effect of a discharge can explain also the behaviour of the curves presented in figures 6.2 – 6.4. If there exists an after-effect of a discharge, the plots $-\ln(p) = F_f(\Phi)$ have not to go through the axes origin. However, if the after-effect is independent of Φ, the plots should still represent straight lines. The plots $-\ln(p) = F_t(\Delta t_{bp})$ should represent straight

lines, which are going through the axes origin, only in the case when the magnitude of the after-effect is independent of Δt_{bp}.

Therefore, the rough statistical model of the streamer formation, presented in section 5, needs improvement. We need to derive the equations, which will describe the formation probability of a streamer also in the presence of the after-effect.

6.3 Improvement of the statistical model

In general, we are not justified to use the equation (5.8), if there exists an after-effect of previous discharges. In this section we show, that after some modification, we still can use the equation (5.8) even if the after-effect is present.

The total flux of ions Φ_T in equation (5.8) can be written as a sum of flux components: $\Phi_T = \Phi_0 + \Phi_{ps} + \Phi_{as} + \ldots + \Phi_{pg} + \Phi_{ag} + \ldots$, where Φ_0 denotes the flux component caused by an external ionizer. $\Phi_{ps}, \Phi_{as}, \ldots$ are the fluxes of residual ions caused by the streamer at previous, antepenultimate, etc. AC cycle. Analogically, $\Phi_{pg}, \Phi_{ag}, \ldots$ are the fluxes of residual ions caused by the glow corona at previous, antepenultimate, etc. AC cycle. The number of AC cycles necessary to be taken into account depends on the magnitude of $\Phi_{ps}, \Phi_{as}, \ldots$ and $\Phi_{pg}, \Phi_{ag}, \ldots$ and on the accuracy required in calculations. In the following discussion we take into account Φ_{ps}, Φ_{as} and $\Phi_g = \Phi_{pg}$.

As a first approximation, we suppose that the ions of each flux component have the same age, whereas the ions of different flux components may have different ages. The probability that a single negative ion initiates a burst pulse may be therefore different for the different components of the ion flux. Let b_0, b_{ps}, b_{as} and b_g denote these probabilities for the ions in the corresponding flux components $\Phi_0, \Phi_{ps}, \Phi_{as}$ and Φ_g, respectively.

Now formula (5.8) can be rewritten for the formation probability of a streamer during a particular AC cycle depending on the type of a discharge during the preceding AC cycles. For an AC cycle preceded by two consecutive AC cycles with glow corona without any streamer we can write:

$$p_{bb} = \exp\left(-\Delta t_{bp}\left(\Phi_0 b_0 + \Phi_g b_g\right)\right). \tag{6.1}$$

If a streamer and accompanying glow corona arise during the antepenultimate AC cycle, and the glow corona without any streamer arises during the previous cycle, then we can write

$$p_{sb} = \exp\left(-\Delta t_{bp}\left(\Phi_0 b_0 + \Phi_{as} b_{as} + \Phi_g b_g\right)\right). \tag{6.2}$$

If the glow corona without any streamer arises during the antepenultimate cycle and a streamer with accompanying glow corona arises during the previous AC cycle, we can write

$$p_{\mathrm{bs}} = \exp\left(-\Delta t_{\mathrm{bp}}\left(\Phi_0 b_0 + \Phi_{\mathrm{ps}} b_{\mathrm{ps}} + \Phi_{\mathrm{g}} b_{\mathrm{g}}\right)\right). \tag{6.3}$$

For an AC cycle preceded by two consecutive AC cycles with streamer and accompanying glow corona we can write

$$p_{\mathrm{ss}} = \exp\left(-\Delta t_{\mathrm{bp}}\left(\Phi_0 b_0 + \Phi_{\mathrm{ps}} b_{\mathrm{ps}} + \Phi_{\mathrm{as}} b_{\mathrm{as}} + \Phi_{\mathrm{g}} b_{\mathrm{g}}\right)\right). \tag{6.4}$$

If we take into account only these AC cycles that are preceded by the cycle with a certain type of discharge, then for short time intervals Δt_{bp} of these cycles the total flux $\Phi_{\mathrm{T}} = \Phi_0 + \Phi_{\text{after-effect}}$ can be considered to be without any pattern. Thus, the assumption is fulfilled that arrival of ions in the birth region of burst pulses is random and independent of arrival of other ions. This justifies the use of Poisson's distribution for arrival moments of those ions and allows us to use equation (5.8) for calculation of the formation probability of a streamer even in the presence of the after-effect.

If we neglect also the after-effect of antepenultimate streamer, the average formation probability of streamer p can be calculated according to equation [II]:

$$p = \frac{p_{\mathrm{bb}}}{1-\left(p_{\mathrm{bs}} - p_{\mathrm{bb}}\right)} = \frac{\exp\left[-\Delta t_{\mathrm{bp}}\left(\Phi_0 b_0 + \Phi_{\mathrm{g}} b_{\mathrm{g}}\right)\right]}{1-\exp\left[-\Delta t_{\mathrm{bp}}\left(\Phi_0 b_0 + \Phi_{\mathrm{g}} b_{\mathrm{g}} + \Phi_{\mathrm{ps}} b_{\mathrm{ps}}\right)\right] + \exp\left[-\Delta t_{\mathrm{bp}}\left(\Phi_0 b_0 + \Phi_{\mathrm{g}} b_{\mathrm{g}}\right)\right]}. \tag{6.5}$$

This equation was used for calculation of curves of the improved model presented in figures 5.1 – 5.5. The values of b_0 and $b_{\mathrm{g}}\,\Phi_{\mathrm{g}}$ were obtained from equation (6.6) by the "method of straight lines" presented in next section. $b_{\mathrm{ps}}\,\Phi_{\mathrm{ps}}$ was calculated according to equation (6.10). The curves that are calculated according to equation (6.5) fit the experimental points considerably better than the curves calculated according to equation (5.8).

6.4 Detection of the after-effect of a discharge by the "method of straight lines". Initiation probability of burst pulses.

The formulae (6.1) – (6.4) can be presented in the following way:

$$\frac{-\ln(p_{\mathrm{bb}})}{\Delta t_{\mathrm{bp}}} = \Phi_0 b_0 + \Phi_{\mathrm{g}} b_{\mathrm{g}}, \tag{6.6}$$

$$\frac{-\ln(p_{\mathrm{bs}})}{\Delta t_{\mathrm{bp}}} = \Phi_0 b_0 + \left(\Phi_{\mathrm{ps}} b_{\mathrm{ps}} + \Phi_{\mathrm{g}} b_{\mathrm{g}}\right), \tag{6.7}$$

$$\frac{-\ln(p_{sb})}{\Delta t_{bp}} = \Phi_0 b_0 + \left(\Phi_{as} b_{as} + \Phi_g b_g\right), \tag{6.8}$$

$$\frac{-\ln(p_{ss})}{\Delta t_{bp}} = \Phi_0 b_0 + \left(\Phi_{ps} b_{ps} + \Phi_{as} b_{as} + \Phi_g b_g\right). \tag{6.9}$$

According to these formulae, the plots $-\ln(p_{bb}) / \Delta t_{bp} = F_{bb}(\Phi_0)$, $-\ln(p_{bs}) / \Delta t_{bp} = F_{bs}(\Phi_0)$, $-\ln(p_{sb}) / \Delta t_{bp} = F_{sb}(\Phi_0)$ and $-\ln(p_{ss}) / \Delta t_{bp} = F_{ss}(\Phi_0)$ should represent straight lines on the assumption that the intensity of the after-effect is independent of Φ_0. The slope of these lines is equal to the probability b_0 that a burst pulse will be initiated by a single negative ion. The intercept with ordinate-axis gives us $\Phi_g b_g$, $\Phi_{as} b_{as} + \Phi_g b_g$, $\Phi_{ps} b_{ps} + \Phi_g b_g$ or $\Phi_{ps} b_{ps} + \Phi_{as} b_{as} + \Phi_g b_g$ respectively. Those products Φb can be considered as quantitative measure of the after-effect [II], as they represent the effective supplementary ion fluxes. According to our oscilloscopic study (see section 4.2), the intensity of the glow corona is approximately the same both after a burst pulse and after a streamer. The after-effect of the glow corona, if it exists, should therefore be present during each AC cycle in equal measure independent of streamers. Substituting the value of $\Phi_g b_g$ from $\Phi_{ps} b_{ps} + \Phi_g b_g$ and $\Phi_{as} b_{as} + \Phi_g b_g$, we will get the effective after-effect of previous and antepenultimate streamer, respectively.

The similar curves like presented in figure 6.2, but with Φ_0 on the abscissa, are recorded for diverse values of airflow velocity v, DC voltage U_{DC}, frequency f and amplitude U_{AC} of the AC voltage. The co-ordinates of intersection of trendlines and abscissa are determined. From those co-ordinates, the quantitative characteristic Φb of the after-effect is calculated and presented in figures 6.5a – 6.8a. The slopes of those trendlines, representing the initiation probability b_0 of burst pulses, are presented in figures 6.10 – 6.13.

6.5 The after-effect of a streamer determined in "single-point measurements"

The after-effect of discharge can be calculated also on the bases of "single-point measurements" [II], that is, calculated using only one and no more preionization level during the measurements. In paper [II], a method for measurement of the after-effect of the previous streamer is presented. The after-effect of the antepenultimate streamer is neglected there. In this section, we extend the method, presented in paper [II], for the measurement of the after-effect of glow corona and antepenultimate streamer. It follows from formulae (6.1 – 6.3) that

$$\Phi_{ps} b_{ps} = \frac{1}{\Delta t_{bp}} \ln\left(\frac{p_{bb}}{p_{bs}}\right), \tag{6.10}$$

$$\Phi_{as} b_{as} = \frac{1}{\Delta t_{bp}} \ln\left(\frac{p_{bb}}{p_{sb}}\right), \tag{6.11}$$

$$\Phi_{g} b_{g} = \frac{1}{\Delta t_{bp}} \ln\left(\frac{1}{p_{bb}}\right) - \Phi_0 b_0 . \tag{6.12}$$

In the similar way, equations (6.2) and (6.4) give

$$\Phi_{ps} b_{ps} = \frac{1}{\Delta t_{bp}} \ln\left(\frac{p_{sb}}{p_{ss}}\right).$$

To use the equation (6.12) for a measurement of the after-effect of the glow corona, we have to know the formation probability of a burst pulse b_0, but it is not always known. At very low level of artificial preionization, the last term in equation (6.12) can be neglected and so the complications due to unknown b_0 can be avoided. However, the discharge inception during every AC cycle must still be warranted, in this case by the after-effect.

6.6 Experimental results

6.6.1 The after-effect

Quantitative characteristics of the after-effect Φb, calculated by the method of straight lines, are presented for gap 3 in figures 6.5a – 6.8a. The A-type uncertainty at confidence level of 95% is also indicated. For comparison, figures 6.5b – 6.8b and 6.9 present the results of the single-point measurement of the after-effect. Here, the after-effects of a streamer ($\Phi_{ps} b_{ps}$ and $\Phi_{as} b_{as}$) are measured at the high preionization level, the after-effect of glow corona ($\Phi_g b_g$) in conditions where the preionization level is close to zero.

Figure 6.5 shows how the after-effect of previous discharges depends on the airflow velocity, v. An increase in the airflow rate weakens the after-effect of both the streamer and the glow corona. The both measurement methods of the magnitude of the after-effect give here the results close to each other.

In figure 6.6, $\Phi_{ps} b_{ps}$, $\Phi_{as} b_{as}$ and $\Phi_g b_g$ are presented as functions of the frequency of the AC voltage. The after-effect of both previous and antepenultimate streamer and that of the glow corona intensify with an increase in the AC frequency.

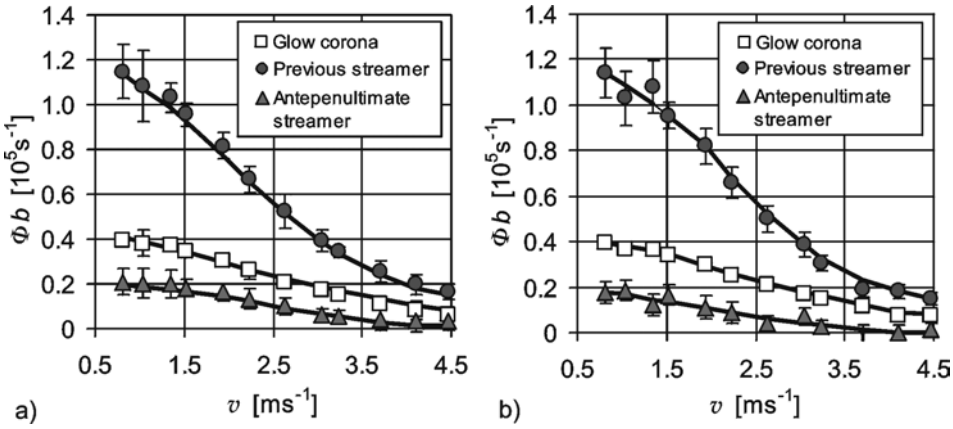

Figure 6.5. After-effect of a discharge versus the airflow rate. (a) method of straight lines (b) single-point measurements. f = 1000 Hz; Gap 3: U_{DC} = 4.27 kV, U_{AC} = 1.52 kV.

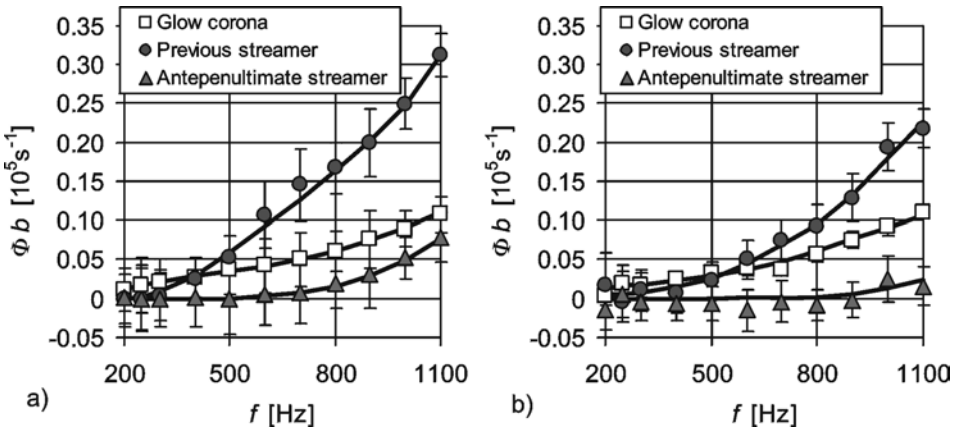

Figure 6.6. After-effect of a discharge versus the AC frequency. (a) method of straight lines (b) single-point measurements. v = 3.7 m/s; Gap 3: U_{DC} = 4.25 kV; U_{AC} = 1.41 kV.

In figure 6.7, the effective ion fluxes $\Phi_{ps} b_{ps}$, $\Phi_{as} b_{as}$ and $\Phi_g b_g$ are presented as functions of the AC voltage. The after-effect of the previous streamer calculated using the results of the single-point measurement is independent of the AC voltage within the limits of the experimental uncertainty. The after-effect of the previous streamer calculated using the method of straight lines increases with amplitude of the AC voltage. The after-effect of the antepenultimate streamer remains independent of the amplitude of the AC voltage. The intensity of the after-effect of the glow corona increases with the AC voltage.

Figures 6.6 – 6.7 indicate that the after-effect of a streamer calculated by the method of straight lines is stronger than the after-effect calculated from results

of a single-point measurement. The after-effect of the glow corona is in both cases in uncertainty limits the same.

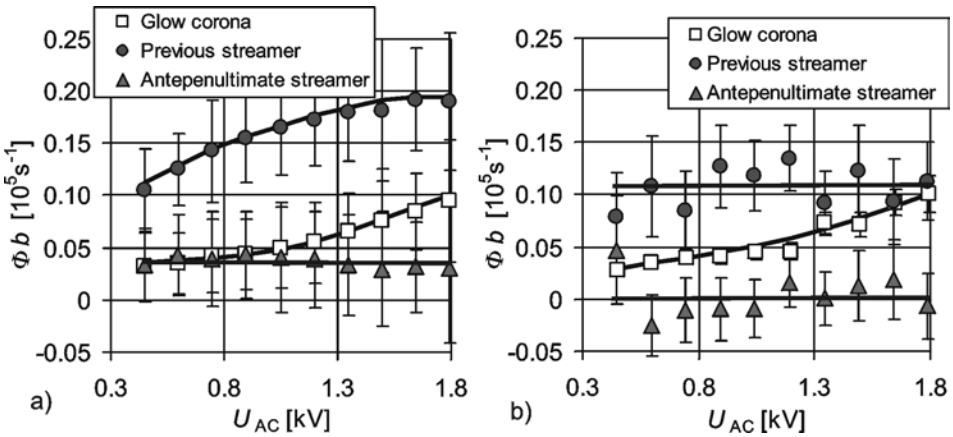

Figure 6.7. After-effect of a discharge versus the AC voltage. (a) method of straight lines (b) single-point measurements. v = 3.7 m/s, f = 1000 Hz; Gap 3: U_{DC} = 4.33 kV.

Figure 6.8 indicates that an increase in the DC voltage decreases the after-effect of both previous and antepenultimate streamer. The after-effect of the glow corona remains almost independent of the DC voltage.

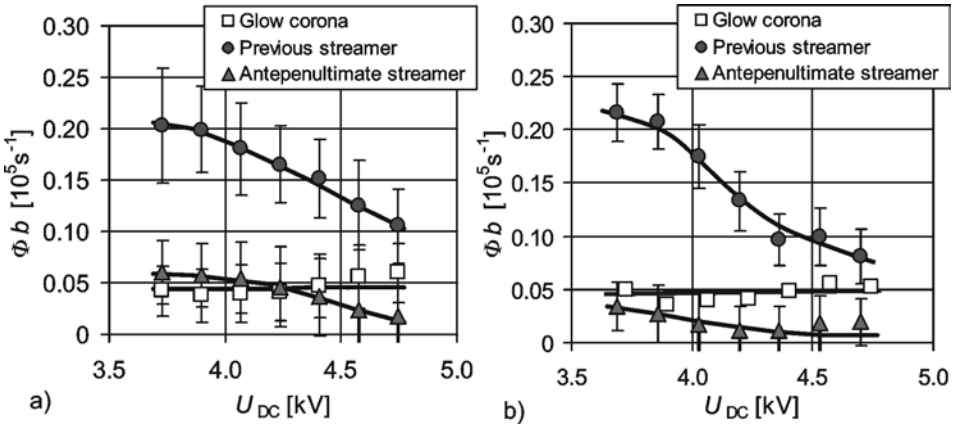

Figure 6.8. After-effect of a discharge versus the DC voltage. (a) method of straight lines (b) single-point measurements. v = 3.7 m/s, f = 1000 Hz; Gap 3: U_{AC} = 0.90 kV.

At airflow rate v = 1.4 m/s, the changes in preionization level have no influence on the intensity of the after-effect caused by a streamer [II]. Figure 6.9 indicates that at airflow rate v = 3.67 m/s, the after-effect of a streamer decreases with an increase of Φ_0. The after-effect of the glow corona can be considered in uncertainty limits independent of preionization level. The values of the after-effect

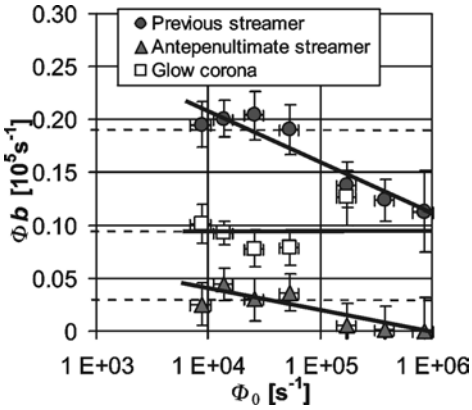

Figure 6.9. After-effect of a discharge versus Φ_0. v = 3.7 m/s, f = 1000 Hz; Gap 3: U_{DC} = 4.33 kV; U_{AC} = 1.80 kV.

calculated using the method of straight lines are indicated in the same figure by dashed lines.

Figure 8 in paper [II] demonstrates that the after-effect of a streamer weakens with an increase in the concentration of water vapour. The same happens with the after-effect of the glow corona.

6.6.2 Initiation probability of burst pulses

Figures below represent the initiation probability of burst pulses depending on the airflow velocity v, on frequency f and amplitude U_{AC} of the AC voltage and on DC voltage U_{DC}. The A-type uncertainty is presented at confidence level of 95%. One can see that the initiation probability b_0 of a burst pulse increases with airflow velocity (figure 6.10) as far as $v \leq 3$ m s^{-1}. Thereafter it decreases a bit.

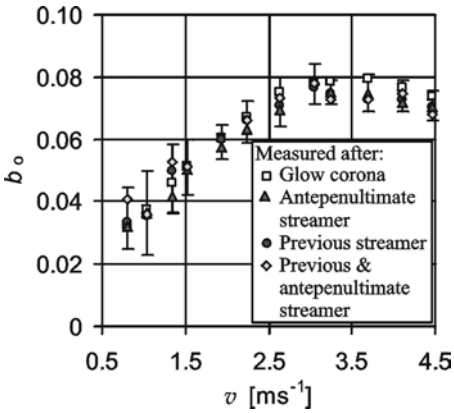

Figure 6.10. Initiation probability of burst pulses b_0 versus airflow velocity. f = 1000 Hz; Gap 3: U_{DC} = 4.27 kV, U_{AC} = 1.52 kV.

The initiation probability b_0 of a burst pulse increases with frequency (figure 6.11) and amplitude (figure 6.12) of the AC voltage. The dependence of b_0 on DC voltage is shown in figure 6.13. One can see that b_0 decreases with an increase in the DC voltage. The experimental points, recorded both after AC cycles with streamer and after AC cycles without streamer, coincide in the limits of the experimental uncertainty.

In figure 6.14, the same initiation probabilities of burst pulses already shown in figures 6.11 – 6.13 are presented versus the time interval Δt_{bp}.

Changes in the DC voltage, AC frequency and amplitude change that time interval. One can see that within the accuracy of 25% all experimental points can be approximated by the same trendline.

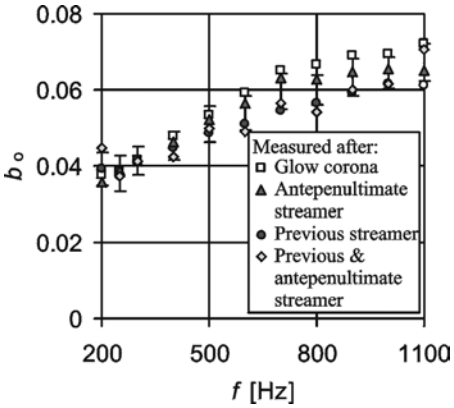

Figure 6.11. Initiation probability of burst pulses b_0 depending on the frequency of the AC voltage. v = 3.7 m/s; Gap 3: U_{DC} = 4.25 kV; U_{AC} = 1.41 kV.

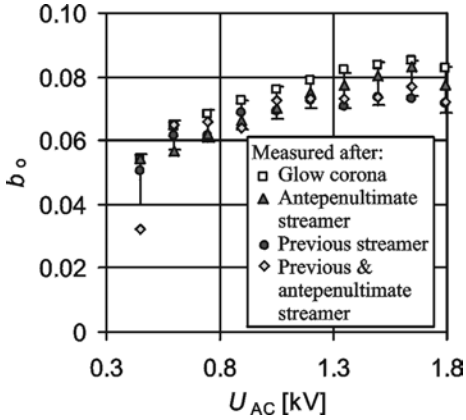

Figure 6.12. Initiation probability of burst pulses b_0 depending on the amplitude of the AC voltage. v = 3.7 m/s, f = 1000 Hz; Gap 3: U_{DC} = 4.33 kV.

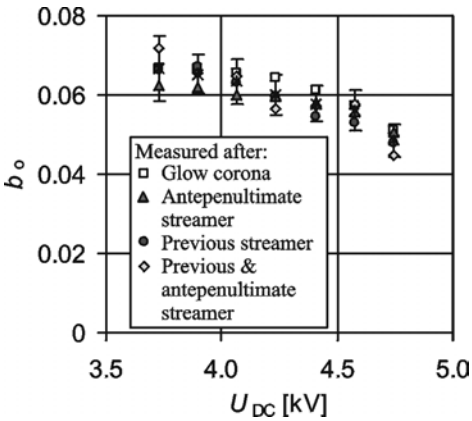

Figure 6.13. Initiation probability of burst pulses b_0 versus DC voltage. v = 3.7 m/s, f = 1000 Hz; Gap 3: U_{AC} = 0.90 kV.

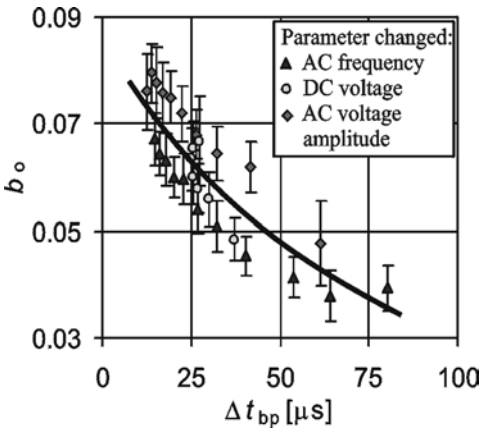

Figure 6.14. Initiation probability of a burst pulse versus time interval Δt_{bp}.

6.7 Discussion of results obtained about b_0 and the after-effect of a discharge

Figure 6.5 indicates that all investigated after-effects decrease with an increase in the airflow rate. It is understandable as the removal of residual products increases with the airflow rate.

From figure 6.6 one can see that the after-effect increases with the AC frequency. The increase is understandable because the higher is the AC frequency the shorter is the removal time of additional ions before the beginning of the discharge formation at the next AC cycle.

Figure 6.8 shows that the after-effect of a streamer decreases with an increase in the DC voltage. That effect can be explained as follows. At a higher DC voltage, the streamers arise still mostly in the time interval Δt_{str}. The time interval between streamers remains approximately the same, equal to the AC period. The streamers arise at the same value of the resultant voltage as at lower values of the DC voltage and the average amplitude of streamers remains unchanged. As the average electric field strength during the AC cycle is higher, the ions generated by a streamer can be removed faster. Higher electric field could remove faster also the ions generated by the glow corona, however, two other effects counteract to that. First, the mean current of the glow corona increases with DC voltage (see section 4.2), and the after-effect increases with the discharge mean current. Second, the time intervals between the end of the glow corona of the previous AC cycle and ignition of a new discharge at the test cycle shortens, which could also increase the after-effect of the glow corona. As a result, last two effects compensate the first one, and the after-effect of the glow corona remains almost independent of DC voltage.

Figure 6.9 indicates that the after-effect of a streamer might depend on the preionization level. The preionization level determines the spread of the time lags of the streamer formation; thus, it determines also the instantaneous voltage at which the streamer will be formed. The mean amplitude of streamer current pulses increases with the applied voltage [Allen and Boutlendj, 1993]. Therefore, the higher is the instantaneous resultant voltage U, the longer are the streamer channels and the higher is the streamer current. The time interval for removing the residual products generated by a streamer is the shorter the later the streamer is formed. Thus, the after-effect of streamer might increase with decrease in the preionization level (figure 6.9).

Our method of straight lines uses measurement points recorded both at high and low preionization level. At low preionization level the streamers are formed considerably later and have a stronger after-effect than at high preionization level. As a result, the magnitude of the after-effect of a streamer calculated by the method of straight lines might be higher. This can be seen in figures 6.6 – 6.7 where the method of straight lines gives us systematically higher results

than the method of single-point measurements at high preionization level. Two different methods of determination of the after-effect give the same result in the case presented in figure 6.5.

Figure 6.7 shows that the after-effect of the glow corona increases with the AC voltage. The oscilloscopic observations showed that the intensity of the glow corona increases with the AC voltage. In addition, during the negative half cycles, the electric field strength decreases with an increase in the AC voltage. Those details can be the reason for an increase in the corresponding after-effect. The after-effect of streamers calculated from results of a single-point measurement is independent of the AC voltage under conditions given in caption of figure 6.7. That one calculated according to the method of straight lines increases. That increase may be caused by the fact that at low preionization level the streamers arise later, well above the onset voltage of streamers. The instantaneous voltage at the inception moment of late streamer is the higher the higher is the increase rate of the resultant voltage. As the increase rate of the resultant voltage increases with the AC voltage, the magnitude of the after-effect of streamers, calculated according to equation (6.7), also increases. At high preionization level or high level of the after-effect, the after-effect of a streamer remains independent of the AC voltage.

Figure 8 in paper [II] indicates that the after-effect of a streamer decreases with an increase in air humidity. The same happens with the after-effect of the glow corona. Due to humidity in air, absorption of the photoionizing radiation increases [Loeb, 1965]. Our numerical estimations show that the number density of photoions increases near the streamer channel and glow region but decreases in that layer where the ions responsible for the after-effect are produced [II]. Humidity causes also a marked decrease in the length and the charge of a streamer [Loeb, 1965], which in its turn reduces the number density of photoions. Moreover, in moist air, the electron detachment from complex ions is less probable [Gallimberti, 1979]. The probability b_0 of initiation of a burst pulse by a residual complex photoion decreases. As a result, the after-effect of a streamer will decrease in moist air [II].

Figures 6.5 – 6.9 show that in general the after-effect of a streamer is higher than that of the glow corona. Figures 5 – 8 in paper [II] and figures 2 – 3 in paper [V] show that the after-effect increases with the point diameter. This effect can be explained by an increase in the discharge current with the point diameter.

The ion composition depends on the ion age [Salm, 1993]. In our experimental device, the velocity of the airflow determines the age of those ions, which are created by the ionizing radiation of the α-source. The higher is the airflow rate, the younger are the ions reaching the discharge gap. Thus, the initiation probability of burst pulses can depend on the magnitude of the airflow rate (figure 6.10).

The physical reason(s) for dependence of b_0 on Δt_{bp} (see figure 6.14) are still unclear for us and they need further investigation. One reason might be the systematic uncertainty in determination of Δt_{bp} by equation (5.9). This systematic uncertainty is caused by inexact determination of onset voltages and by neglecting the effect of overlapping of voltage regions of burst pulses and streamers.

Lowke [1991] is of the opinion that streamers produce metastable particles, which increase the probability of electron detachment from negative ions. If those metastable particles will be present in the birth region of burst pulses during Δt_{bp}, they should favour the destruction of negative ions formed due to the α-source. Consequently, the metastable particles increase the formation probability b_0 of burst pulses and b_0 can not be considered independent of f, U_{AC} and U_{DC} any more. After an AC cycle with a streamer that effect should be more pronounced than after an AC cycles without a streamer. Our experiment shows that this is not a case — b_0 is independent of the type of the discharge during the preceding AC cycle. Thus we conclude that in our experiments the metastable particles generated by a streamer have no detectable influence on the magnitude of the after-effect.

Gosho [1981 and 1982] explains the appearance of an after-effect by the production of nitrous oxides in the corona. Figure 8.7 in chapter 8 indicates that an increase in concentration of NO_x increases the formation probability of a streamer. In contrary, the experimental results presented in this chapter indicate that the after-effect decreases the formation probability of a streamer. Thus we conclude that in our experiments the production of nitrous oxides is not the main cause of the after-effect.

According to the discussion presented above, it remains to suppose that the detected after-effect is caused by negative ions. The possible mechanisms of production of those ions will be discussed in section 6.10.

6.8 Comparison of two proposed methods for detection of the after-effect of a discharge

In general, the after-effect of a streamer calculated according to the method of straight lines is higher than that calculated from the results of single-point measurement. This might be caused by the fact that the assumption about independence of the after-effect of the preionization level is not always correct for streamers (see figure 6.9). Under certain conditions, the spread of time lags of the streamer formation may increase with a decrease in Φ_0. As a result, the after-effect of a streamer may increase too (figure 6.9).

The method of straight lines and the method of single-point measurement give similar results for the after-effect of the glow corona.

The method of single-point measurement has an advantage in comparison with the method of straight lines: the calculated after-effect is independent of the measurement quality of the preionization level. In addition, we don't have to know the form of ion trajectories inside the detector gap. Thus, the measurement procedure is much more convenient and there is no need to change the preionization level during the measurements. However, during the measurement of the after-effect of streamers, the preionization level has to be high enough to warrant the inception of most streamers at a resultant voltage close to U_{str}. Otherwise the assumption, that the intensity of the after-effect of the glow corona is the same both after a burst pulse and after a streamer, is incorrect. Another possibility to eliminate the effect of the delayed streamers, valid for both methods, is to modify the computer program so that only those AC cycles will be taken into account, where a streamer appears at the voltage close to U_{str}.

Measurement of the after-effect of the glow corona is possible by the single point method, if the preionization level is close to zero or we know the value of Φ_0 and the initiation probability of burst pulses.

Possibility to estimate also the initiation probability of burst pulses is an advantage of the method of straight lines.

6.9 Modelling of ion trajectories in the streamer counter

6.9.1 Calculation of the electric field strength

The mechanism of discharge inception in conditions of the combined voltage and the background of those ions that supply the seed electrons are understood incompletely. We try to clear up some problems by modelling the ion trajectories in our discharge gaps. In numerical two-dimensional (three-dimensional axis-symmetric) calculations, the motion of ions is evaluated as a resultant drift caused by both the electric field and the air flux. The distribution of the Laplacian electric field is computed by the finite difference method. The successive over-relaxation method [Zhou, 1993] is used in first iterations. Gauss-Seidel iterative condition [Zhou, 1993] is used to obtain the final results.

The rectangular computation region is taken a little larger than the discharge gap. On the open boundaries, the potential $U = 0$ V is considered except the boundary, perpendicular to the gap axis behind the point, where the potential distribution is considered to be the same as that between infinite coaxial cylinders. On the gap axis, the condition of symmetry [Serdyuk *et al*, 2001] is used. The computation domain is divided first into a uniform square grid having 40 nodes per millimetre. In the vicinity of the point electrode, additional iterations are made. That domain is divided into a square grid having maximally 3200 nodes per millimetre. For the convergence criterion of the iterations is

taken the requirement that the relative residual in the iterative process should not exceed 10^{-12} at each interior node.

The air flux is taken into account as an additional electric field $\vec{E}_a(r) = \vec{v}(r)/\mu$, where $\vec{v}(r)$ is the vector of the airflow velocity and μ is the mobility of ions [II]. Computations are carried out on the assumption that the mobility of negative ions $\mu = 2$ cm^2(Vs)$^{-1}$ [II]. The airflow profile inside the signal electrode is calculated according to the empirical power-law equation

$$v(r) = v(0)\left(1 - \frac{r}{R_0}\right)^{\frac{1}{1.66\log(\mathrm{Re})}},$$

where r is a radial co-ordinate, R_0 is the co-ordinate of the wall of the signal electrode, $v(r)$ is the airflow velocity at point r, and Re is the Reynolds number [Miller, 1989]. In our experiments and calculations, Re ranges from 275 – 6950.

The accuracy of the computing algorithm was tested by the numerical evaluation of the well-known field distributions of coaxial cylinders and concentric spheres. The difference between analytical and numerical results was less than 0.5%.

It is impossible to obtain an exact analytical solution for the electric field distribution in our discharge gaps. In numerical calculation of the electric field strength we use the Deutsch approximation, which assumes that the electric field direction is unaffected by the corona space charge and remains Laplacian in shape [Bouziane *et al*, 1997]. Thus, in absence of the airflow, the ion drift trajectories will coincide with these lines. The magnitude of the electric field, however, can in general be affected by the corona space charge [Bouziane *et al*, 1994]. Thus, the space charge can affect the drift trajectories provided the electric field and the air flux act simultaneously. However, in our case, those trajectories remain unaffected near the point electrode even in the presence of the airflow, as the drift due to the electric field prevails there. Far from the point, the drift due to the airflow prevails.

6.9.2 Demarcation of the birth region of burst pulses

At the onset of burst pulses only these avalanches, which develop close to the axis of the discharge gap, can launch the burst pulses. The size (number of electrons) of those avalanches is considered critical [II]. According to our calculations, the critical avalanche consists of $(1.1 – 2.9)\cdot 10^4$ electrons depending on the point diameter [II]. An increase in the point diameter decreases the size of the critical avalanche [II]. The data for ionization coefficient, used in our calculations, are taken from the survey [Dutton, 1975].

For comparison, the mean size of $2.7 \cdot 10^4$ electrons is proposed in literature for the critical avalanche [Loeb, 1965].

Once the onset voltage of burst pulses is exceeded, also the off-axis electrons can launch the burst pulses [II]. We denote the radial distance between the gap axis and the utmost lateral start position of a critical avalanche with r_c. It characterizes the lateral expansion of the birth region of burst pulses at a given voltage. In the present theses, r_c is calculated numerically for the onset voltage of streamers. The ratio $r_c / r_0 \approx 0.68$ for all three gaps [II]. Here r_0 is the radius of the point electrode.

6.9.3 Limiting trajectories of those negative ions which can trigger the discharge

In figure 6.15, the ion trajectories terminating at the lateral boundary of the birth region of burst pulses are presented for those negative ions which reach this boundary at the moment when $U = U_{str}$. The ion trajectories are computed for different velocities of the airflow and are shown in the plane of the gap axis. Calculations reveal that the higher is the airflow rate the closer the limiting trajectories are to the gap axis. At low airflow rate, those trajectories can start even from the signal electrode. If $v > 0.4$ m s^{-1}, the limiting trajectories in all our gaps do not touch the signal electrode any more. The limiting trajectories will be the closer to the gap axes the smaller is the diameter of the point electrode [II].

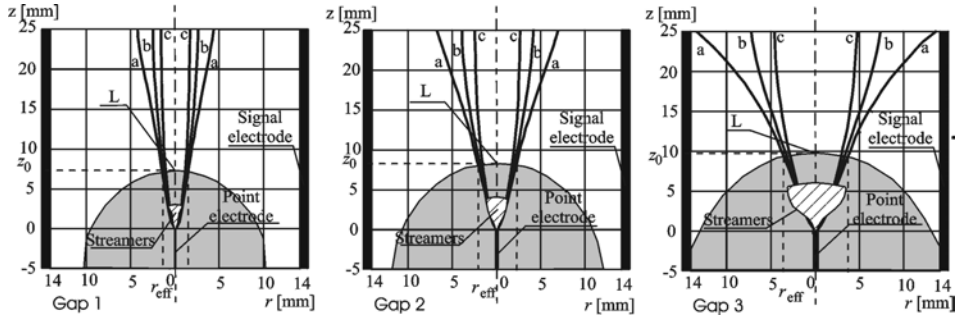

Figure 6.15. Trajectories of ions terminating at the lateral boundary of the birth region of burst pulses. $f = 1000$ Hz; Gap 1: $U_{DC} = 2.47$ kV; $U_{AC} = 0.720$ kV. Gap 2: $U_{DC} = 3.21$ kV; $U_{AC} = 0.950$ kV. Gap 3: $U_{DC} = 4.40$ kV; $U_{AC} = 1.50$ kV.
(a) $v = 0.4$ m s^{-1}; (b) $v = 1.4$ m s^{-1}; (c) $v = 3.6$ m s^{-1}. The grey area presents the space region from which the ions will be collected to the point electrode during the time interval when the discharge is extinguished. $v = 0.4$ m s^{-1}.

Using limiting trajectories of ions and measured intensity of the ion flux Φ at the entrance of the detector gap, we calculate the intensity of the flux Φ_0 of ions reaching the birth region of burst pulses in each discharge gap.

6.9.4 The space region from which the ions will be collected to the point electrode during Δt_{free}

We determine numerically, under the assumptions of our model, the co-ordinates of the space region inside which the negative ions will be collected on the point electrode during the time interval Δt_{free} (see figure 4.1a) when the discharge is extinguished. In figure 6.15, the sectional view of this space region in the plane of the gap axis for $v = 0.4$ m s^{-1} is painted grey. The gap axis intersects the boundary of this space region at $z = z_0$.

Our numerical calculations show that the value of z_0 increases with a decrease in the AC frequency and with an increase in the DC voltage. An ion layer labelled L in figure 6.15 is located between the limiting trajectories immediately beyond that boundary. The thickness of that layer at distance r is $v_i(r)\,\Delta t_{bp}$, where $v_i(r) = v(r) + \mu E(r)$ denotes the velocity of ions in the layer L. The ions of this layer are responsible for the initiation of the burst pulse during the time interval Δt_{bp} at the next AC period. The region occupied by streamer channels is indicated in the same figure. One can see that the length of the streamer is always less than z_0.

6.10 Background of negative ions responsible for the after-effect

Calculation of ion trajectories, presented in section 6.9, enable us to make some conclusion about background of the negative ions responsible for the after-effect.

In principle, the negative ions can arise due to the photoeffect on the wall of the signal electrode and subsequent attachment of the photoelectrons to oxygen molecules [Beattie, 1975; II]. However, the calculation of ion trajectories show that these ions are unable to reach the birth region of burst pulses in our discharge gaps, if the airflow is laminar and the flow rate is higher than 0.4 m s^{-1} (see figure 6.15). Thus, they are unable to participate in the initiation of the discharge.

The negative ions can be born in the streamer channel or glow corona layer. However, the streamer length is about two times less than the extent of the space region inside which the negative ions are collected on the point electrode during the time interval when the discharge is extinguished (in conditions of figure 6.15). Hence, the ions born in the streamer channel are unable to contribute to the after-effect. The same is valid for ions produced in the layer of the glow corona, as the extent of the glow corona layer is by an order of magnitude smaller than the length of streamers.

The negative ions may be produced by the photoionizing radiation of a discharge (streamer or glow corona) [Loeb, 1965; Teich, 1967; Penney and

Hummert, 1970; Morrow, 1997]. The rate of photoionizing radiation was measured experimentally by Teich [1967] and by Penney and Hummert [1970]. The quantitative theory of photoionization is presented by Zheleznyak *et al* [1982] and it is consistent with experimental results of Teich [1967].

We calculated numerically, using the photoionization data obtained by Teich [1967], the flux of those ions, as if the ions were generated by the radiation of a streamer or glow corona only. One example of those calculations is presented in paper [II] for streamers. The calculation shows that the ions produced by the photoionizing radiation can be responsible for the detected after-effect. The calculated flux and the measured one are in close agreement [II]. On the one hand, this result demonstrates that the investigated after-effect of discharges is caused by photoionization. On the other hand, it confirms that the methods proposed in sections 6.4 and 6.5 are suitable for quantitative evaluation of the after-effect [II].

7 GENERATION MECHANISM OF THE PHOTOIONIZING RADIATION IN CORONA DISCHARGES

It is generally accepted that the corona discharge in air generates photoionizing radiation. Concerning the generation mechanism of this photoionizing radiation, two very different opinions exist.

1. The radiation is emitted by gas atoms and/or molecules exited by electron collision. The dominant processes leading in air to photoionization of oxygen molecules are believed to be the excitation of nitrogen molecules to energies of 12.1 – 13.6 eV with subsequent emission of photons [Badaloni and Gallimberti, 1972]; and the dissociation of oxygen molecules with subsequent emission of photons by excited oxygen atoms [Badaloni and Gallimberti, 1972]. To cause the photoionization of oxygen molecules, the energy of those emitted photons has to be above the ionization potential of oxygen molecules (12.1 eV). The ionization potential of nitrogen molecule is higher (13.6 eV); therefore the electron collision processes leading to the excitation of nitrogen to energies above the ionization potential are believed to be less probable.
2. The radiation is generated due to the bombardment of the anode surface by electrons, accelerated in a high electric field near the anode [Akishev *et al*, 1999b, c].

To check the second hypotheses, presented above, Akishev *et al* carried out a simple experiment using a point-to-plane discharge gap where the cathode was replaced by a metal mesh. Close behind the mesh-electrode, they placed the x-ray spectroscopy film wrapped in dense black paper to screen the film from the visible and UV radiation [Akishev *et al*, 1999a, b]. After exposition of the film to the radiation generated by the positive corona and subsequent development, the dark spots were observed on the film around the axis of symmetry of the discharge. Therefore, Akishev *et al* believed that the "bremsstrahlung" from the anode is the most important ionizing agent in a positive corona [Akishev *et al*, 1999a]. In the paper [III], however, we show that the above-described photographic detection of photoionizing radiation is improbable and in similar experiments we were unable to get dark spots on the x-ray spectroscopy film [III]. Moreover, no imprint of the mesh is seen on the photographs published by Akishev *et al*. Evidently, dark spots on the photographs published by Akishev *et al* do not prove the x-ray generation by the corona discharge. The processes causing those spots need further explanation.

To get some additional experimental confirmation for or against the hypothesis of bremsstrahlung, we developed a method for detection of the photoionizing radiation. The method bases on an internal gas discharge counter. Description of the principle of the method and experimental setup used is presented in paper [III]. Dependencies Ψ versus PX are presented in figure 2 of paper [III], where P denotes the gas pressure and Ψ is the number of photoions created in a layer

of unit thickness at distance X from the radiation source, per ionizing collision in the discharge, at unit pressure. One can see that within the limits of experimental uncertainty, Ψ does not depend on the material of the point electrode. The values of Ψ are a little higher in the case of negative corona [III].

If the photoionizing radiation were produced by collision of accelerated electrons with anode surface, at least two characteristic tendencies should appear [III]. First, the intensity of the photoionizing radiation should be the higher the greater is the atomic weight of the material of the anode. Second, the spectral characteristics of the photoionizing radiation should depend on the polarity of the applied voltage. In case of negative corona, the electric field strength near the anode is weak and the electrons are unable to gather the sufficient energy to cause the bremsstrahlung. As a result, the radiation intensity in the negative corona should be less than that in the positive corona. The both above-mentioned tendencies should have an effect on the shape of Ψ versus PX curves. However, like it was seen in figure 2 in paper [III], the radiation intensity was independent of the anode material and, in the contrary of the secondly expected tendency, that intensity was a little higher for negative corona than for positive corona. We conclude that different materials of electrodes or different polarities of the applied voltage cause no significant differences in the generation mechanism of the photoionizing radiation.

As a result we consider that mainly gas molecules and atoms emit the photoionizing radiation in corona discharge, like it was widely accepted before the work of Akishev *et al*. The hypothesis that “the bremsstrahlung from the anode is an important ionizing agent in a positive corona” is not enough confirmed at the moment.

8 FORMATION PROBABILITY OF STREAMER AS A MEASURE OF CONTENT OF ELECTRONEGATIVE TRACE GASES IN AIR

8.1 Dependence of streamer formation probability and amplitude on the concentration of admixtures

Figures below present the streamer formation probability p and average amplitude A of the streamer versus the fractional concentration C of different admixtures. The number of streamers is counted during $\tau = 30$ s at each measurement point. Voltages applied to the point electrodes are given in table II. The frequency f of the AC voltage is 500 Hz. The airflow velocity in the discharge gaps is 3.6 m/s. The ion flux Φ at the inlet of each discharge gap is $6.2 \cdot 10^6$ s^{-1}, the age of ions being approximately 0.12 s. The temperature of the gas is 31ºC.

Table II Applied voltages reduced to the standard conditions and Δt_{bp} for point electrodes used.

Gap number, i	1	2	3
d /mm/	0.13	0.25	0.5
U_{DC} /kV/	2.64	3.44	4.69
U_{AC} /kV/	0.79	1.04	1.61
Δt_{bp} /μs/	25.5	32.2	30.4

Influence of water vapour on the formation probability and average amplitude of streamer is presented in figure 8.1. One can see that the formation probability of a streamer increases and the average amplitude decreases with increasing concentration of water vapour. At the same time, an increase in concentration of water vapour influences neither the width of the voltage region of streamer occurrence nor the position of this region relative to the phase of the AC voltage.

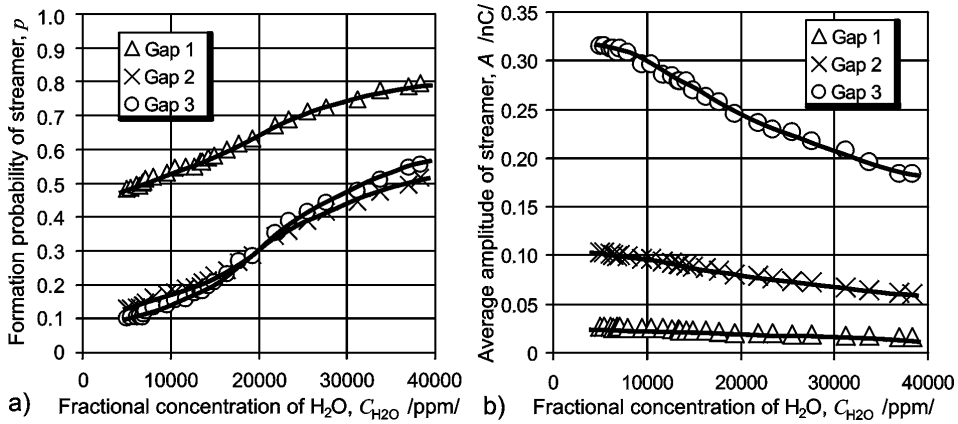

Figure 8.1. Dependence of streamer formation probability and average amplitude on the fractional concentration of water vapour C_{H2O}.

Small amounts of additional carbon dioxide have no influence on the average amplitude of streamers, on the width of the voltage region of streamer occurrence and on the position of this region relative to the phase of the AC voltage. The formation probability of a streamer increases only a little with an increase in the concentration of CO_2 up to 3000 ppm (figure 8.2).

A rise in concentration of CO_2 above 10 000 ppm causes a slight shift of the voltage region of streamer occurrence towards a later phase of the AC voltage. The number of streamers per AC cycle increases over one and the streamers arise on the point electrode all the time the resultant voltage is above U_{str}. The higher is the concentration of CO_2 the more streamers will arise during the same AC cycle. The maximum repetition rate of streamers reaches 50 kHz under the conditions given in caption of figure 10 in paper [I].

Visual observations reveal that a rise in concentration of CO_2 is accompanied by essential changes in the discharge structure. From a certain concentration on, more and more streamers form in zones adjacent to the point tip. Finally the streamers are distributed almost uniformly over the whole hemispherical tip of the electrode [I]. Branching of each streamer seems to be reduced. The burst pulse following a streamer becomes weaker the higher is the repetition rate of the streamers. Finally the specific glow of burst pulses disappears on the point surface almost completely [I]. Beattie [1975] reported a similar result – concentration of CO_2 much less than one percent is sufficient to extinguish the glow.

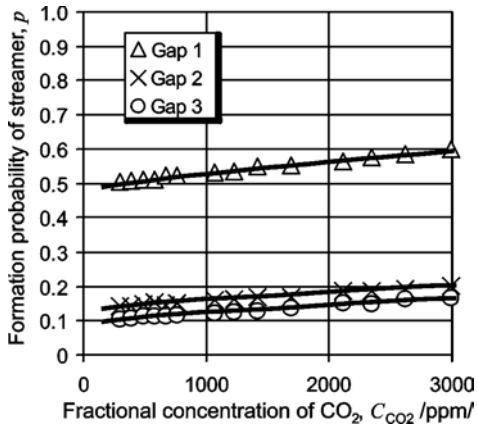

Figure 8.2. Dependence of streamer formation probability on the fractional concentration of CO_2 C_{CO2}. Fractional concentration of H_2O is 6500 ppm.

The number of streamers versus phase angle of the AC voltage is presented in figure 8.3. One can see a number of maximums in each histogram. The first peak has the smallest width; last peaks are wider and cover oneself. The width of the peaks is the narrower the smaller is the point diameter. According to the visual and oscilloscopic observations presented in section 4, the amplitude of streamer increases with point diameter. We can conclude that a streamer prevents the formation of another streamer for a certain time interval and that time interval depends on the amplitude of the streamer – the more powerful the streamer is the later the new streamer will arise. In spite of the difference in initiation moments of streamers, the amplitude of streamers remains unchanged.

An increase in concentration of ozone up to 5 ppm increases the formation probability of streamers. At 5 ppm, the formation probability of a streamer reaches the saturation value (see figure 8.4). The average amplitude of streamers, the width of the voltage region of streamer occurrence and the position of this region relative to the phase of the AC voltage are independent of the concentration of O_3.

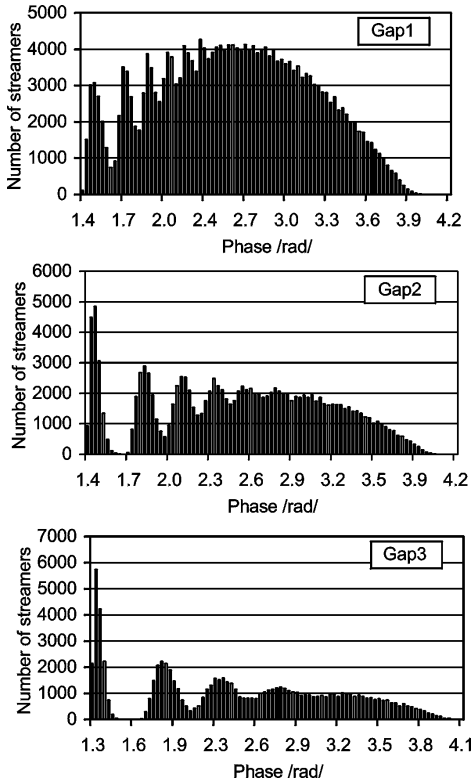

Figure 8.3. Number of streamers versus phase of the combined voltage. C_{CO2} = 28 000 ppm.

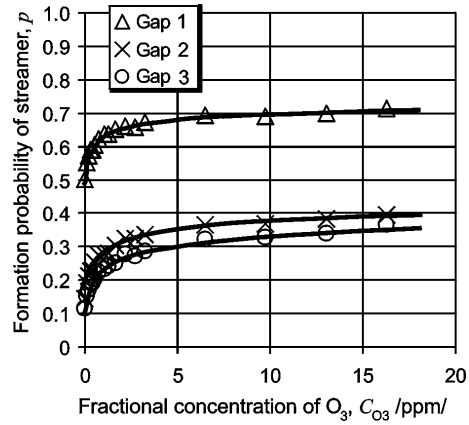

Figure 8.4. Dependence of the streamer formation probability on the fractional concentration of ozone C_{O3}. Fractional concentration of H_2O is 8400 ppm.

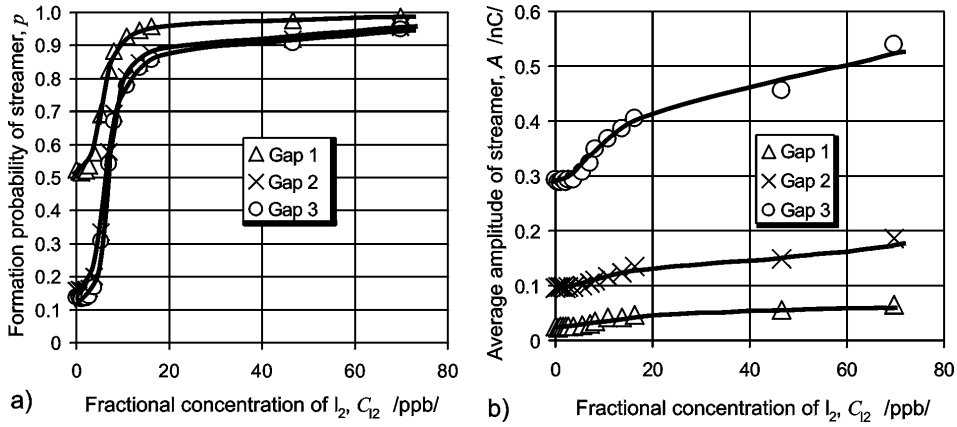

Figure 8.5. Dependence of streamer formation probability and average amplitude on the fractional concentration of iodine C_{I2}. Fractional concentration of H_2O is 8800 ppm.

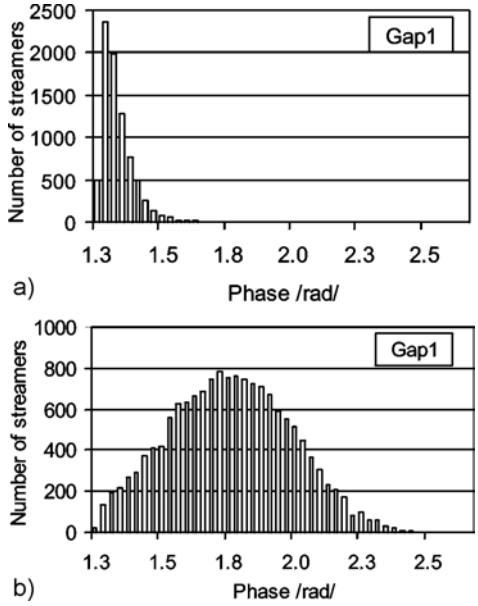

Figure 8.6. Number of streamers versus phase of the combined voltage. (a) C_{I2} = 0 ppb; (b) C_{I2} = 70 ppb.

Influence of iodine on both the formation probability and the average amplitude of streamers is presented in figure 8.5. One can see that the formation probability of a streamer increases remarkably under the influence of iodine and $p \approx 0.95$ in all discharge gaps if $C_{I2} > 30$ ppb. Average amplitude of a streamer increases with the concentration of I_2 as well. The voltage interval of streamers broadens (figure 8.6), at the same time, the voltage region of streamer occurrence starts at the same phase of the AC voltage independent of the amount of the iodine admixture.

$O_3 + NO_x$ has a similar effect on the formation probability and the average amplitude of streamers (see figure 8.7) like iodine does. The formation probability of a streamer increases remarkably — $p \approx 0.9$ in all discharge gaps, if $C_{O3+NOx} > 1$ ppm. Average amplitude of a streamer increases with the concentration of $O_3 + NO_x$ as well. The voltage region of streamer occurrence starts at the same phase of the AC voltage independent of $O_3 + NO_x$ concentration. The width of this voltage region increases two-three times, when C_{O3+NOx} increases from 0 to 1 ppm.

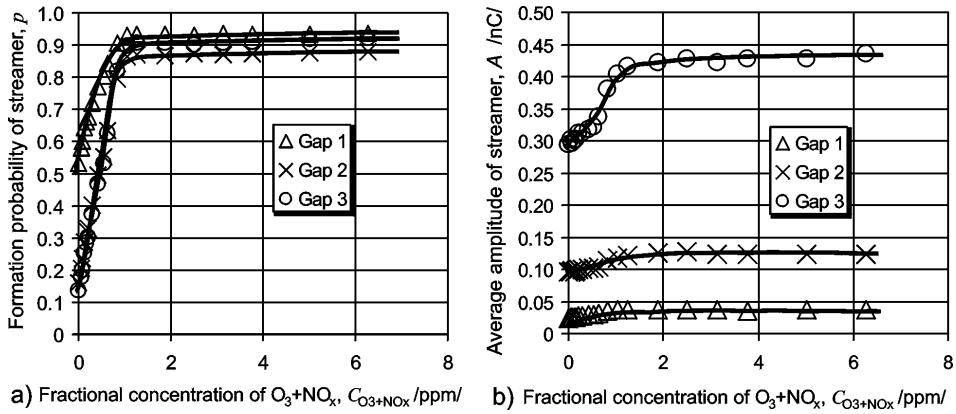

Figure 8.7. Dependence of streamer formation probability and average amplitude on the fractional concentration of ozone and NO_x C_{O3+NOx}. Fractional concentration of H_2O is 9100 ppm.

Influence of sulphur hexafluoride on the formation probability and the average amplitude of streamers is presented in figure 8.8. One can see that the average amplitude of streamers decreases remarkably with increasing concentration of SF_6 and constitutes at SF_6 concentration of 400 ppm only a quarter of that at 0 ppm. At the same time, an increase in the concentration of SF_6 increases only a little the formation probability of a streamer and has no influence on both the width of the voltage region of streamer occurrence and the position of this region relative to the phase of the AC voltage.

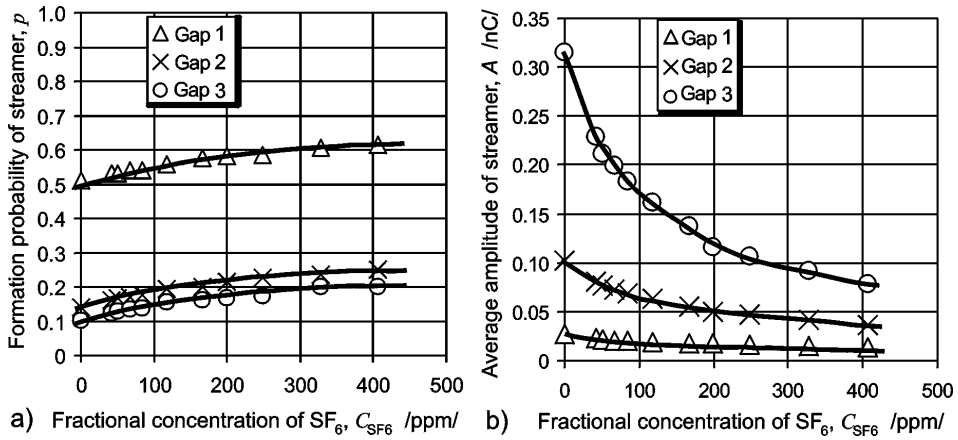

Figure 8.8. Dependence of streamer formation probability and average amplitude on the fractional concentration of sulphur hexafluoride C_{SF6}. Fractional concentration of H_2O is 5100 ppm.

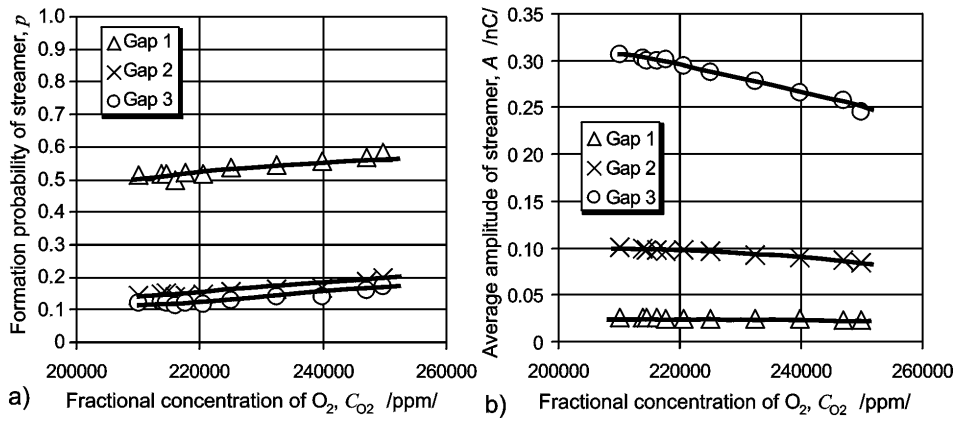

Figure 8.9. Dependence of streamer formation probability and average amplitude on the fractional concentration of oxygen C_{O2}. Fractional concentration of H_2O is 6800 ppm.

Influence of oxygen on the formation probability and average amplitude of streamers is presented in figure 8.9. One can see that the formation probability of a streamer increases and the average amplitude of streamers decreases with

an increase in the concentration of O_2. An increase in the concentration of O_2 has no influence on the width of the voltage region of streamer occurrence or on the position of this region relative to the phase of the AC voltage.

In our investigation [I], we have shown that in air the formation probability of a streamer increases also with the concentration of such admixtures as HNO_3, HCl, H_2SO_4, H_3PO_4, $CHCl_3$, C_6H_6, NH_4OH, CH_3COOH, $C_{10}H_{16}O$, HCHO, Cl_2. Ethyl ether $C_2H_5OC_2H_5$ and ethyl acetate $C_4H_8O_2$ decrease the repetition rate of streamers [I].

8.2 Discussion

One can see in figures of the previous section that p increases with fractional concentration of all electronegative admixtures used, in all gaps. Under the influence of an electronegative admixture, the number of ions with high probability to initiate burst pulses decreases due to the conversion reactions, and the number of ions with lower probability to initiate burst pulses increases [IV, VI, VII]. The primary negative ions formed at the ionizer or due to the after-effect of a discharge are supposed to be the molecular ions of oxygen O_2^-. In the drift region, between the ionizer and the point electrode, a conversion of those negative ions takes place and various complex ions are formed. According to the numerical simulation [Luts and Salm, 1994], the concentration of the primary oxygen ions will be close to zero already within 10^{-8} s. The composition and concentration of resulting ions depends on the concentration of humidity and other electronegative additives. Some of molecules of strongly electronegative additives will collide with the complex ions and new, very stable ions will be formed. Electrons attached to such molecules are then practically unavailable for triggering a corona discharge [I]. The composition and concentration of ions reaching the active zone of the discharge depends also on the time of flight of ions through the drift region. This time is determined mainly by the flow rate of the air stream. The experiments carried out with a buffer section between ionizer and the detector gap showed that the lengthening of the time of flight in the presence of halogen additive increases the repetition rate of streamers remarkably [I].

Small amounts of the additive do not change the propagation mechanism of a discharge (they do not change values of the ionization coefficient α, attachment coefficient η, coefficient of absorption of photoionizing radiation). Thus, they have no effect on the development of an already initiated streamer or burst pulse. An electronegative additive causes only a reduction in the number of seed electrons because the detachment probability of electrons from the ions decreases.

Higher amounts of the additive alter the discharge development already substantially. First, the amplitude of streamers will change (like in above-reported experiments with H_2O, SF_6 and O_2). Second, the DC voltage interval of streamers expands (as for $C_{H2O} > 15\,000$ ppm and $C_{CO2} > 3000$ ppm [I]). Third, the number of streamers per cycle may grow over one, if the concentration of the additive exceeds some percent.

8.3 Modification of the equation that describes the streamer formation probability

In the general case, the number m of different types of ions reaching the birth region of burst pulses is greater than one. For the probability p_j that the ions of j^{th} type will not initiate a burst pulse during the time interval Δt_{bp}, we can write an equation similar to equation (5.8):

$$p_j = \exp\left(-\Delta t_{bp} \Phi \varphi_j g_j b_j\right).$$

Here φ_j denotes the fractional flux of ions of j^{th} type, which is defined as the ratio of the flux Φ_j of ions of that type to the flux Φ. Factor g_j characterizes the possibility that an ion of j^{th} type will reach the birth region of burst pulses. g may be different for ions of different type because of difference in mobilities. b_j denotes the probability that one ion of j^{th} type initiates a burst pulse.

The probability, that none of ions of m different type initiates a burst pulse during the time interval Δt_{bp}, is equal to the product of all p_j:

$$p = \prod_{j=1}^{m} p_j = \exp\left(-\Phi \Delta t_{bp} \sum_{j=1}^{m} \varphi_j g_j b_j\right). \qquad (8.1)$$

This probability equals also to the formation probability of a streamer, as according to our experimental conditions a streamer arises whenever a burst pulse is not formed during Δt_{bp} (see section 4.2). According to equation (8.1), the changes in ion flux composition result in changes of p as the average initiation probability of a burst pulse and the factor g change upon introduction of an electronegative admixture [IV, VII].

8.4 Limitations on detection of electronegative trace gases by the streamer counter with one discharge gap

According to experimental results presented above, the electronegative additives increase the streamer formation probability. Especially high sensitivity is observed in the case of halogens. For example, a detectable change in the formation probability of a streamer takes place at fractional concentration of iodine $C_{I2} = 1$ ppb [I]. Thus, the streamer counters can be used as simple and cheap detectors of electronegative trace gases.

The simple streamer counter with only one discharge gap has a disadvantage – the lack of selectivity [IV, VI, VII]. It is possible to detect the presence of an electronegative admixture in laboratory air but it is impossible to distinguish between different electronegative admixtures (see for example figure 4 in paper [VII]).

The experimental results presented above show that the influence of electronegative additives on the average amplitude of streamers depends on the nature of an additive. Some stuff increase, some other decrease the amplitude of a streamer, and some do not have any detectable influence on it.

Simultaneous measurements of formation probability and amplitude of streamers give us a possibility to differentiate between different additives. One can see that the additives can be divided at least in four groups.

- Gases (O_3, CO_2), which increase the formation probability of a streamer and have no effect on the amplitude of streamers. To that group belong also these gases (I_2, $O_3 + NO_x$), which increase the average amplitude of streamers due to the shift of initiation moments of streamers in the voltage scale to higher instantaneous values of the combined voltage.
- Gases (O_2, H_2O), which increase the formation probability and decrease somewhat the amplitude of streamers.
- Gases ($CHCl_3$ (chloroform) [I] and SF_6), which increase the formation probability and decrease remarkably the amplitude of streamers.
- Additives which decrease the formation probability of streamers ($C_2H_5OC_2H_5$ (ethyl ether) and $C_4H_8O_2$ (ethyl acetate), for example) [I]. These additives form a fourth group. The amplitude of streamers was not investigated experimentally for this group of additives

8.5 Streamer counter with several discharge gaps

The simultaneous use of several discharge gaps improves the capability of a streamer counter to differentiate between electronegative additives. The probability b_j for a certain ion to initiate a burst pulse depends on the decomposition probability of the ion, which in turn depends strongly on the electric field strength (at constant gas number density). At the onset of streamers, the maximum field strength on the axis of the discharge gap is the higher the smaller is the curvature radius of the point tip. According to numerical calculations (see section 6.9) for our discharge gaps, the maximum field strength $E_{max} = 250$ kV/cm if the point diameter $d = 0.13$ mm, and $E_{max} = 120$ kV/cm if $d = 0.5$ mm, provided that $U = U_{str}$. Thus it can be supposed that the probability b of initiating a burst pulse by a negative ion depends on the tip radius of the point electrode and, furthermore, the dependence of b on the tip radius is different for different kind of ions. The

dependence of b on different admixtures is due to difference in their electron affinities, molecule masses and their structure [VI]. Using m - 1 point electrodes with different curvature of the tip we get a set of linear equations

$$\begin{cases} p_1 = \exp\left(-\Delta t_1 \Phi (a_{1,1}\varphi_1 + a_{1,2}\varphi_2 + ... + a_{1,\mathrm{j}}\varphi_\mathrm{j} + ... + a_{1,\mathrm{m}}\varphi_\mathrm{m})\right) \\ p_2 = \exp\left(-\Delta t_2 \Phi (a_{2,1}\varphi_1 + a_{2,2}\varphi_2 + ... + a_{2,\mathrm{j}}\varphi_\mathrm{j} + ... + a_{2,\mathrm{m}}\varphi_\mathrm{m})\right) \\ ... \\ p_\mathrm{i} = \exp\left(-\Delta t_\mathrm{i} \Phi (a_{\mathrm{i},1}\varphi_1 + a_{\mathrm{i},2}\varphi_2 + ... + a_{\mathrm{i},\mathrm{j}}\varphi_\mathrm{j} + ... + a_{\mathrm{i},\mathrm{m}}\varphi_\mathrm{m})\right) \\ ... \\ p_{\mathrm{m}-1} = \exp\left(-\Delta t_{\mathrm{m}-1} \Phi (a_{\mathrm{m}-1,1}\varphi_1 + a_{\mathrm{m}-1,2}\varphi_2 + ... + a_{\mathrm{m}-1,\mathrm{j}}\varphi_\mathrm{j} + ... + a_{\mathrm{m}-1,\mathrm{m}}\varphi_\mathrm{m})\right) \\ 1 = \varphi_1 + \varphi_2 + ... + \varphi_\mathrm{j} + ... + \varphi_\mathrm{m} \end{cases} \qquad (8.2)$$

Here index i indicates the gap number and index j the type of ions. p_1, p_2,..., $p_{\mathrm{m}-1}$ are streamer formation probabilities measured in different gaps. $a_{\mathrm{i,j}}$ denotes the product $b_{\mathrm{i,j}}\, g_{\mathrm{i,j}}$. Constancy of the sum of fractional ion fluxes yields the additional condition $\sum_\mathrm{j} \varphi_\mathrm{j} = 1$, which is presented in the last row of set (8.2).

If the numerical values of $a_{\mathrm{i,j}}$ are known, then solving this set of equations yields the values of φ_j. In that way we get a distribution of the ion flux by values of $a_{\mathrm{i,j}}$, that is, a spectrum of ions by $a_{\mathrm{i,j}}$. The spectrum shape depends on gas composition. Once the spectrum is known, some conclusions about gas composition are possible.

The relative increase in p with fractional concentration of an admixture is different in different gaps. For instance, look at figure 8.1, where the H_2O-curves for gaps 2 and 3 are even intersecting. This is in accordance with our hypothesis that the initiation probability b of a burst pulse depends on the point diameter differently for different ion species.

8.6 Calibration of the detector

The coefficients $a_{\mathrm{i,j}}$ of equations (8.2) can be determined, if we know the ion composition of the gas. We determined the values of $a_{\mathrm{i,j}}$ for our three-gap device using the known ion composition of clean humid air. According to Allen and Gallimberti, the most populous ions in clean humid air are the ions of $O_2^-(H_2O)_\mathrm{x}$, with x = 2 ... 5 [Allen, 1985; Gallimberti, 1979]. As a first approximation, we take into account only those ions and calculate the fractional concentration $\varphi_\mathrm{x}^*(h)$ of those ions using the formulae proposed by Allen [1985]. Thereafter, using the curve fitting method, we find the coefficients $a'_{\mathrm{i,x}}$ such that curves $\mathrm{f_i}(h) = \sum_\mathrm{x} a'_{\mathrm{i,x}} \varphi_\mathrm{x}^*(h)$ fit experimental points on $-(\Delta t \Phi)^{-1}\ln(p(h))$

versus *h* plots for all three gaps as well as possible [IV]. The calibration procedure is described in detail in paper [IV]. The obtained values of $a'_{i,x}$ are presented in the first three rows of the matrix **A**:

$$\mathbf{A} = \begin{pmatrix} 7.90\cdot10^{-3} & 5.47\cdot10^{-3} & 5.16\cdot10^{-4} & 2.18\cdot10^{-6} \\ 2.85\cdot10^{-2} & 1.01\cdot10^{-2} & 2.29\cdot10^{-3} & 8.43\cdot10^{-6} \\ 3.96\cdot10^{-2} & 1.17\cdot10^{-2} & 1.05\cdot10^{-3} & 5.13\cdot10^{-6} \\ 1 & 1 & 1 & 1 \end{pmatrix} \tag{8.3}$$

The first row corresponds to gap 1, the second to gap 2, the third to gap 3. The first column consists of coefficients $a'_{i,2}$, the second of coefficients $a'_{i,3}$, the third of coefficients $a'_{i,4}$, and the fourth of coefficients $a'_{i,5}$. Coefficients of the condition $\sum_j \varphi_j = 1$ are presented in the fourth row of the matrix **A**.

By solving the equation

$$\mathbf{A} \cdot \varphi = \mathbf{q} \tag{8.4}$$

for φ, where $\varphi = \begin{pmatrix} \varphi_1 \\ \varphi_2 \\ \varphi_3 \\ \varphi_4 \end{pmatrix}$ and $\mathbf{q} = \begin{pmatrix} -(\Delta t_1 \Phi)^{-1} \ln p_1 \\ -(\Delta t_2 \Phi)^{-1} \ln p_2 \\ -(\Delta t_3 \Phi)^{-1} \ln p_3 \\ 1 \end{pmatrix}$,

the four components of φ (fractional fluxes) can be determined [IV]. Each flux component is characterized by certain values of $a_{i,j}$. Ions constituting flux component with subscript 1 have the greatest probability to initiate a burst pulse, ions with subscript 4 – the smallest, close to zero [IV].

8.7 The response of the detector in the form of a four-bar (pseudo)spectra

In the general case, some different trace gases are present in air, and the number *m* of ion species with different values of *a* may be great enough. If the number of gaps *n* is smaller than *m* - 1, then the actual spectrum of ions by *a* can not be resolved because the number of unknowns is greater than the number of equations. Nevertheless, it is possible to find a solution for the set (8.4) that consists of *n* + 1 equations [IV]. Below, the solution of equation (8.4) using matrix (8.3) is named the device response. It can be presented as a spectrum as well, but in the general case it differs from the actual spectrum of ions – the number of components of the actual spectrum may be different from four, and the values of *a* corresponding to each component of the actual spectrum may be different from values of $a_{i,j}$ chosen for the components of the response. Despite of these differences, the calculation of a detector response using matrix (8.3) enables us to distinguish between some admixtures.

The response φ of the detector depending on the concentration of different admixtures is presented in paper [IV]. Some characteristic results are presented also in figure 8.10 for pure laboratory air and for laboratory air with artificially increased concentration of H_2O, CO_2 and O_2. To accent the possible difference between the detector response and the actual spectrum of ions, these histograms will be named pseudospectra below.

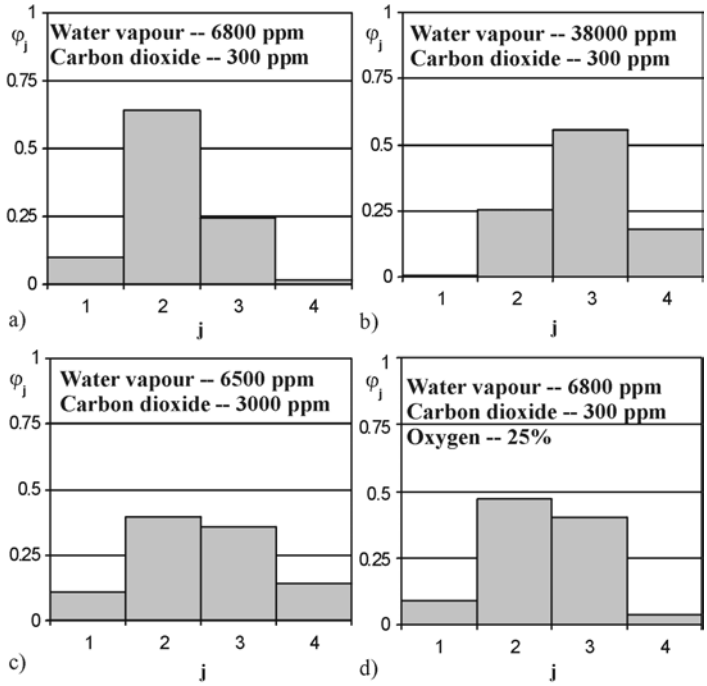

Figure 8.10. Response of the detector (a) in laboratory air; (b) in laboratory air with increased concentration of H_2O; (c) in laboratory air with increased concentration of CO_2 (d) in laboratory air with increased concentration of O_2.

One can see that the spectrum of clean laboratory air has his maximum at j = 2.

At high concentration of H_2O, the maximum is moved to j = 3. Under the influence of CO_2 or O_2, φ_1 and φ_4 stay practically unchanged whereas φ_3 increases and φ_2 decreases with increase in concentration of admixture. However, the initial relationship among the components of φ, $\varphi_2 > \varphi_3 > \varphi_1 \approx \varphi_4$, remains unchanged over the investigated range of concentrations of CO_2 and O_2.

Figure 8.11 presents some characteristic results in the case when some strongly electronegative trace gases are present in laboratory air.

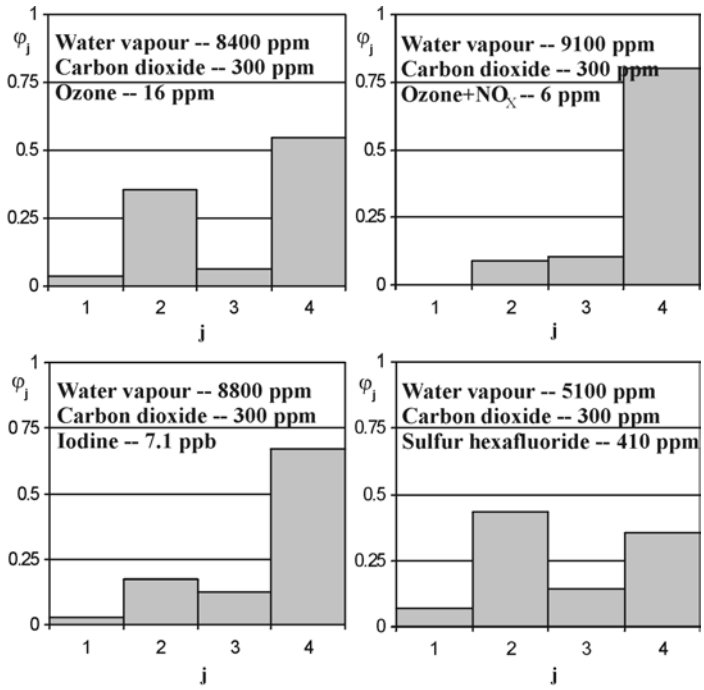

Figure 8.11. Response of the detector in laboratory air with addition of small quantity of different strongly electronegative admixtures.

The influence of strongly electronegative trace gases on the shape of the pseudospectrum is quite similar in case of each admixture. The values of φ_1, φ_2 and φ_3 decrease and that of φ_4 increases with an increase in the concentration of an electronegative admixture [IV]. In the case of I_2 or O_3+NO_x, the pseudospectrum obtains one maximum at j = 4. In the case of O_3 or SF_6, another maximum at j = 2, specific for clean air of low humidity, remains observable as well.

As can be seen from figure 8.11, in the presence of I_2, O_3 or O_3+NO_x in air, the component φ_4 acquires the highest value among the components of φ. Under influence of SF_6 (figure 8.11) or H_2O (figure 8.10), φ_4 increases as well but here the component φ_2 or φ_3 has the highest value [IV]. In the case of CO_2 or O_2, the initial relationship among the components of φ remains unchanged. Therefore it is possible to distinguish the presence of some strongly electronegative trace gas (I_2, O_3, O_3+NO_x, SF_6) in air on the basis of the four-bar pseudospectrum [IV]. Once the admixture is identified, the concentration of it can be determined on the bases of formation probability of a streamer versus admixture concentration curve (like those presented in figures 8.1 – 8.2, 8.4 – 8.5 and 8.7 – 8.9) [IV]. Accurate measurements of concentration of an admixture are possible if only

one admixture is present in air. Applicability of the detector in the case when several admixtures are present at the same time needs further investigation [IV].

To increase the selectivity of the detector, the number of gaps used in the streamer counter can be stepped up. The electrodes for the new gaps have to be chosen so that the electric field strength near the point at the onset voltage of streamers and the degree of inhomogeneity would be remarkably different from the corresponding values of the already existing gaps [VII]. As one can see in paper [IV], the scattering of points around the smoothed curves in figures 5 - 10 is relatively great compared to that in figures 2 - 4. This is caused by the fact that relative changes in p due to addition of a particular admixture are quite similar in different gaps. Thus, the accuracy in determination of φ decreases rapidly with an increase in the number of gaps [IV], and determination of the optimal number and geometry of gaps need further investigation.

Another thing in need of further investigation is the optimal choice of the matrix **A**. We have obtained the matrix **A** by changing the concentration of H_2O. Applying this matrix to other admixtures gives only a pseudospectrum [IV]. Another matrix **A**, obtained by changing the concentration of some other admixture, might lead to the spectra of another shape (see for example figure 3 in paper [VI], where the matrix **A** was obtained in a different way than in paper [IV]). What kind of matrix is the best one, might depend on the admixtures used. However, the responses like presented above in the form of four-bar pseudospectra seem to be quite proper for the present task - to distinguish strongly electronegative trace gases from additional H_2O, CO_2 [IV] and O_2 in air.

8.8 Preferable operating conditions of the streamer counter.

To determine the best operating condition for the streamer counter, we proceed from the limits of applicability of the equation (5.8) and experimental results about the dependence of the after-effect on AC frequency, airflow rate and DC voltage. Presence of the after-effect complicates the interpretation of the response of the streamer counter, as the ion composition can depend on the place of origin of ions. Thus, we try to choose the working parameters of the streamer counter in such a way that the after-effect of streamers and glow corona would be minimized. If the after-effect can be neglected, the equation (5.8) takes a form:

$$p = \exp\left(-\Phi_0 b_0 \Delta t_{\mathrm{bp}}\right). \tag{8.5}$$

Application of high AC frequencies is preferred, because they enable to opt for shorter counting times and ensure a lower scatter of the experimental data. Figure 6.6 indicates that the after-effect of streamers increases remarkably with

the AC frequency, if the frequency is higher than 500 Hz. Thus, the highest value of the acceptable AC frequency is about 500 Hz.

Figure 6.5 shows us that the after-effect of a discharge decreases remarkably with an increase in the airflow rate v. Therefore, the high airflow rates are preferable. However, the airflow rate should be low enough to avoid the possible turbulence in the discharge gaps. Reynolds numbers $\mathrm{Re} > 7000$ indicate the presence of an excessive strong turbulence [Miller, 1989]. The velocities $v > 4.3\ \mathrm{m\ s^{-1}}$ correspond to those Reynolds numbers. Weak turbulence exists already above $\mathrm{Re} = 4000$ (corresponding $v = 2.5\ \mathrm{m\ s^{-1}}$). As one can see, the fully laminar air flux and the effective removal of the residual ions are not always the compatible requirements. If all residual ions are to be certainly removed before the formation of the next discharge, then a weak turbulence should be accepted. The limits for acceptable airflow rate are $2.5\ \mathrm{m\ s^{-1}} < v < 4.3\ \mathrm{m\ s^{-1}}$.

The concrete values of optimal f and v are valid in the case of our discharge gaps. In the case of discharge gaps of other dimension, the optimal f and v can be different. However, the methodology of their determination presented above is valid also in that case.

The main advantage of the combined voltage is that it makes the repetition rate of streamers in the streamer counter insensitive to small variations in air pressure and temperature [I]. For that, the time interval Δt_{bp} has to remain in certain limits with changes in the DC voltage. For example, if we allow Δt_{bp} to differ maximally 20% from Δt_{bp} at $U_{DC} = U_{str}$, the DC voltage has to satisfy the condition $U_{str} - 0.6\ U_{AC} < U_{DC} < U_{bp} + 0.6\ U_{AC}$. Figure 6.8 indicates that the after-effect of streamers decreases with an increase in the DC voltage. Therefore, higher DC voltages are preferred. However, according to the assumptions of equation (5.8), the DC voltage has to be low enough to warrant the discharge extinction at the end of every AC cycle. In our opinion, the preferable choice of the DC voltage is $U_{str} < U_{DC} < U_{bp} + 0.6\ U_{AC}$.

According to the assumptions of equation (5.8), the resultant voltage has to stay in the discharge-free voltage region for some time and traverse voltage regions of burst pulses, streamers and glow corona. The amplitude of the AC voltage has to be high enough to warrant that. In addition, $\Delta t_{bp} + \Delta t_{str}$ has to be short enough to warrant that the burst pulse eliminates the inception of the streamer during the same AC cycle. The time interval Δt_{str} has to be short enough to eliminate the inception of more than one streamer during the same AC cycle. The higher is the amplitude of the AC voltage, the better the above requirements are fulfilled. The onset voltage U_{bs} of breakdown streamers limits the highest peak value of U_{AC} to the magnitude $U_{AC} < U_{bs} - U_{DC}$. In practice, it is necessary to consider also the after-effect of the glow corona under high AC voltages (see

figure 6.7). Therefore, we have chosen for our streamer counter the voltages presented in table II.

Finally, the acceptable preionization level should be chosen according to the repetition rate of streamers applicable for detection of electronegative trace gases. We will choose the repetition rate of streamers so that the detector will be as sensitive as possible to small variations in the average initiation probability of a burst pulse caused by changes in the ion composition of the gas under test. Equation (5.8) gives that the maximal sensitivity of the detector is reached at $p \approx 0.37$. The corresponding preionization level $\Phi = \frac{1}{gb\Delta t_{\mathrm{bp}}}$. In our streamer counter with several discharge gaps, only one gap can be optimized for sensitivity. To optimize all discharge gaps, the design of the streamer counter has to be modified so that the regulation of Φ would be possible in every gap separately.

9 CONCLUSIONS

The positive corona was investigated experimentally under the combined voltage (DC + AC). The dependence of the repetition rate of streamers on DC voltage, AC voltage amplitude and frequency, airflow rate, preionization level, diameter of the point electrode and on the concentration of some electronegative admixtures was recorded.

The main results of the present work are the following.

- The probability of discharge inception under conditions of combined voltage is described mathematically. This description relates the formation probability of a streamer with values of DC and AC voltage, AC frequency, preionization level, and to characteristics of the corona gap – onset voltages of burst pulses and streamers and initiation probability of burst pulses.
- Two methods were developed to measure the after-effect of a discharge on the formation of the following streamer. One of them is preferable for measurement of the after-effect of a streamer, another for measurement of the after-effect of the glow corona. Both methods are based on the statistical analysis of sequences of streamers under the conditions of the combined voltage.
- The negative ions left into the discharge gap by a streamer or glow corona cause the after-effect. The analysis of the experimental results, as well as the numerical simulation of the ion drift reveal that in our discharge gaps those negative ions are the products of photoionization in gas.
- The after-effect of both streamer and glow corona increases with discharge current and AC frequency. The after-effect decreases with an increase in airflow rate and air humidity.
- A method for detection of photoionizing radiation, based on an internal gas discharge counter, was developed. The production of photoions by negative and positive coronas was recorded in air at atmospheric pressure. It is shown that the bremsstrahlung caused by electron bombardment of the anode surface constitutes so small fraction of the total radiation that it is indistinguishable from the total radiation by our experimental method. According to the earlier widely admitted hypothesis, mainly gas molecules and atoms emit the photoionizing radiation in a corona discharge. The present experiments leave this hypothesis in force.
- A method was developed to estimate the average probability of the burst pulse initiation by one negative ion. This probability was determined for point electrode of 0.5 mm in diameter.
- Using properties of the streamer corona, a detector can be designed for detection of electronegative trace gases in air. The detector is sensitive to admixtures such as H_2O, CO_2, O_3, O_3+NO_x, SF_6, HNO_3, HCl, H_2SO_4, H_3PO_4, $CHCl_3$, C_6H_6, NH_4OH, CH_3COOH, $C_{10}H_{16}O$, HCHO, I_2, Cl_2. The detection limit for halogen concentration in air is about 1 ppb.

- A streamer counter with three discharge gaps has the capability to distinguish at least four strongly electronegative trace gases (I_2, O_3, O_3+NO_x, SF_6) from H_2O or CO_2 background in air. Once the admixture is identified the concentration of it can be determined on the bases of formation probability of a streamer versus admixture concentration plots. Accurate measurements of concentration are possible, if only one additional gas is present in air.
- Measuring the repetition rate and amplitude distribution of streamers simultaneously improves the ability of the streamer counter to distinguish between different admixtures.

As a result of the present work, a mock-up of a three-gap computer-linked detector of electronegative trace gases was built. The methodology was developed for optimization of parameters of detector such as amplitude and frequency of the AC voltage, DC voltage, airflow rate and preionization level.

Open problems

The initiation probability of a burst pulse depends on Δt_{bp} (see figure 6.14). The physical reasons for that need a further investigation and theoretical explanation.

In addition, next aspects need further investigations:

- Applicability of the streamer counter as a detector of electronegative trace gases in situations where several admixtures are present at the same time;
- The optimal number of discharge gaps in a multi-gap detector;
- Optimization of electrode configuration of discharge gaps.

SUMMARY IN ESTONIAN

Positiivne koroona segapingel

Uurimistöö eesmärgiks oli täpsustada positiivse koroona tekkemehhanismi (initsieerimist) segapingel (alalis- + vahelduvpinge) atmosfääriõhus, välja selgitada elektronegatiivsete lisandgaaside mõju koroona karakteristikutele ja selgitada koroonal baseeruva elektronegatiivsete lisandgaaside detektori (nn. striimerloenduri) täiustamise võimalusi.

Eksperimentaalselt uuriti positiivset koroonalahendust atmosfääriõhus segapingel, kui elektroodidele oli samaaegselt rakendatud nii alalis- kui ka vahelduvpinge. Registreeriti striimerite kordussageduse sõltuvus vahelduvpinge amplituudist ja sagedusest, alalispingest, gaasi voolukiirusest, eelionisatsiooni tasemest, poolsfäärilise tipuga silindrilise teravikelektroodi diameetrist ja rea elektronegatiivsete lisandgaaside kontsentratsioonist.

Käesoleva töö põhitulemused on järgmised.

- Koostati striimerloenduris asetleidvate protsesside matemaatiline mudel, mis kirjeldab striimerite tekketõenäosust sõltuvalt alalispingest, vahelduvpinge amplituudist ja sagedusest, eelionisatsioonitasemest, purskeimpulsside ja striimerite lävepingest ning purskeimpulsi algatamise tõenäosusest.
- Striimerid ja pidev koroona võivad avaldada järelmõju järgneva lahenduse süttimise tõenäosusele. Järelmõju suuruse mõõtmiseks töötati välja kaks meetodit, mis põhinevad striimerite jadade statistilisel analüüsil. Üks meetoditest on eelistatav pideva koroona järelmõju mõõtmisel, teine striimeri järelmõju mõõtmisel.
- Lahenduse järelmõju põhjustavad lahendusvahemikku jäänud negatiivsed ioonid. Eksperimenditulemuste analüüs ja ioonide triivi numbriline modelleerimine näitavad, et uuritud lahendusvahemikes põhjustavad järelmõju negatiivsed ioonid, mis tekivad õhu fotoioniseerimisel lahenduse ultraviolettkiirguse poolt.
- Nii striimeri kui ka pideva koroona järelmõju tugevneb vahelduvpinge sageduse ja lahendusvoolu kasvades. Järelmõju nõrgeneb õhuvoolu kiiruse ja õhu niiskusesisalduse suurenedes.
- Töötati välja metoodika fotoioniseeriva kiirguse mõõtmiseks gaaslahenduspõhise loenduri abil. Mõõdeti nii positiivse kui ka negatiivse koroona fotoioniseeriv kiirgus atmosfäärirõhul. Näidati, et anoodi pinna elektronpommitamise tagajärjel tekkida võiv pärsskiirgus moodustab nii väikese osa kogu fotoioniseerivast kiirgusest, et meie eksperimentides polnud teda võimalik kogukiirguse foonil registreerida. Seetõttu jääb jõusse seni laialdaselt aktsepteeritud hüpotees, et koroonalahenduse fotoioniseeriva kiirguse allikaks on peamiselt gaasi ergastatud molekulid või aatomid.

- Töötati välja meetod, mis võimaldab leida keskmise tõenäosuse, millega üks negatiivne ioon initsieerib purskeimpulsi. Selle tõenäosuse väärtus määrati 0.5 mm diameetriga teravikelektroodi jaoks.
- Kasutades striimerkoroonat on võimalik konstrueerida õhu elektronegatiivsete lisandgaaside detektor. Striimerloendur on tundlik näiteks H_2O, CO_2, O_3, O_3+NO_x, SF_6, HNO_3, HCl, H_2SO_4, H_3PO_4, $CHCl_3$, C_6H_6, NH_4OH, CH_3COOH, $C_{10}H_{16}O$, HCHO, I_2 ja Cl_2 lisandite suhtes. Halogeenide detekteerimisel õhus on detektori tundlikkuse lävi umbes 1 ppb.
- Eksperimentaalselt näidati, et kolme lahendusvahemikuga striimerloendur on kasutatav lisandgaasi detektorina, mis suudab eristada vähemalt nelja tugevalt elektronegatiivset lisandgaasi (I_2, O_3, O_3+NO_x, SF_6) veeauru või süsihappegaasi foonist õhus. Kui lisandgaas on identifitseeritud, siis saab tema kontsentratsiooni hinnata striimeri tekketõenäosuse ja lisandgaasi kontsentratsiooni vahelise sõltuvuse graafikult. Korrektsed mõõtmised on võimalikud ainult siis, kui õhk ei sisalda rohkem kui ühte lisandgaasi.
- Striimerloenduri võimet eristada lisandgaase saab parandada, kui mõõta üheaegselt striimerite kordussagedust ja amplituudi.

Uurimistöö tulemusena valmistati arvutiga sidestatud elektronegatiivsete lisandgaaside detektori makett. Töötati välja metoodika detektori tööparameetrite – vahelduvpinge amplituudi ja sageduse, alalispinge, gaasi voolukiiruse ja eelionisatsiooni taseme – optimaalsete väärtuste määramiseks.

REFERENCES

1. Acker F E and Penney G W 1968 Influence of Previous Positive Streamers on Streamer Propagation and Breakdown in a Positive Point-to-Plane Gap *J.Appl.Phys.* **39** 2363-9
2. Aints M Kudu K and Haljaste A 1977 Investigation of the primary-secondary streamer sequence in the air *Acta Comment. Universitatis Tartuensis* **443** 3-20 (in Russian)
3. Akishev Yu S Grushin M E Deryugin A A Napartovich A P Pankin M V and Trushkin N I 1999a Self-oscillations of a positive corona in nitrogen *J. Phys. D: Appl. Phys.* **32** 2399-409
4. Akishev Yu S Grushin M E Deryugin A A Napartovich A P Pankin M V and Trushkin N I 1999b Integral and local characteristics of an extended positive corona in the regime of non-linear oscillations: experiment *Plasma Phys. Rep.* **25** 867-76
5. Akishev Yu S Grushin M E Deryugin A A Napartovich A P Pankin M V and Trushkin N I 1999c Integral and local characteristics of an extended positive corona in the regime of non-linear oscillations: theory *Plasma Phys. Rep.* **25** 877-81
6. Allen N L 1985 The effect of humidity on positive corona discharges in air *Proc. 17th Int. Conf. on Phenomena in Ionized Gases* Invited Papers (Budapest) 62-72
7. Allen N L and Boutlendj M A 1993 Pre-breakdown streamer pulses in long air gaps under positive direct voltage *J.Phys.D: Appl. Phys.* **26** *760-766*
8. Allen N L and Ghaffar A 1995a The conditions required for the propagation of a cathode-directed positive streamer in air *J.Phys.D: Appl. Phys.* **28** *331-7*
9. Allen N L and Ghaffar A 1995b The variation with temperature of positive streamer properties in air *J.Phys.D: Appl. Phys.* **28** *338-43*
10. Allen N L and Mikropoulos P N 1999 Dynamics of streamer propagation in air *J. Phys. D: Appl. Phys.* **32** 913-9
11. Anderson D R Sweeney D J and Williams T A 1981 *Introduction to statistics. An applications approach* (St. Paul: West) 602 p.
12. Andersson N E and Hertz C H 1955 Positive corona as an hygrometer of small inertia *Z. Ang. Phys.* **7** 361-6 (in German)
13. Andersson N E 1958 An investigation of the positive point streamer corona. Part I. The time distribution of the streamers *Arkiv Fysik* **13** 399-422
14. Babaeva N Yu and Naidis G V 1996a Two-dimensional modelling of positive streamer dynamics in non-uniform electric fields in air *J. Phys. D: Appl. Phys.* **29** *2423-31*
15. Babaeva N Yu and Naidis G V 1996b Simulation of positive streamers in air in weak uniform electric fields *Phys. Letters A* **215** *187-90*

16. Badaloni S and Gallimberti I 1972 *Basic data of air discharges UPee–72/05* (Padova University) 91 p.
17. Bazelyan E M and Raizer J P 1998 *Spark Discharge* (Boca Raton: CRC) 294 p.
18. Beattie J 1975 The Positive Glow Corona Discharge PhD thesis (University of Waterloo) 283 p.
19. Berger G Johnson P C and Goldman M 1972 Influence of an electrical discharge on the development of a subsequent discharge in a positive point-to-plane gap *Proc. 2nd Int. Conf. Gas Discharges* (London) 236-8
20. Berger 1974 Influence of a corona discharge on the subsequent one in atmospheric air *Proc. 3rd Int. Conf. Gas Discharges* (London) 294-7
21. Berger G 1980 Statistical time-lags of a positive corona discharge in atmospheric air PhD thesis (Université de Paris-Sud) 242 p. (in French)
22. Blair D T A 1978 Breakdown Voltage Characteristics In: *Electrical Breakdown of Gases* ed J M Meek and J D Craggs (Wiley) p 533-653
23. Bogdanova N B and Popkov V I 1973 Appearance of a corona discharge and breakdown in air gaps (Moscow: Elektritshestvo) **8** 27-34 (in Russian)
24. Bogdanova N B Pevchev B G Polevoy S V 1976 Measurement of electrical field strength on the electrode during corona *Proc. 4th Int. Conf. Gas Discharges* (Swansea) 231-4
25. Bogdanova N B Pevchev B G and Popkov V I 1978 Electric field strength on the surface of the positive electrode in conditions of contraflux of negative ions (Moscow: Energetika i transport) **1** 96-102 (in Russian)
26. Bouziane A Hidaka K Taplamacioglu M C and Waters R T 1994 Assessment of corona models based on the Deutsch approximation *J. Phys. D: Appl. Phys.* **27** 320-9
27. Bouziane A Taplamacioglu M C Hidaka K and Waters R T 1997 Non-Laplacian ion trajectories in mutually interacting corona discharges *J. Phys. D: Appl. Phys.* **30** 1913-21
28. Van Brunt R J and Kulkarni S V 1989 Method for measuring the stochastic properties of corona and partial-discharge pulses *Rev. Sci. Instrum.* **60** 3012-23
29. Dawson G A and Winn W P 1965 A model for streamer propagation *Z. Phys.* **183** 159-71
30. Dutton J A 1975 Survey of electron swarm data *J. Phys. Chem. Ref. Data* **4** 577-856
31. Fouad L F Abdel-Salam M Zeitoun A G and Gohar M K 1978 Performance Characteristics of Alpha-Particle Corona-Streamer Counter *IEEE Trans. Ind. Applicat.* **14** 510-5
32. Fouad L F and El-Hazek S T M 1996 Temperature Effect on the Performance Characteristics of Beta Rays Open Air Corona Streamer Counter *IEEE Trans. Ind. Applicat.* **32** 221-6
33. Gallimberti I 1979 The mechanism of the long spark formation *J. Physique* **40** C7 193-250

34. Georghiou G E Morrow R and Metaxas A C 1999 The theory of short-gap breakdown of needle point-plane gaps in air using finite-difference and finite-element methods *J. Phys. D: Appl. Phys.* **32** 1370-85
35. Grangé F Soulem N Loiseau JF and Spyrou N 1995 Numerical and experimental determination of ionizing front velocity in a DC point-to-plane corona discharge *J. Phys. D: Appl. Phys.* **28** 1619-29
36. Goldman M and Goldman A 1978 Corona Discharges In: *Gaseous Electronics Vol 1 Electrical Discharges* ed M N Hirsh and H J Oskam (Academic Press) 219-90
37. Gosho Y 1981 Enhancement of DC positive streamer corona in a point-plane gap in air due to addition of a small amount of an electronegative gas *J. Phys. D: Appl. Phys.* **14** 2035-46
38. Gosho Y 1982 Considerable change in DC breakdown characteristics of positive-point-plane gaps due to varying concentrations of NO_x, CO_2 and H_2O in air and intensity of irradiation *J. Phys. D: Appl. Phys.* **15** 1217-25
39. Gosho Y and Harada A 1982 A new technique for detecting initial electrons by using Geiger counter region of positive corona *Proc. 7th Int. Conf. on Gas Discharges and Applications* (London) 193-5
40. Gosho Y and Saeki M 1987 Triggering of dc positive corona by pulsed UV irradiation *J. Phys. D: Appl. Phys.* **20** 526-9
41. Hartmann G and Gallimberti I 1975 The influence of metastable molecules on the streamer progression *J. Phys. D: Appl. Phys.* **8** 670-80
42. Hepworth J K Klewe R C and Tozer B A 1972 The effect of charged particles on impulse corona and breakdown in divergent field gaps *Proc. Int. Conf. Gas Discharges* (London) 227-9
43. Hõrrak U Iher H Luts A Salm J Tammet H 1994 Mobility spectrum of air ions at Tahkuse Observatory *J.Geophys.Res.* **99** 10 697-700
44. Kip A F 1939 Onset Studies of Positive Point-to-Plane Corona in Air at Atmospheric Pressure *Phys. Rev.* **55** *549-56*
45. Kudu K 1960 *About the initial stage of point-discharges in air* (Tartu) 56 p. (in Russian)
46. Kudu K and Veimer V 1970 On conditions of the positive corona streamer appearance *Trans. Tartu State University* **240** *221-33* (in Russian)
47. Kudu K 1980 Some possible applications of a streamer counter *Proc. 6th Int. Conf. on Gas Discharges & Applications* (Edinburgh Heriot-Watt University Press) **1** 275-8
48. Kudu K Lågstad I H and Sigmond R S 1998 Positive point-to-plane corona discharge forms in O_2-N_2 mixtures *Czechoslovak J. Phys.* **48** *1180-92*
49. Kulikovsky A A 1997 Positive streamer between parallel plate electrodes in atmospheric pressure air *J. Phys. D: Appl. Phys.* **30** 441-50
50. Kulikovsky A A 2000a The role of the absorption length of photoionizing radiation in streamer dynamics in weak fields: a characteristic scale of ionization domain *J. Phys. D: Appl. Phys.* **33** L5-7

51. Kulikovsky A A 2000b The role of photoionization in positive streamer dynamics *J. Phys. D: Appl. Phys.* **33** 1514-24
52. Laan M and Paris P 1992 Formation of corona pulses *9th Symp. on Elementary Processes and Chemical Reactions in Low Temperature Plasma* Invited papers (Small Carpathy, Slovakia) 201-16
53. Laan M and Paris P 1994 The multi-avalanche nature of streamer formation in inhomogeneous fields *J. Phys. D: Appl. Phys.* **27** 970-8
54. Levitov V I 1975 *The AC corona. Problems of theory, methods of investigation and experimental characteristics* (Moscow) 280 p. (in Russian)
55. Loeb L B 1965 *Electrical Coronas: Their Basic Physical Mechanisms* (Berkeley and Los Angeles: University of California Press) 694 p.
56. Lowke J J 1992 Theory of electrical breakdown in air – the role of metastable oxygen molecules *J. Phys. D: Appl. Phys.* **25** 202-10
57. Luts A and Salm J 1994 Chemical composition of small atmospheric ions near the ground *J.Geophys.Res.* **99** 10 781-5
58. Luts A 1995 Evolution of negative small ions at enhanced ionization *J.Geophys.Res.* **100** 1487-96
59. Martinez P and Brandvold D K 1996 Laboratory and field measurements of NO_x produced from corona discharge *Atmospheric Environment* **30** 4177-82
60. McAllister I W Crichton G C and Bregnsbo E 1979 Experimental study on the onset of positive corona in atmospheric air *J. Appl. Phys.* **50** 6797-805
61. Miller R W 1989 *Flow Measurement Engineering Handbook* 2nd edn (New York: McGraw-Hill) 1073 p.
62. Miyoshi Y and Hosokawa T 1973 The formation of a positive corona in air *J. Phys. D: Appl. Phys.* **6** 730-3
63. Mohr E I and Weissler G L 1947 Positive Corona in Freon-Air Mixtures *Phys. Rev.* **72** 294-7
64. Morrow R 1997 The theory of positive glow corona *J. Phys. D: Appl. Phys.* **30** 3099-114
65. Nasser E 1971 *Fundamentals of Gaseous Ionization and Plasma Electronics* (New York) 456 p.
66. Nagato K and Ogava T 1998 Evolution of tropospheric ions observed by an ion mobility spectrometer with a drift tube *J. Geophys. Res.* **103** 13 917-25
67. Naidis G V 1997 Modelling of plasma chemical processes in pulsed corona discharges *J. Phys. D: Appl. Phys.* **30** 1214-8
68. Pancheshnyi S V Starikovskaia S M and Starikovskii A Yu 2001 Role of photoionization processes in propagation of cathode-directed streamer *J. Phys. D: Appl. Phys.* **34** 105-15
69. Paris P 1994 Initiation of corona pulses PhD thesis (University of Tartu) 145 p.
70. Pedersen A 1989 On the electrical breakdown of gaseous dielectrics *IEEE Trans. on Electrical Insulation* **24** 721-39

71. Penney G W and Hummert G T 1970 Photoionization Measurements in Air, Oxygen, and Nitrogen *J. Appl. Phys*. **41** 572-7
72. Peyrous R and Lapeyre R-M 1982 Gaseous products created by electrical discharges in the atmosphere and condensation nuclei resulting from gaseous phase reactions *Atmospheric Environment* **16** 959-68
73. Phelps A V and Pack J L 1961 Collisional detachment in molecular oxygen *Phys. Rev. Lett.* **6** 111-3
74. Radsig A A and Smirnov B M 1980 *Handbook of atom- and molecular physics* (Moscow: Atomizdat) 240 p. (in Russian)
75. Raether H 1964 *Electron Avalanches and Breakdown in Gases* (London: Butterworths) 191 p.
76. Raizer Yu P 1987 *Gas discharge physics* (Moscow) 591 p. (in Russian)
77. Rees J A 1978 Fundamental processes in the Electrical Breakdown of Gases In: *Electrical Breakdown of Gases* ed J M Meek and J D Craggs (Wiley) 1-128
78. Reess Th Ortega P Gibert A Domens P and Pignolet P 1995 An experimental study of negative discharge in a 1.3 m point-plane air gap: the function of the space stem in the propagation mechanism *J. Phys. D: Appl. Phys.* **28** 2306-13
79. Roos H and Hilpus A 1977 On the possibility of using a gas discharge counter of ions for the detection of small halogen concentrations in the air *Acta Comment. Universitatis Tartuensis* **409** 73-83 (in Russian)
80. Rusanov V D and Fridman A A 1984 *Physics of chemically active plasma* (Moscow) 415 p. (in Russian)
81. Salm J 1993 Ions of the near-Earth layer of the atmosphere In: *Plasma chemistry* (Moscow: Energoatomizdat) 194-217 (in Russian)
82. Samoilovitsh V G Gibalov V I and Kozlov K V 1989 *Physical chemistry of barrier discharge* (University of Moscow) 175 p. (in Russian)
83. Serdyuk Yu V Larsson A Gubanski S M and Akyuz M 2001 The propagation of positive streamers in a weak and uniform background electric field *J. Phys. D: Appl. Phys.* **34** 614-23
84. Sigmond R S 1978 Corona discharges In: *Electrical Breakdown of Gases* ed J M Meek and J D Craggs (Wiley) 319-84
85. Sigmond R S and Goldman M 1983 Corona Disharge Physics and Application In: *Electrical Breakdown and Discharges in Gases* **89B** (New York) 1-64
86. Sigmond R S 1983 Basic corona phenomena: the roles of space charge saturation and secondary streamers in breakdown *Proc. 16th Int. Conf. on Phenomena in Ionized Gases* Invited papers (Düsseldorf, Germany) 174-86
87. Sigmond R S 1984 The residual streamer channel: Return strokes and secondary streamers *J. Appl. Phys.* **56** 1355-69
88. Sigmond R S 1989 Mass transfer in corona discharges *Rev. Int Hautes Temp. Réfract.* **25** 201-6

89. Sigmond R S Goldman A and Goldman M 1992 Ring vortex gas flow in negative point coronas *Proc. 10th Int. Conf. on Gas Discharges and their Applications* (Swansea, UK) 330-3
90. Sigmond R S and Lågstad I H 1993 Mass and species transport in corona discharges *High Temp. Chem. Processes* **2** 221-9
91. Smirnov B M 1978 *Negative ions* (Moscow: Atomizdat) 176 p. (in Russian)
92. Spyrou N Held B Peyrous R Manassis Ch and Pignolet P 1992 Gas temperature in a secondary streamer discharge: an approach to the electric wind *J. Phys. D: Appl. Phys.* **25** 211-6
93. Tammet H 1996 Atmospheric electricity. Air ions *CRC Handbook of Chemistry and Physics 77th edn* ed Lide D R and Frederikse H P R (Boca Raton: CRC) **14** 30-2
94. Trichel G W 1938 The Mechanism of the Negative Point to Plane Corona Near Onset *Phys. Rev.* **54** *1078-84*
95. Trichel G W 1939 The Mechanism of the Positive Point-to-Plane Corona in Air at Atmospheric Pressure *Phys. Rev.* **55** *382-90*
96. Teich T H 1967 Emission of gasionizing radiation from electron avalanches *Z. Phys.* **199** 378-410 (in German)
97. Vaska M 1960 The streamers of positive corona as an indicator of halogens Diploma thesis (University of Tartu) 37 p. (in Estonian)
98. Waters R T Jones R E and Bulcock C J 1965 Influence of atmospheric ions on impulse corona discharge *Proc. IEE* **112** 1431-8
99. Waters R T Rickard T E and Stark W B 1972 Electric field measurements in D.C. corona discharges *IEE Int. Conf. Gas Discharges 188-90*
100. Waters R T 1978 Spark Breakdown in Non-uniform Fields In: *Electrical Breakdown of Gases* ed J M Meek and J D Craggs (Wiley) 385-532
101. Wetzer J M and Wen C 1991 Different avalanche types in electronegative gases *J. Phys. D: Appl. Phys.* **24** 1964-73
102. Zheleznyak M B Mnatsakanian A Kh and Sizykh S V 1982 Photoionization of nitrogen-oxygen mixtures by radiation of gas discharge *Teplofiz. Vysokih Temp.* **20** 423-8 (in Russian)
103. Zhou P 1993 *Numerical Analysis of Electromagnetic Fields* (Berlin: Springer) 406 p.

ACKNOWLEDGEMENTS

First, I am indebted to associated professor Kalju Kudu, the founder and long time leader of the Gas Discharge Laboratory, who fostered my interest in gas discharge physics and brought me into the Gas Discharge Laboratory. Furthermore, he was the man who first got the idea to use streamer corona under combined voltage for detection of trace gases.

I am greatly indebted to my supervisor Dr. Ants Haljaste and Dr Märt Aints for their advises, suggestions and discussion during my studies.

I want to express my sincere thanks to the whole Gas Discharge Laboratory for a pleasant working atmosphere and moral support throughout all these years.

My deepest gratitude belongs to my family for their continuos support and encouragement.

The Estonian Science Foundation has financed this work under the grants 88, 3024 and 4518. Support was received also from the EU Copernicus Grant CIPA-CT94-0186. All these grants are gratefully acknowledged.

PUBLICATIONS

I

Aints M Haljaste A Kudu K and Plank T
Repetition rate of streamers as a measure of content of electronegative additives in the air *J. Phys. D: Appl. Phys*. (1997) **30** 210-20
http://www.iop.org/Journals/JPhysD

J. Phys. D: Appl. Phys. **30** (1997) 210–220. Printed in the UK PII: S0022-3727(97)74871-X

Repetition rate of streamers as a measure of content of electronegative additives in the air

M Aints, A Haljaste, K Kudu and T Plank

Institute of Experimental Physics and Technology, University of Tartu, EE2400 Tartu, Estonia

Received 8 May 1996, in final form 29 August 1996

Abstract. This paper demonstrates that the positive streamer corona may be useful for the detection of electronegative impurities in gas (ambient air). The measurements of the repetition rate of streamers are carried out in a point-to-coaxial cylinder gap where DC voltage and AC voltage at a frequency of up to some kilohertz (the so-called 'mixed voltage') are applied simultaneously. The repetition rate of streamers is investigated depending on the airflow rate, on the amplitude and frequency of the AC voltage, on the level of gas preionization and on the amount of moisture and impurities of different kinds in air. Results presented in the form of counting-rate characteristics of streamers show that under the action of halogens (I_2, Cl_2) the detectable changes in characteristics take place if the halogen concentration exceeds 1–10 ppb. Principles of operation of the proposed detector and possible basic physical mechanisms of the influence of impurities on the counting response are discussed. It has been demonstrated that a simple statistical model for the inception of streamers under the conditions of a mixed voltage enables calculation of the counting-rate characteristics of streamers in satisfactory agreement with the experimental results.

1. Introduction

There exists an urgent need for fast-response but simple and inexpensive detectors of electronegative noxious impurities in process gases or in ambient air. Well known methods of chemical analysis are mostly time consuming and inconvenient. Those based on absorption of light or on mass spectrometry require quite complicated and costly equipment [1]. Interesting possibilities arise when one attempts to use properties of corona discharges in this field. For example, it is widely admitted that the voltage range of the positive onset streamers of the DC corona and their number per unit time depend on the geometry of the discharge gap as well as on the properties of the filling gas [2, 3]. The properties in question are pressure and temperature, velocity of the gas flux, the preionization level and the chemical composition of the gas.

Andersson and Hertz [4] made the first known attempt to use the repetition rate of DC corona streamers in practice. They tried to measure humidity in the air.

A modified technique to estimate the humidity or concentration of halogen in air was developed by Kudu [5], who suggested a simultaneous application of a DC voltage and an AC voltage of 50 Hz frequency to the gap. The main advantage of this kind of mixed voltage is the appearance of a plateau on the counter characteristic curve. Owing to the plateau the results of the fixed-point measurements in the centre of the plateau are practically insensitive to possible variations in pressure and temperature of the ambient air.

The aim of our measurements at a mixed voltage is to investigate the dependence of the counting rate versus voltage characteristics of streamers on different factors—the amplitude and frequency of the AC voltage, the airflow rate, the level of preionization, and the gas composition. We discuss the physical processes that could affect the shapes of counting-rate characteristics.

2. Experimental set-up

A sketch of the experimental set-up is presented in figure 1.

The air under test entered the air channel of the device through an electric filter formed by the pipeline and a coaxially arranged rod electrode (1). The filter blocked the passage of primary air ions. Subsequently the preionization level was driven to a desired value using an α-active source (2) or a corona ionizer (3). The preionization level was adjusted in steps by orifice plates of different apertures D in front of the α-source.

It is common to use preferably radioactive sources as sources of ions in various instrumentations. Unfortunately, such instrumentation requires certification and regular leak tests according to governmental standards in force [6]. To avoid these inconveniences we investigated the potential of a corona ionizer to be used as an adjustable nonradioactive

0022-3727/97/020210+11$19.50

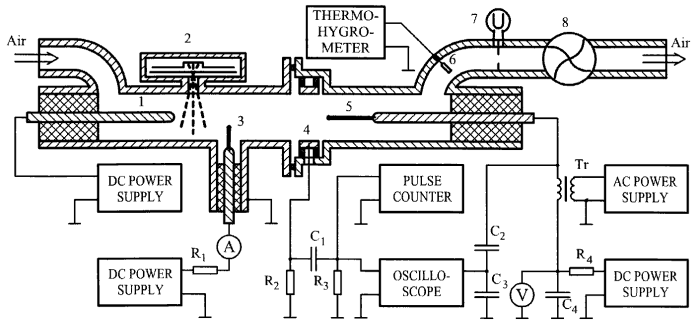

Figure 1. Schematic diagram of the experimental apparatus.

human-friendly alternative. The negative corona was excited on a conically tipped platinum wire (3) of 0.2 mm in diameter. Here setting the preionization level was achieved by adjustment of the current intensity of the negative corona.

The preionized air was directed to the positively stressed point electrode (5) of the main discharge gap. By 'preionization level' we mean fixed values Φ of the flux of negative ions in the cross section of the air channel just at the tip of the point electrode (5). To determine the preionization level dependence on the aperture of the orifice plates, on the current intensity of the corona ionizer, and on the airflow rate the thin point electrode (5) was replaced by a rod of 3 mm in diameter. The ion current collected by the rod was measured to estimate the degree of preionization. During these measurements the potential of the stressed rod was kept low (+100 V) to avoid ionization phenomena.

During the corona investigations the electrode (5) was a hemispherically capped platinum wire of 0.2 mm in diameter and 15 mm in length anchored to a rod of 5 mm in diameter. The opposite electrode was formed by walls of the air channel, a metallic pipeline of 10 mm in inner diameter. A part of the pipeline was electrically insulated to form a signal electrode (4) for the detection of corona pulses at the point electrode.

A high DC voltage was applied to the point electrode through the secondary winding of a transformer Tr. This allowed a stepped-up AC voltage at various frequencies (20–3000 Hz) and a DC voltage to be applied to the gap simultaneously. The DC voltage was measured to an accuracy within $\pm 0.5\%$ by an electrostatic voltmeter and the AC voltage, to an accuracy within $\pm 3\%$, by a dual-channel 100 MHz oscilloscope and a capacitance voltage divider C_2–C_3.

Pulses induced on the signal electrode (4) by a discharge were examined by an oscilloscope and counted by a pulse counter. The differentiating circuit R_2–C_1–R_3 was used for the suppression of the background induced by the AC voltage.

The humidity and air temperature were measured by a digital thermohygrometer provided with a remote capacitive transducer (6). In the range from 4 to 99% relative humidity the error was $\pm 3\%$ of the indication. The measured temperature values exhibited an error $\pm 0.5\%$.

The airstream through the pipeline was produced and controlled using a ventilator (8). The volumetric flow rate of the airstream was measured within an accuracy of $\pm 10\%$. A differential flowmeter (7) was used [7].

The investigated agents were extracted from a cylinder (carbon dioxide), produced by the evaporation of liquid and solid substances (acetone, ethyl ether, ethanol, hydrochloric acid, sulphuric acid, nitric acid, water, iodine, etc), or they were generated by electrolysis (chlorine). The concentration of additives was calculated from the flow measurements, by weighing the evaporated quantities of agents, or by using the laws of electrolysis.

3. Experimental results

3.1. Discharge appearances at mixed voltages

We start the presentation of experimental results with a description of events observed in an oscilloscopic study of a corona at mixed voltage. An insight into the typical behaviour of the discharge was undertaken under the following conditions: (i) the AC component of the mixed voltage had a frequency 50 Hz and a peak value $U_{AC} > U_g - U_{bp}$, where U_g and U_{bp} are the onset potentials of the steady glow corona and of the burst pulses in the DC case respectively; (ii) the DC voltage U_{DC} satisfied the restriction $U_{str} - U_{AC} < U_{DC} < U_{str} + U_{AC}$ with U_{str} the onset potential of streamers in the DC case; (iii) artificial preionization was not used and the electric filter was switched off; (iv) the flow rate of the laboratory air through the discharge gap was about 0.5 l s^{-1}.

Oscillograms of the discharge current indicated the existence of discharge modes well known to researchers of DC corona. There were cycles of AC voltage during which the discharge commenced as a streamer followed by steady glow. Under these conditions no more than one streamer arose during one cycle of AC voltage. During some other cycles only steady glow was observed. It was pure chance whether a discharge arose either as a streamer or as a glow corona. Moreover, there existed a certain probability for discharge-free cycles.

A more detailed examination of oscillograms showed that a streamer arose on the positive slope of the AC wave at an instantaneous value U which was somewhat higher than the onset potential U_{str} of DC streamers. During no-streamer cycles of AC voltage the glow corona arose at an instantaneous value of mixed voltage which fell within a voltage interval applicable to burst pulses in the DC case ($U_{bp} \leq U < U_{str}$).

Lowering of the preionization level with the help of the electric filter showed that the mean repetition rate of streamers decreased with an increase in filter voltage. Increasingly dischargeless cycles of AC voltage occurred. At the same time the spread of the onset instants of streamers increased. At filter voltages sufficient to suppress the passage of most light ions, the formation of a streamer was probable even on the negative slope of the AC wave.

When the preionization level was enhanced with the help of an ionizer, the mean repetition rate of streamers passed through a maximum. If the rise in preionization continued, the repetition rate fell off to zero. When the streamers disappeared under the action of preionization, the steady glow corona was the only discharge mode observed during each period of AC voltage. The glow corona was observed at the point electrode all the time, the resultant voltage being higher than the onset potential of burst pulses ($U > U_{bp}$).

3.2. Variations of a counter characteristic curve with applied voltage

Counting-rate characteristics of streamers under a mixed voltage represent the number of streamers per unit time (the mean repetition rate) n plotted against the DC voltage U_{DC}. The peak value of the AC voltage is considered as a parameter. The relative repetition rate n/f of streamers, that is the mean repetition rate of streamers divided by the AC frequency, is laid as the ordinate in most diagrams. This facilitates a better comparison of results obtained at different AC frequencies.

All values of voltage measured in various experiments were numerically reduced to the standard conditions and the reduced data are presented below. The common procedure of reduction is described by the relation

$$U_0 = \frac{p_0 T}{p T_0} U$$

where p stands for the pressure and T for the temperature [8]. Here the subscript 0 refers to data at the standard conditions ($p_0 = 101.325$ kPa; $T_0 = 293$ K) but it is omitted below. The linear procedure of reduction ensures a scatter of reduced onset potentials less than 1% provided that variations of air density remain below 5% relative to the standard density. The shift of counting-rate characteristics along the voltage axis, which occurs due to variations of air pressure and temperature, disappears as a result of the application of the above reduction procedure. Under the standard conditions the onset potentials of the burst pulses U_{bp}, of the streamers U_{str} and of the steady corona U_g at DC voltage were 2.44, 2.52 and 2.59 kV respectively.

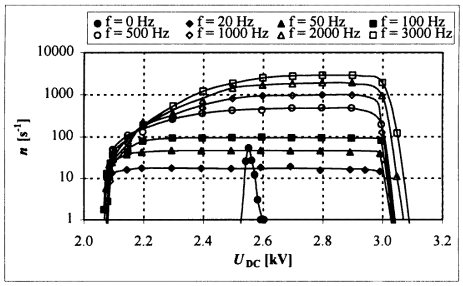

Figure 2. Counting-rate characteristics depending on the frequency of the AC voltage (U_{AC} = 480 V; V = 1 l s^{-1}; $\Phi \simeq 2.5 \times 10^5$ s^{-1}).

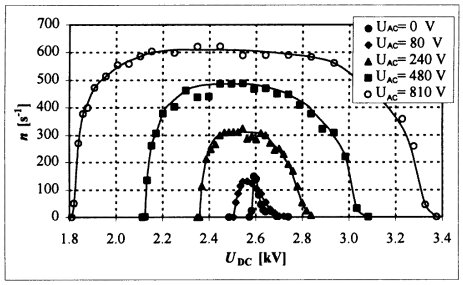

Figure 3. Counting-rate characteristics depending on the amplitude of the AC voltage (f = 1000 Hz; V = 1 l s^{-1}; $\Phi = 1.8 \times 10^6$ s^{-1}).

Figure 2 shows typical counter characteristic curves for room air in the case of seven AC frequencies provided the peak value of the AC voltage is kept constant at $U_{AC} =$ 480 V. For comparison, the counting-rate characteristic at DC voltage is also presented. Each experimental point on these graphs was obtained as an average over four sequential measurements. The duration of a single counting period was 1 s. As seen from the figure, the counter characteristic curves at mixed voltages are much wider than those at DC voltage. The width of the characteristic depends not on the frequency but on the amplitude of the AC voltage (figure 3), with a centre of characteristic lying at $U_{DC} \simeq U_{str}$.

Results in figure 2 and 3 correspond to the airflow rate $V = 1$ l s^{-1} through the discharge gap. The counting characteristics in figure 2 were recorded at the level of natural ionization ($\Phi = 2.5 \times 10^5$ s^{-1}) whereas the ionization level applicable to figure 3 was higher ($\Phi = 1.8 \times 10^6$ s^{-1}).

3.3. Effect of preionization and airflow rate

Figure 4 illustrates how the preionization level of air under test affects the counting-rate characteristics of streamers. The measurements under consideration were carried out at

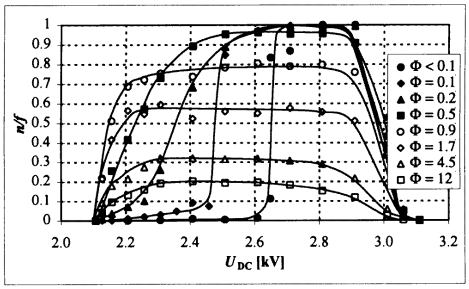

Figure 4. Counting-rate characteristics depending on the level of preionization (U_{AC} = 480 V; f = 1000 Hz; V = 1 l s^{-1}). Flux Φ of negative ions is given in units of 10^6 s^{-1}.

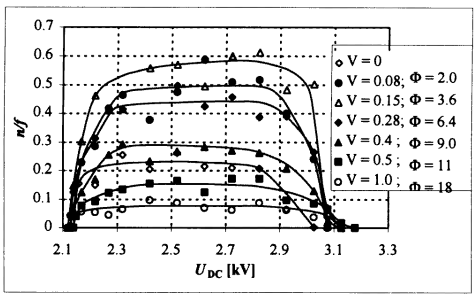

Figure 5. Counting-rate characteristics depending on the airflow rate (U_{AC} = 480 V; f = 100 Hz). Airflow rate V is given in units l s^{-1}, flux Φ of negative ions is given in units of 10^5 s^{-1}.

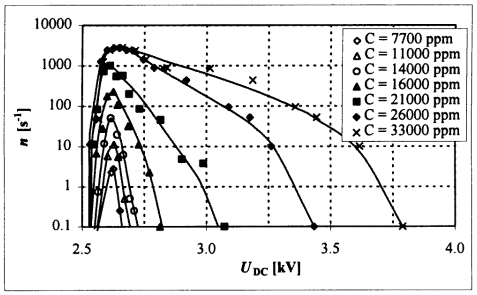

Figure 6. Counting-rate characteristics depending on the air humidity (U_{AC} = 0 V; V = 1 l s^{-1}; Φ = 1.8 × 10^6 s^{-1}).

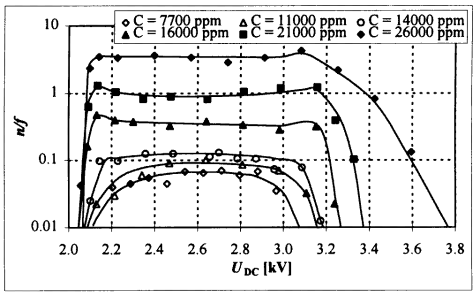

Figure 7. Counting-rate characteristics depending on the air humidity (U_{AC} = 480 V; f = 100 Hz; V = 1 l s^{-1}; Φ = 1.8 × 10^6 s^{-1}).

$f = 1000$ Hz with the energized electric filter and a corona ionizer. The filter blocked the passage of all entering ions having a mobility higher than 0.2 cm^2 V^{-1} s^{-1}.

The counting-rate characteristics at low levels of preionization ($\Phi \leq 1 \times 10^5$ s^{-1}) are extremely asymmetric. At lower values of the DC voltage the streamers occur very rarely, if at all. The oscilloscopic observations under such conditions show that often there is no discharge activity during the no-streamer cycle of the AC voltage (see section 3.1). At higher values of the DC voltage, on the contrary, the relative counting rate $n/f \simeq 1$. The asymmetry of the counting-rate characteristics emerges all the more the higher the AC frequency is. The asymmetry is reduced as the preionization level is enhanced: the repetition rate of streamers increases at lower values of the DC voltage and decreases to some extent at higher values of the DC voltage. The characteristics become nearly symmetric if the corona ionizer maintains a preionization level $\Phi \geq 1 \times 10^6$ s^{-1}. A further increase in the preionization level results in a monotonic decrease in the repetition rate of streamers to the full extent of the plateau of the counting-rate characteristic.

An example of the effect of airflow rate on the counting-rate characteristics is shown in figure 5 for $f = 100$ Hz under the proviso that the aperture of the orifice plate of the α-source is $D = 4$ mm. The airflow gives rise to an increase in the plateau of counting-rate characteristics followed by a decrease at higher flow rates ($V > 0.2$ l s^{-1}). The higher the frequency of the AC voltage, the higher are the flow rates needed to reach the maximum height of the plateau of the counting-rate characteristic for a given ionizer.

3.4. Sensitivity with respect to humidity and carbon dioxide

The absolute humidity in ambient air usually ranges from a few to 20 g m^{-3}. The atmosphere contains a little more than 0.03% of its volume as CO_2 with an allowable indoor concentration up to 0.1%. Both these agents—H_2O and CO_2—are electronegative characterized by electron affinities 0.9 and 1.11 eV respectively [9].

The counting-rate characteristics of streamers are presented over a range of humidity concentrations C = 7700–33 000 ppm (a = 5.7–24 g m^{-3}) for a DC voltage in figure 6 and for a mixed voltage in figure 7. Here the preionization level was such that in the DC case the streamers were suppressed practically completely provided

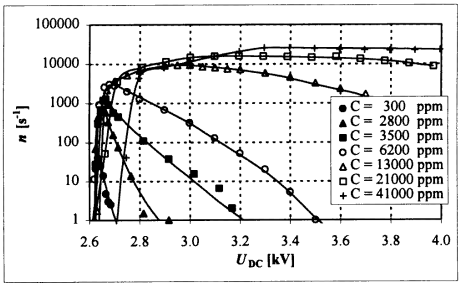

Figure 8. Counting-rate characteristics depending on the concentration of carbon dioxide (U_{AC} = 0 V; V = 1 l s^{-1}; $\Phi = 1.8 \times 10^6$ s^{-1}).

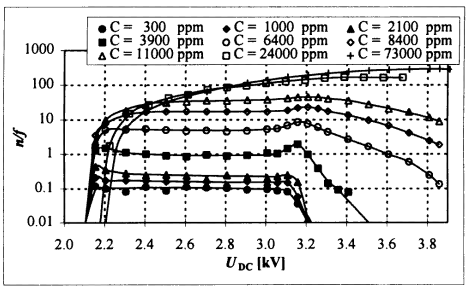

Figure 9. Counting-rate characteristics depending on the concentration of carbon dioxide (U_{AC} = 480 V; f = 100 Hz; V = 1 l s^{-1}; $\Phi = 1.8 \times 10^6$ s^{-1}).

the humidity was less than 4000 ppm. An increase in the humidity led to an increase in the repetition rate of streamers and to a broadening of the DC voltage interval for which they were observed. At a humidity level of 33 000 ppm the maximal repetition rate reached 4500 s^{-1} and the width of the voltage interval was 1.1 kV.

In the case of a mixed voltage the repetition rate of streamers also increased with the absolute humidity, but the sensitivity of the characteristics to humidity was appreciably lower.

Two or more streamers during a cycle of AC voltage were observed under conditions where the density of water vapour was higher than 20 000 ppm. The second streamer generally arose on the negative slope of the AC wave.

According to expectations carbon dioxide should have an effect comparable to that of water vapour. In practice it was verified that in the case of equal concentrations of H_2O and CO_2, higher than ∼2500 ppm, the latter agent resulted in a wider voltage region for the existence of streamers and in an appreciably higher repetition rate of streamers for both DC (figure 8) and mixed voltage (figure 9).

It can be seen clearly in figure 9 that at a mixed voltage the characteristic curve is wider the higher the concentration of CO_2. In case of medium concentrations of CO_2 the relative repetition rate of streamers is typically higher at

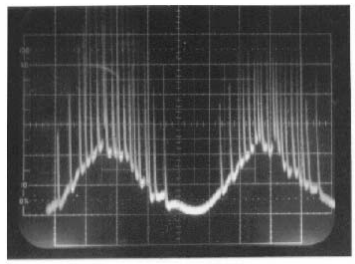

Figure 10. Distribution of streamers over AC cycles for a high concentration of CO_2 in air (U_{DC} = 3.2 kV; U_{AC} = 480 V; f = 1000 Hz; V = 0.3 l s^{-1}; $\Phi \simeq 1 \times 10^5$ s^{-1}; C_{CO_2} = 10 000 ppm). Sweep rate, 0.2 ms per division.

the beginning and at the end of the counting curve than on the plateau between these regions. The same is true for water vapour (figure 7), though the tendencies are less pronounced.

An increase in the concentration of CO_2 up to the level of 2500 ppm caused the formation of another streamer during the same cycle of the AC voltage. The higher the concentration of CO_2, the larger the number of streamers during a cycle of AC voltage. The maximal repetition rate of streamers reached 50 kHz under the reported conditions (figure 10). The oscillogram presented in figure 10 was recorded as follows. Applied to the point electrode, the AC voltage (480 V) was attenuated by the capacitance voltage divider $C_2 - C_3$ (see figure 1). The attenuated AC signal was fed to the first channel of the oscilloscope. The induced discharge current issued from the capacitive probe (4) was applied to the second channel (vertical deflection factor was 0.1 V per division). These signals were algebraically added using ADD mode of operation on the vertical amplifier system of the oscilloscope. Only the algebraic sum is displayed in figure 10. Hence, besides the distribution of streamers in time, this oscillogram carries additional information about the correlation between streamer activity and phase angle of the AC voltage.

Visual observations revealed that the rise in concentration of CO_2 is also accompanied by essential changes in the discharge structure. It is typical of a DC streamer in ambient air to start from the tip of the hemispherically capped point electrode and for the remaining part of the hemisphere to be covered by a following burst pulse. Starting positions of all subsequent streamers are the same on the hemisphere, so the stems of streamers overlap [10]. The rise in concentration of CO_2 has no effect on the described state at the outset. Beginning from a certain concentration, more and more streamers rise in zones adjacent to the point tip. Finally the streamers are distributed almost uniformly over the whole hemispherical tip of the electrode. Branching of each streamer seems to be reduced while the range of propagation is scaled down slightly. As the burst pulse following a streamer becomes weaker, the repetition rate of the streamers becomes higher. Finally the specific glow of burst pulses disappears on the point surface almost completely.

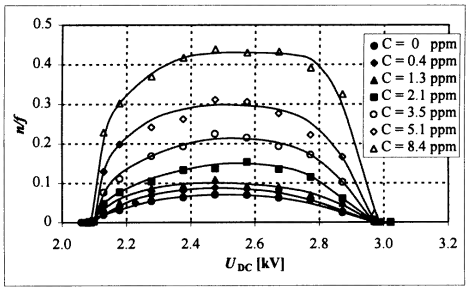

Figure 11. Counting-rate characteristics depending on the concentration of ozone (U_{AC} = 480 V; f = 1000 Hz; V = 1 l s^{-1}; $\Phi = 1.5 \times 10^7$ s^{-1}).

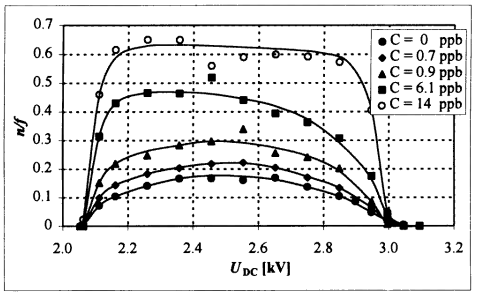

Figure 13. Counting-rate characteristics depending on the concentration of iodine (U_{AC} = 480 V; f = 1000 Hz; V = 1 l s^{-1}; $\Phi = 1.5 \times 10^7$ s^{-1}).

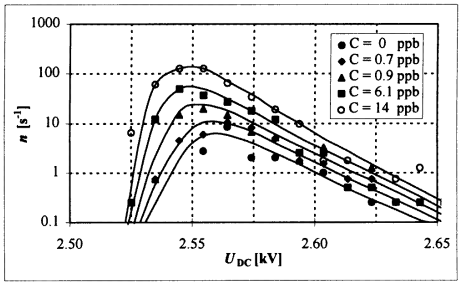

Figure 12. Counting-rate characteristics depending on the concentration of iodine (U_{AC} = 0 V; V = 1 l s^{-1}; $\Phi = 1.5 \times 10^7$ s^{-1}).

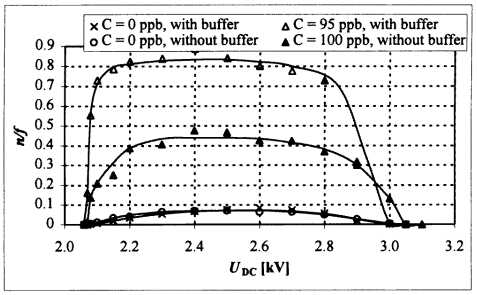

Figure 14. Influence of buffer volume on counting-rate characteristics (chlorine; U_{AC} = 480 V; f = 1000 Hz; V = 1 l s^{-1}; $\Phi = 1.5 \times 10^7$ s^{-1}).

One marked difference between the effects of water vapour and CO_2 appears in the relation of the peak value of the streamer current pulse, which is recorded by the capacitive probe ((4) in figure 1), to the concentration of these additives. The decrease in peak current with an increase in additive concentration is about four times as fast in water vapour as it is for CO_2.

3.5. Effect of strongly electronegative agents

The effects of ozone (electron affinity $EA_{O_3} = 2.1$ eV), iodine ($EA_{I_2} = 2.55$ eV) and chlorine ($EA_{Cl_2} = 2.38$ eV) on the counting-rate characteristics of streamers were investigated. Ozone was produced using a small-scale plate ozonizer and dissolved subsequently in the air stream to the required concentration. The measurements were carried out at $f = 1000$ Hz. Results are presented in figure 11. One can see that detectable changes in the repetition rate of streamers take place if the concentration of ozone is higher than 0.5 ppm.

The counting-rate characteristics of streamers were very sensitive to iodine both at DC (figure 12) and mixed voltages (figure 13). The experimental data presented were recorded at such a high preionization level ($\Phi = 1.5 \times 10^7$ s^{-1}) that under a DC voltage the repetition rate of streamers underwent a tenfold reduction in comparison with the repetition rate at the natural preionization level (see also figure 2). A detectable increase in the counting rate was recorded with a concentration of iodine as little as 1 ppb both under DC conditions and mixed voltage conditions. At the same time the width of the characteristic curves remained practically unchanged.

The sensitivity of the counting-rate characteristics regarding chlorine (10 ppb) was to some extent inferior to that for iodine.

The time of flight of ions from the ionizer to the point electrode of the test gap was varied in the chlorine experiments. This time was generally 7.5 ms for the data presented here. By adding a buffer section into the pipeline the time of flight was prolonged up to 1 s. The results are presented in figure 14. The preionization level was chosen so that the plateau of the counting-rate characteristic was a little below the level $n/f = 0.1$ under a deficiency of chlorine. The presence of the buffer section had no impact on this zero reading (figure 14). Chlorine in concentrations of 95 ppb caused the plateau to rise to the level $n/f = 0.4$ provided the time of flight was 7.5 ms. When the buffer section was made a part of the pipeline, the plateau rose to the level $n/f = 0.8$.

3.6. Some other active impurities

The influence of other impurities on the counting-rate characteristics of streamers at mixed voltage was briefly as follows.

Vapours of hydrochloric acid (HCl), nitric acid (HNO_3) and sulphuric acid (H_2SO_4) elicited a similar response as with the electronegative impurities described above. For example, under the very same conditions as in the iodine experiment, the addition of HCl at 105 ppm concentration instead of iodine increased the repetition rate of DC streamers by a factor of 10 000 and stretched the voltage range of their existence by about 1 kV. Chloroform ($CHCl_3$) also increased the repetition rate of streamers noticeably, but as a characteristic property chloroform reduced the amplitude of streamers very effectively.

Phosphoric acid (H_3PO_4), acetic acid (CH_3COOH), benzene (C_6H_6), ammonium hydroxide (NH_4OH), formalin (HCHO), and camphor ($C_{10}H_{16}O$) also increased the probability of formation of streamers. However, their impacts on the counting-rate characteristics were less pronounced than those of the substances listed above.

Ethyl ether ($C_2H_5OC_2H_5$) and ethyl acetate ($C_4H_8O_2$) caused an opposite effect to that described above: they reduced the repetition rate of streamers.

Finally, the counting-rate characteristics showed no response to vapours of ethyl alcohol (CH_3CH_2OH) and butyl alcohol ($CH_3CH_2CH_2CH_2OH$).

4. Discussion

4.1. Rise of streamers at mixed voltage

Under a mixed voltage and flowing gas conditions the behaviour of a corona discharge shows some notable peculiarities. They can be explained by the model described below.

Let us consider the applied mixed voltage $U = U_{DC} + U_{AC}$ plotted against time in figure 15. The onset potentials are indicated for burst pulses (U_{bp}), onset streamers (U_{str}), and steady glow corona (U_g) under DC conditions. The resultant voltage U traverses the regions $\Delta U_{bp} = U_{str} - U_{bp}$ and $\Delta U_{str} = U_g - U_{str}$ of DC burst pulses and streamers.

Let us begin with an examination of the operation of the experimental device under conditions where the air passing through the corona gap has not been previously mixed with additives. Hence the voltage regions ΔU_{bp} and ΔU_{str} are quite narrow (see section 3.2). Triggering electrons are assumed to appear due to electron detachment from negative ions.

If the applied voltage is higher than the onset potential of burst pulses U_{bp} and a negative ion falls into the active zone before the voltage has exceeded U_{str}, then there is a certain probability for detachment and for the rise of a burst pulse. The space charge of the burst pulse prevents the rise of a streamer for some time. During this time interval the instantaneous value of the mixed voltage exceeds the onset potential U_g of the steady glow corona. It stands to reason that the discharge continues as a steady glow corona. When the mixed voltage traverses down the region of DC streamers ΔU_{str}, the formation of a streamer is still impossible. Now the preventive effect is due to the space charge produced by the steady glow corona. Consequently, if a burst pulse arises during a time interval Δt_{bp}, when $U_{bp} \leq U < U_{str}$, then the formation of a streamer is impossible during the same cycle of AC voltage.

If no free electron appears in the active zone during the time interval Δt_{bp}, then a burst pulse does not arise. The appearance of a negative ion at a voltage higher than U_{str} means that (with very high probability) the discharge is set off as a streamer. The streamer is followed by a burst pulse that has a high chance of turning into a steady glow. Again, this steady glow rules out the formation of another streamer during this AC cycle. Hence, during each period only one or no streamer can arise.

At low preionization levels the dischargeless cycles of AC voltage (see section 3.1) are due to a lack of triggering electrons. There is a low probability that during a relatively short time interval Δt_{bp} a negative ion will fall into the active zone. More probably an ion finds itself there over a considerably longer time interval when $U > U_{str}$ (see figure 15). This is why at low preionization levels the probability of rise of either a burst pulse or a streamer tends to favour production of a streamer.

The described model could be summarized as follows. During each cycle of AC voltage the mixed voltage traverses up and down the regions of burst pulses, streamers and steady glow corona. The rise of a discharge as a burst pulse or a streamer is a matter of chance. It depends on the presence of an appropriate triggering electron, that is on the presence of a negative ion able to undergo detachment. The formation of a burst pulse during Δt_{bp} excludes the rise of a later streamer during the same cycle of AC voltage.

4.2. Mechanisms responsible for the influence of gaseous electronegative agents on the repetition rate of streamers in airflux

At low preionization levels the repetition rate of streamers increases with preionization level (see figure 4), because the number of dischargeless cycles of AC voltage decreases. This decrease takes place due to the increase in the number of negative ions (triggering electrons). Hence the recorder of the repetition rate of streamers operates essentially in the mode of a usual Geiger counter under conditions of mixed voltage. The Geiger mode is well suited to estimate the ionization degree by means of streamer repetition rate. In this mode the repetition rate is only weakly affected by small amounts of electronegative additives. The probability of rise of a streamer is slightly dependent on whether the triggering electron appears due to detachment from an O_2^- ion or from an ion of a significantly more electronegative substance.

If the preionization level is enhanced so as to raise the probability of burst pulses above that of streamers, then the recorder of the repetition rate of streamers operates in a reverse mode to that of a Geiger counter, that is a growth in the preionization degree results in a decrease in the repetition rate of streamers [11]. The essential difference in comparison with the Geiger mode lies in the

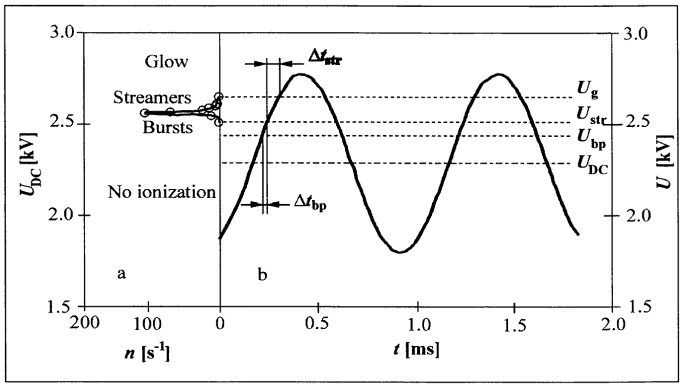

Figure 15. Counting-rate characteristic for DC voltage (*a*) and mixed voltage (*b*).

influence of the ion composition (besides the preionization level) on the repetition rate of streamers. If strongly electronegative impurities are present in air, their negative ions are formed. The detachment probability for these ions is essentially less than that for the negative ions of molecular oxygen. Hence, in the voltage range $U_{bp} \leq U < U_{str}$ the number of potential triggering electrons decreases and thus the probability of the appearance of a burst pulse is reduced. Consequently the probability of the appearance of streamers increases with an increase in the concentration of an electronegative additive. This phenomenon forms the basis for the detection of electronegative trace gases using the repetition rate of streamers.

It is expedient to treat the ion–molecular processes in two space regions separately. The first of the regions is formed by the section of the pipeline between the ionizer and the active zone of the main discharge gap. The active zone is considered to be the second region.

The preliminary negative ions are mainly the molecular ions of oxygen O_2^- formed in three-body collisions in a region in which the field is very low. In the first space region a conversion of negative ions takes place, so this region may be called the conversion zone. Various complex ions are formed there. Their composition spectrum and concentrations depend on the time given for the transition of ions through the conversion zone. Some of the molecules of the strongly electronegative additive will collide either with some oxygen molecular ions or with some complex ions. New very stable negative ions are formed with participation of the additive. This happens as a result of a probable charge transfer or due to some other reaction of conversion. Electrons attached to such molecules are then unavailable as triggering electrons.

If the concentration of an electronegative additive is very low, then its effect is reduced to the dependence of the number density of triggering electrons on the number density of additive ions. The presence of an electronegative additive has no effect on the development of an already initiated discharge pulse.

It follows from the above discussion that under the condition of a fixed flow rate the repetition rate of streamers as a measure of the content of electronegative additives should depend on the volume of the pipeline between the ionizer and the point electrode, that is on the time allowed for conversion reactions. The experiments carried out with a buffer section (see figure 14) corroborate this conclusion. They show that a lengthening of conversion time indeed results in an increase of sensitivity to a strongly electronegative additive. Consequently the detection limit of the streamer counter is improved for strongly electronegative impurities the more ions are converted into impurity ions.

If the concentration of an additive is so high that the composition of the gas is essentially altered, then processes which are negligible for low concentrations of the additive may produce a marked effect on the repetition rate of streamers.

In the active zone the effectiveness of secondary mechanisms, which maintain the development of burst pulses, seems to be altered substantially. This is probably the primary reason why, in the case of higher concentrations of CO_2 and several other additives, the DC voltage interval of streamers expands, the intensity of burst pulses is reduced, and many streamers arise during the same cycle of the AC voltage. The probable relevant physical mechanisms are dissociation of additive molecules (photodissociation at the outer boundary of the active zone and dissociative attachment within the active zone) and changes in length of the photoabsorption mean free path. The weak maxima at the beginning and at the end of counting-rate characteristics, observed both at higher concentrations of water vapour and in CO_2 concentrations in the range of 2100–11 000 ppm (see figure 9), have analogous backgrounds. These maxima appear under conditions where one of the extreme values of voltage falls into the voltage interval ΔU_{str} of DC streamers. In such a case the mixed voltage stays in the above voltage region for a long time, hence more streamers are recorded.

4.3. Dependence of the counting rate on the operating conditions of a counter

The mean repetition rate of streamers is determined by a number of state variables (peak value and frequency of the AC voltage, airflow rate, preionization level, etc). Physical mechanisms responsible for the effect of some state variables are discussed below.

Proceeding from the above principles of operation of an experimental device, it is easy to come to the conclusion that at mixed voltages the width of a counting-rate characteristic ΔU_{CRC} has to be nearly equal to the peak-to-peak value of the AC voltage: $\Delta U_{CRC} \simeq 2U_{AC}$. Under such conditions that $\Delta U_{str} \ll U_{AC}$ and during one cycle of the AC voltage no more than one streamer could arise. A more exact consideration of experimental results gives $\Delta U_{CRC} = 2U_{AC} - \Delta U'$. Here $\Delta U' \leq \Delta U_{bp}$ indicates how much the mixed voltage has to sink below the level of U_{str} to interrupt the glow corona for a while at a given frequency of the AC voltage.

If the restriction $\Delta U_{str} \ll U_{AC}$ is not satisfied and more than one streamer may arise during one cycle of the AC voltage under conditions of high concentration of additives, the width of a counting-rate characteristic appears to be $\Delta U_{CRC} = 2U_{AC} + \Delta U_{str} - \Delta U''$. Here $\Delta U''$ indicates how much the mixed voltage has to sink below the level of U_g to restore the conditions for streamers to penetrate through the glow. Thus in the general case the constraint on the width of a counting-rate characteristic may be represented as $(2U_{AC} - \Delta U_{bp}) \leq \Delta U_{CRC} < (2U_{AC} + \Delta U_{str})$.

If $U_{AC} \gg \Delta U_{bp} + \Delta U_{str}$ and U_{DC} is close to U_{bp} or U_{str}, then the time Δt_{bp} of the growth of mixed voltage through a narrow voltage interval ΔU_{bp} (see section 3.1, figures 2, 3, and 14) varies little with DC voltage. This is the reason for the emergence of the plateau on the characteristic curves under mixed voltage conditions. If the peak value of the AC voltage should be increased, then the resultant voltage traverses the region of burst pulses more swiftly. The probability of the appearance of burst pulses decreases, that of streamers increases both in the case of high (figure 3) and low preionization levels, and as a result the height of the plateau on the characteristic curve of the counter increases.

Increases in the AC frequency produce directly opposite effects depending on whether the preionization level is high or low: in the first case the formation probability of a streamer increases with frequency (compare curve $U_{AC} = 480$ V in figure 3 with that of $V = 1.0$ l s^{-1} in figure 5); in the second case it diminishes (see figure 2). An explanation of such a phenomenon is as follows. The rise in frequency means that the resultant voltage traverses a given voltage interval faster the higher the frequency. Thus, in the case of a high preionization level, the explanation given above for the increase in the probability of formation of streamers with increases in peak AC voltage remains in force when we increase the AC frequency. The decrease in the streamer formation probability with AC frequency at a low preionization level is due to a lack of primary particles, so that during some cycles of the AC voltage no discharge arises. Consequently, when increasing the AC frequency under conditions of high preionization intensity, it is still necessary to increase the preionization intensity if the height of the plateau on the counting-rate characteristic remains at the former level.

The airflow performs four tasks in the experimental device:

(1) it transports the gas (air) under investigation into the corona gap;

(2) it controls, through the flow rate, the concentration of an additive when the air is prepared for the test by mixing of two fluxes;

(3) it controls the preionization level by means of the flow rate;

(4) it should remove residual products of a discharge pulse before the next one arises.

The changes in the counting rate of streamers resulting from variations in the airflow rate (see figure 5) may have the following interpretation.

Under no-flow conditions the repetition rate of streamers is governed by the speed of clean-out of the positive space charge under the action of an electric field, and by the presence of suitably located triggering electrons (negative ions) at the right instants of time. The ionizer has no effect. A faint airflux reduces the space charge near the point electrode, hence its inhibitory effect on the rise of streamers. The repetition rate of streamers increases. Simultaneously the effect of ionizer as an ion source increases nearly proportionally with the airflux. The number density of negative ions, and consequently that of triggering electrons, increases at the boundary of the active zone. At flow rates higher than 0.2 l s^{-1} the device goes into reverse Geiger counter mode. Accordingly the formation probability for burst pulses rises and that for streamers decreases with further increases in the airflow rate (figure 5).

Short-wave radiation of a discharge in the described corona device gives rise to problems similar to those which occur in a Geiger counter [2]. For example, at low levels of preionization the explicit asymmetry of the counting-rate characteristics of streamers (see figure 4) is above all due to the enhanced positive feedback between streamers at higher values of the DC voltage U_{DC}. This positive feedback could be caused by negative ions formed due to the attachment of photoelectrons to electronegative molecules in the stagnant air layer in the immediate vicinity of the cathode. The photoelectrons are produced by the photoeffect on the cathode.

4.4. The mathematical interpretation of a counting-rate characteristic of streamers

According to the model presented in section 4.1 the counting rate of streamers is given by the probability of detachment in the active zone as well by the mutual relationship of probabilities of subsequent events (that is, formation of a burst pulse or a streamer). In the simplest case this relationship can be phrased in the following way: the rise of a burst pulse during Δt_{bp} rules out the possibility of a streamer during the relevant period of

the AC voltage. Thus the counting-rate characteristic of streamers is a representation of a probabilistic process and so it is mathematically describable as follows.

Suppose Φ is a stationary flux of negative ions reaching the tip of the point electrode. B and S are the probabilities that a negative ion, entering the active zone at a given instantaneous value of the applied mixed voltage, undergoes detachment and initiates a burst pulse or a streamer respectively. Let Q denote the probability of rise of a streamer during a particular cycle of the AC voltage. This can be presented as a product of two probabilities:

$$Q = Q_1 Q_2.$$

Here

$$Q_1 = \exp\left(- \Phi \int_{\Delta t_{bp}} B \, \mathrm{d}t \right)$$

is the probability that no burst pulse arises in the time interval Δt_{bp} during which the instantaneous values of the mixed voltage lie within the limits $U_{bp} \leq U < U_{str}$. The second factor

$$Q_2 = 1 - \exp\left(- \Phi \int_{\Delta t_s} S \, \mathrm{d}t \right)$$

gives the probability that a streamer arises in the time interval Δt_s during which $U > U_{str}$. For a given configuration of electrodes the probabilities B and S depend on the type of ions and on the instantaneous value of the mixed voltage only. Therefore B and S may be represented as functions of time. The time intervals Δt_{bp} and Δt_s may be calculated simply, if the onset potentials U_{bp}, U_{str}, and U_g of different discharge modes are known, and the frequency f and peak value U_{AC} of the AC voltage as well the value U_{DC} of the DC voltage are given.

Taking into account that the streamer rise probability increases rapidly with the increase of voltage above the onset potential of streamers, the probability S may be taken to be approximately unity for $U \geq U_{str}$. The determination of the voltage dependence of the probability B calls for suitable experiments. If no experiments are carried out, then it is possible to operate in a first approximation on the average probability $\bar{B}$ over the time interval Δt_{bp}. On these assumptions the counting rate of streamers is given by the expression

$$n/f \equiv Q = [1 - \exp(-\Phi \Delta t_s)] \exp(-\Phi \bar{B} \Delta t_{bp}).$$

Under conditions of high-rate preionization the factor $1 - \exp(-\Phi \Delta t_s) \simeq 1$ and hence

$$n/f = \exp(-\Phi \bar{B} \Delta t_{bp}).$$

The derived equation enables us to calculate the counting-rate characteristics of streamers. Experimental values of the flux Φ specified in figure captions should be considered only as upper limits of the flux Φ of negative ions hitting the point tip under fixed conditions. This is the reason why we have used the product of Φ and $\bar{B}$, instead of $\bar{B}$ only, to calibrate the computed counting-rate characteristics. The calibration could be carried out at an arbitrary point of an experimental characteristic.

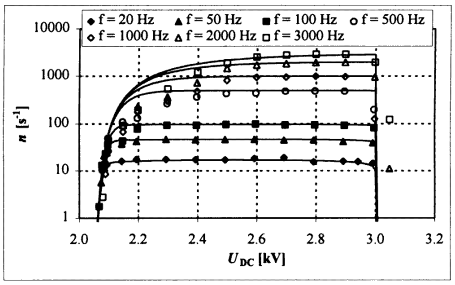

Figure 16. Measured and calculated counting-rate characteristics depending on the amplitude of the AC voltage (f = 1000 Hz; V = 1 l s^{-1}; $\Phi = 1.8 \times 10^6$ s^{-1}).

The counting-rate characteristics, computed under the conditions of figure 2 according to the above statistical model, are presented in figure 16. The points correspond to experimental data (see figure 2) and the full curves depict the counting-rate characteristics computed according to the above model. The results of the computation are in satisfactory agreement with those of the experiment. The most likely reasons for discrepancies may be: (i) neglect of the voltage dependence of probabilities B and S; (ii) the inadequacy of the model in the region of higher values of the DC voltage, where the instantaneous values of the mixed voltage do not drop below the onset potential of burst pulses; (iii) variations in the intensity of the ion flux, which may be interpreted as being caused by a feedback between successive streamers, etc.

An electronegative additive affects the shape of the counting-rate characteristic through probabilities B and S.

4.5. Conclusions

A simple corona device constructed for the detection of electronegative additives in air was investigated under different conditions of operation. The counting-rate characteristics of streamers, that is the curves representing the repetition rate of streamers as a function of the applied DC or mixed (DC + AC) voltage, were recorded to detect changes in the gas medium. The study has shown the following.

(1) The repetition rate of streamers is related to the concentration of electronegative molecules and their affinities.

(2) The effect of electronegative impurities in ambient air can be investigated using the counting-rate characteristics of corona streamers.

(3) The counting-rate characteristics of streamers have wide plateaus under conditions of mixed voltage and high intensity of preionization.

(4) Halogens in air can be detected at concentrations higher than 1 ppb.

(5) High concentrations of some additives (CO_2, halogens, HCl, HNO_3) cause both a noticeable expansion

of the voltage interval in which the streamers exist and a considerable increase in their repetition rate.

(6) Calculated counting-rate characteristics give satisfactory agreement with measured characteristics.

Acknowledgments

The authors are grateful to Professor R S Sigmond and Professor M Goldman for their collaboration and support in the development of new pollution detectors. This work was financially supported by the Estonian Science Foundation under Grant 88.

References

[1] Günzler H *et al* (eds) 1980–1996 *Analytiker-Taschenbuch* vols 1–13 (Berlin: Springer)

[2] Loeb L B 1965 *Electrical Coronas: Their Basic Physical Mechanisms* (Berkeley: University of California Press)

[3] Sigmond R S and Goldman M 1983 Corona discharge physics and application *Electrical Breakdown and Discharges in Gases* ed E E Kunhardt and L H Luessen (New York: Plenum) pp 1–64

[4] Andersson N E and Hertz C H 1955 Positive Spitzenentladung als Hygrometer geringer Trägheit *Z. Ang. Phys.* **7** 361–6

[5] Kudu K 1980 Some possible applications of a streamer counter *Proc. 6th Int. Conf. on Gas Discharges & Applications* (Edinburgh: Heriot-Watt University Press) Pt 1 pp 275–8

[6] Eiceman G A and Karpas Z 1994 *Ion Mobility Spectrometry* (Boca Raton: CRC)

[7] Miller R W 1989 *Flow Measurement Engineering Handbook* 2nd edn (New York: McGraw-Hill)

[8] Razevig D V and Sokolova M V 1977 *Analysis of Onset and Breakdown Voltages of Gas Gaps* (Moscow: Energiya) in Russian

[9] Lide D R and Frederikse H P R (ed) 1994 *CRC Handbook of Chemistry and Physics* 75th edn (Boca Raton: CRC)

[10] Aints M, Kudu K and Haljaste A 1977 Investigation of the primary–secondary streamer sequence in the air *Acta Comm. Univ. Tartuensis* **443** 3–20 in Russian

[11] Andersson N E 1958 An investigation of the positive point streamer corona. Part I. The time distribution of the streamers *Arkiv Fysik* **13** 399–422

II

Plank T Haljaste A and Aints M
The after-effect of streamers of positive corona under combined voltage
J. Phys. D: Appl. Phys. (2000) **33** 2791-7
http://www.iop.org/Journals/JPhysD

J. Phys. D: Appl. Phys. **33** (2000) 2791–2797. Printed in the UK PII: S0022-3727(00)14763-1

The after-effect of streamers of positive corona under combined voltage

T Plank, A Haljaste and M Aints

Institute of Experimental Physics and Technology, University of Tartu, 51010 Tartu, Estonia

Received 16 June 2000

Abstract. The rise probabilities of positive corona streamers initiated by a flux of negative ions are investigated under the combined voltage (dc + ac) in point-to-coaxial cylinder discharge gaps in atmospheric air. A method is developed to detect and to estimate quantitatively an after-effect of the preceding streamer on the rise probability of the following one during the next cycle of the ac voltage. The method is based on the statistical analysis of sequences of streamers. The dependence of the intensity of the after-effect on dc and ac voltage, ac frequency, pre-ionization level, air humidity and airflow velocity is investigated. The causes of the after-effect of streamers are discussed.

1. Introduction

In our previous works, we have investigated physical phenomena in a streamer counter [1, 2]. The streamer counter is a corona-based device where the dependence of the repetition rate of corona streamers on the concentration of electronegative additives is used for the detection of electronegative trace gases in air [3]. Under some experimental conditions in the streamer counter, the preceding streamer changed the rise probability of the following one [1]. This after-effect of streamers complicated both the detector calibration and the interpretation of the readings.

In air, the after-effect of a discharge on the rise and development of the next discharge is usually attributed to residual ions [4, 5], chemical products (ozone, nitrous oxides, etc) [6, 7] and neutral excited species [5]. Detachment of electrons from negative ions under the influence of the applied electric field is the dominant creation process of free electrons for triggering a corona discharge [4, 5, 8–13]. The changes in rise probability of a discharge are caused mainly by the residual negative ions. They come from a discharge channel; they may be produced by a previous corona pulse due to the photoeffect at the surface of the opposite electrode or due to the photoionization of gas molecules.

Although different manifestations of the after-effect of corona pulses are widely investigated, special methods for their detection are poorly developed. Very few attempts have been made with the aim of quantifying these phenomena under controlled conditions.

This paper deals with the after-effect of a streamer upon the rise of the streamer during the next cycle of the combined (dc + ac) voltage. The main objective of this investigation was to develop a method suitable for the detection of the after-effect of streamers and quantitative estimation of its intensity. The after-effect was investigated depending on dc and ac voltage, ac frequency, airflow rate, pre-ionization level, humidity of the air, and geometry of the discharge gap. In order to clarify the physical background of the after-effect in a streamer counter, we simulated numerically the ion trajectories in the discharge gaps and measured the length of streamers. Finally, the flux of negative ions created by the previous streamer and responsible for the after-effect was calculated numerically under the assumption that ions were formed only due to the photoionization. The experimental and computed results were compared.

2. Detection of an after-effect of streamers under combined voltage: theoretical background of the method

A better understanding of the proposed method requires a brief description of some features characteristic to the discharge mechanism in a streamer counter under the combined voltage. Here, we use some oscillograms (figure 1) recorded in our experimental device (see section 3 for more information). In figure 1, the upper oscillogram represents the combined voltage, which is applied to the point electrode. Here U_{bp} denotes the onset voltage of burst pulses, U_{str} that of streamers, and U_g that of steady glow corona. Δt_{bp} is the time interval during which the resultant voltage increases from U_{bp} to U_{str}. Negative ions, created by an ionizer and carried by the air stream and by the electric field to the discharge gap, are the source of triggering electrons. Free electrons for triggering a corona discharge appear via collisional detachment from negative ions under the influence of the strong electric field near the point electrode. Due to the stochastic nature of the appearance of triggering electrons the discharge arises during each cycle either as a burst pulse or a streamer [1].

0022-3727/00/212791+07$30.00

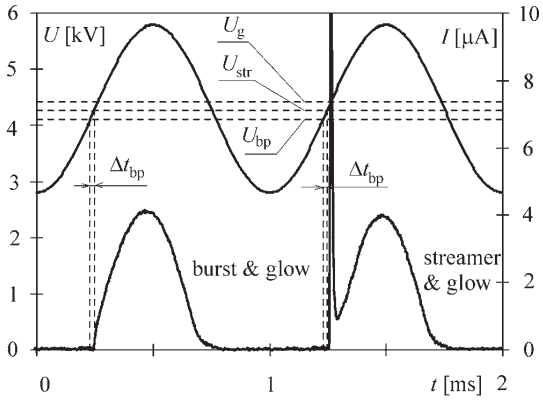

Figure 1. Typical oscillograms of applied voltage and discharge current: point diameter $d = 0.5$ mm.

A certain probability exists for the rise of a burst pulse, if an electron appears in the active zone during Δt_{bp}. The burst pulse spreads over the hemispherical tip of the point. The positive space charge of the burst pulse blocks the rise of a streamer [14, 15] for a time sufficient for the increasing voltage to reach the onset voltage of the steady glow corona, U_g. Thus, the burst pulse is transformed smoothly into the steady glow corona and no streamer is able to develop at this ac cycle. In figure 1, the first pulse in the current oscillogram corresponds to that situation.

If an appropriately placed triggering electron does not appear during Δt_{bp}, then such a later electron initiates a streamer during that ac half-cycle [1]. In figure 1, the second current pulse illustrates this case. Under the conditions of our experiments, only a single streamer arises during one ac cycle. The streamers are followed by the glow corona. The intensity of the glow corona is approximately the same, both after a burst pulse and after a streamer. The steady glow corona burns on the point electrode as long as the resultant voltage, U, is above U_{bp}. When the resultant voltage sinks below U_{bp}, the corona interrupts.

If the rise of a burst pulse during the time interval Δt_{bp} excludes the rise of a streamer during this ac cycle, then the rise probability, P , of a streamer is given by the formula [1]

$$P = \exp\left(-\Phi_T b \Delta t_{bp}\right). \tag{1}$$

Here Φ_T is a stochastic flux of negative ions reaching this part of the active zone ahead of the point electrode where a detached electron can initiate a burst pulse. Below this region of the active zone at $U = U_{str}$ will be referred to as the birth region of burst pulses. The calculation of the lateral boundary of this region will be discussed in section 4.

In expression (1), b denotes the mean (averaged over the voltage interval $U_{bp} \leqslant U \leqslant U_{str}$ and over the birth region of burst pulses) probability of initiation of a burst pulse by a single negative ion. The value of b depends on the diameter of the point electrode [16] and the nature of ions. Expression (1) is valid, if the pre-ionization level is high enough to ensure the discharge inception at each ac cycle. In practice, we get the rise probability of a streamer, P, by dividing the total number of streamers by the total number of the consecutive ac cycles examined.

Let us suppose now that some negative ions left in the discharge gap by a streamer and glow corona are available during the next increase in the combined voltage so that they form a supplementary ion flux into the birth region of burst pulses in addition to the flux from the ionizer. This supplementary ion flux increases the rise probability of a burst pulse and decreases the rise probability of a streamer. The intensity of the supplementary ion flux caused by a streamer and a following glow is evidently different from the flux caused solely by the glow corona. From the above, we conclude that the rise probability of a discharge during the given ac cycle may depend on the type of the discharge of the preceding ac cycle. For the detection of such an after-effect of a discharge, we introduce two more rise probabilities of a streamer, P_{as} and P_{ab}, as follows.

(1) P_{as} denotes the rise probability of a streamer for an ac cycle that is preceded by the ac cycle with a streamer.
(2) P_{ab} denotes the rise probability of a streamer for an ac cycle that is preceded by the ac cycle without any streamer; that is, during the foregoing cycle the discharge has been started as a burst pulse which is followed by the glow corona without any streamers.

For the calculation of P_{as} and P_{ab}, a sequence of streamers must be recorded synchronously with the ac voltage. The set of recorded ac cycles should be split up into two subsets. The first subset includes all these ac cycles that are preceded by the cycle with a streamer and glow. The second one includes all remaining ac cycles; that is, the cycles which are preceded by the cycle with a burst pulse and glow without any streamers. Dividing the number of streamers in the first subset by the number of ac cycles in this subset, we get P_{as} (probability after streamer). In the second subset, the analogous procedure gives P_{ab} (probability after burst pulse). Probabilities P, P_{as} and P_{ab} are related according to the formula

$$P = \frac{P_{ab}}{1 - (P_{as} - P_{ab})}.$$

The total flux, Φ_T, of negative ions into the birth region of burst pulses may consist of up to three components, if the after-effect of a previous discharge exists. The first component, Φ_0, is due to the external ionizer. The second component, Φ_s, is due to the residual ions of the preceding streamer. The third component, Φ_g, is caused by the residual ions left in the gap by the preceding glow corona. As a first approximation, we suppose that the ions of each flux component have the same age, whereas the ions of different flux components have different ages. The probability of initiation of a burst pulse by a single negative ion may therefore be different for the different components of the ion flux. Let b_0, b_s and b_g denote these (mean) probabilities for the ions in the corresponding flux components Φ_0, Φ_s and Φ_g, respectively. Now formula (1) can be rewritten for P_{as} and P_{ab} as follows:

$$P_{as} = \exp\left\lfloor -\left(\Phi_0 b_0 + \Phi_g b_g + \Phi_s b_s\right) \Delta t_{bp} \right\rfloor \tag{2}$$

$$P_{ab} = \exp\left\lfloor -\left(\Phi_0 b_0 + \Phi_g b_g\right) \Delta t_{bp} \right\rfloor. \tag{3}$$

The intensity of the glow corona is approximately the same, both after a burst pulse and after a streamer (see figure 1).

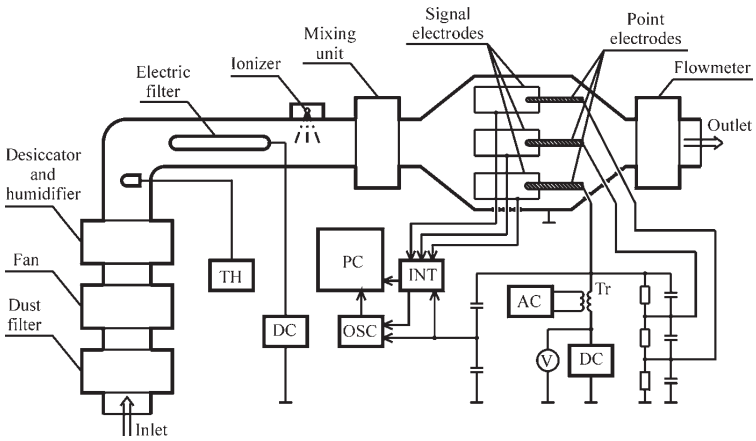

Figure 2. Experimental set-up.

The after-effect of the glow corona, if it exists, should be present therefore during each ac cycle in equal measure, independent of streamers. Regarding this, it follows from formulae (2) and (3):

$$\Phi_s b_s = \frac{1}{\Delta t_{bp}} \ln\left(\frac{P_{ab}}{P_{as}}\right). \tag{4}$$

The product $\Phi_s b_s$ can be considered as a quantitative measure of the after-effect of a streamer, because it represents the effective supplementary ion flux during the time interval Δt_{bp}.

Only few words have been said above about the role of the residual positive ions. In specific cases, the positive space charge of a decaying streamer channel can affect the rise probability of the next streamer because the field conditions may be changed. Under our conditions, the positive space charge ahead of the point electrode is predominantly removed long before the rise of the next discharge due to drift and diffuse scattering of the charges, and the negative ions play the major role in the after-effect studied. In principle, an effect of the positive ions may appear at high ac frequencies.

3. Experimental set-up

We investigated the after-effect of discharge pulses in an electrode arrangement designed for a streamer counter. Figure 2 shows a diagram of the experimental set-up. Hemispherically tipped platinum wires of different diameter, d, ($d = 0.13$, 0.25 and 0.50 mm) served as point electrodes. Each of these was surrounded by a coaxial cylinder as an opposite electrode of 28 mm in inner diameter and 30 mm in length. The point tip was placed 25 mm distant from the front edge of the cylinder. The cylinders served as signal electrodes. In the following, these discharge gaps of the multielectrode streamer counter will be called channel 1, channel 2 and channel 3, respectively. High dc and ac voltages, U_{dc} and U_{ac}, were applied to the point electrodes through a common rc voltage divider. Frequency of the ac voltage, f, was varied from 200–1100 Hz. Circuit arms of the voltage divider were chosen so that the combined voltage reached the onset voltage of streamers for all gaps simultaneously. The dc voltage was adjusted close to the onset voltage of streamers. The onset voltages of different discharge modes are presented in table 1.

Table 1. Onset voltages.

Point diameter, d (mm)	0.13	0.25	0.50
U_{bp} (kV)	2.46	3.08	4.10
U_{str} (kV)	2.54	3.18	4.26
U_g (kV)	2.84	3.43	4.42

A digital dual-channel 60 MHz oscilloscope recorded the pulses induced on the signal electrodes. A personal computer, PC, with a special interface, INT, stored both the sequences of streamers and the ac voltage synchronously. The time resolution and the recording time were 1 μs and 5 s, respectively.

A dust filter eliminated particles larger than 10 nm in diameter from the laboratory air. A desiccator filled with silica gel removed moisture from the air. The desired level of humidity was adjusted thereafter by evaporation of distilled water in a humidification unit. A digital thermohygrometer, TH, measured the humidity and air temperature. The experiments were carried out at a pressure of 1.01×10^5 Pa, at a temperature of 20 °C and at an absolute humidity $\rho = 3.1$ g m^{-3}. The volumetric flow rate of the gas stream was measured by a differential flowmeter.

An electric filter neutralized primary air ions. A subsequent α-active ionizer generated free electrons and ions in the air. Under normal air conditions, the free electrons have a characteristic attachment lifetime of $\sim 10^{-8}$ s [17]. They attach to electronegative atoms and molecules in the zero field near the ionizer. A homogeneous mixture of ions was obtained in a mixing unit. The ion flux, Φ, at the inlet of the signal electrodes was measured with an electrometer in additional experiments. Below, while discussing the pre-ionization level, we consider just this ion flux. The age of ions in the flux, Φ, was approximately 0.3 s. During the experiments, the pre-ionization level was always such that the increase in pre-ionization decreased the rise probability of streamers. At the same time, the pre-ionization level was too low for changing the discharge mechanism.

4. Computer modelling of ion flow

The aim of the computer modelling was to discover whether the residual negative ions responsible for the after-effect come from a discharge channel; whether they are produced due to the photoeffect at the surface of the opposite electrode or due to the photoionization of gas molecules.

In numerical two-dimensional calculations, we evaluated the motion of ions as a resultant drift caused by both the air flux and the electric field. The distribution of the axisymmetric Laplacian electric field, $E(r, z)$, in the cylindrical coordinates was computed by the finite difference method using the Gauss–Seidel iterative condition [18]. The rectangular computation area was divided into a square grid having maximally 3200 nodes per millimetre. It was taken for the convergence criterion of the iterations that the relative residual in the iterative process must be less than 10^{-12} at each interior node.

The air flux was taken into account as an additional electric field $\vec{E}_{\text{flow}}(r) = \vec{v}(r)/\mu$, where $\vec{v}(r)$ was the vector of the airflow velocity, r was a radial coordinate, and μ was the mobility of ions. Computations were carried out on the assumption that the mobility of negative ions, μ, was 2 cm^2 (Vs)$^{-1}$. The airflow profile inside the signal electrode was calculated according to the empirical power-law equation $v(r) = v(0)(1 - r/R_0)^{1/1.66\log(Re)}$, where R_0 was the coordinate of the wall of the signal electrode and Re was the Reynolds number [19]. In our experiments and calculations, Re ranged from 1240–5500.

At the onset of burst pulses only these avalanches, which develop close to the axis of the discharge gap, can launch the burst pulses [14]. We consider the size (number of electrons) of those avalanches to be critical and calculate it using the numerically computed Laplacian field, and the data for the ionization coefficient from the survey [20]. Our estimate of the size of the critical avalanche is, depending on the point diameter, $(1.1 - 2.9) \times 10^4$ electrons. The size of the critical avalanche is larger for fine point electrodes.

Once the onset voltage of burst pulses is exceeded, it is possible for the electrons in the off-axis positions to launch burst pulses. The upper voltage limit for burst pulses is U_{str}. The utmost off-axis start position of a critical avalanche at $U = U_{\text{str}}$ determines the lateral boundary of the birth region of burst pulses. The computed ratio of the distance of that lateral boundary from the gap axis and the radius of the point electrode is approximately 0.68 for all three channels.

Figure 3 presents for channel 3 ($d = 0.50$ mm) the ion trajectories terminating at the lateral boundary of the birth region of burst pulses in the case of different velocities, v, of the airflow. These ion trajectories, later called limiting trajectories, are computed and displayed inside the signal electrode in the plane of the gap axis. Similar calculations for finer point electrodes reveal that the smaller the diameter of the point electrode is, the closer the limiting trajectories are to the gap axis.

We determined numerically the coordinates of the space region inside which the negative ions were collected on the point electrode during the time interval $1/f - \Delta t_{\text{bp}}$. The sectional view of this space region in the plane of the gap axis for $v = 0.8$ m s^{-1} is painted grey in figure 3. The gap

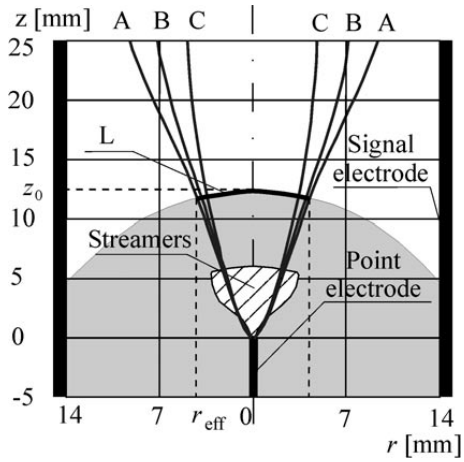

Figure 3. Trajectories of ions, terminating at the lateral boundary of the birth region of burst pulses: $d = 0.5$ mm; $f = 1000$ Hz; $U_{\text{dc}} = 4.40$ kV; $U_{\text{ac}} = 1500$ V. (A) $v = 0.8$ m s^{-1}; (B) $v = 1.4$ m s^{-1}; (C) $v = 3.2$ m s^{-1}.

axis intersects the boundary of this space region at $z = z_0$. The value of z_0 increases with a decrease in the ac frequency and with an increase in the airflow rate or dc voltage. An ion layer, labelled L in figure 3, is located between the limiting trajectories immediately beyond that boundary. The ions of this layer are responsible for the initiation of the discharge one ac period later, during the time interval Δt_{bp}. The radial extent of the layer, L, we denote with r_{eff}. The thickness of the layer is equal to $v_{\text{i}}\Delta t_{\text{bp}}$, where $\vec{v}_{\text{i}} = \vec{v} + \mu\vec{E}$ is the velocity of ions in the layer, L. The region occupied by streamer channels is indicated in the same figure. The length of streamers, l, was measured visually and photographically using a signal electrode with a hole for visual observations. The lengths of streamers were 2.4, 3.6 and 5.9 mm for point diameters $d = 0.13$ mm, $d = 0.25$ mm and $d = 0.50$ mm, respectively.

5. Results and discussion

Figure 4 shows that in channel 1 the probabilities P_{as} and P_{ab} coincide within the limits of experimental accuracy over all the dc voltage range except the beginning of the curves. In channel 2, the initially different probabilities become equal at $U_{\text{dc}} > 3.6$ kV. In channel 3, the probabilities differ markedly over the whole range of the dc voltage. The difference between P_{as} and P_{ab} indicates that the after-effect of a streamer exists.

Calculation of ion trajectories enables us to clarify the background of the negative ions responsible for the after-effect. The negative ions can arise due to the photoeffect on the wall of the signal electrode and the subsequent attachment of photoelectrons to the oxygen molecules near the wall. If the airflow is laminar and $v > 0.8$ m s^{-1}, then in all three channels these ions are unable to reach the birth region of burst pulses (see figure 3) and to participate in the initiation of the discharge.

In figure 3, we can see that the streamer length is at least two times less than z_0. Hence, the ions born in the steamer channel should be removed before the rise of the

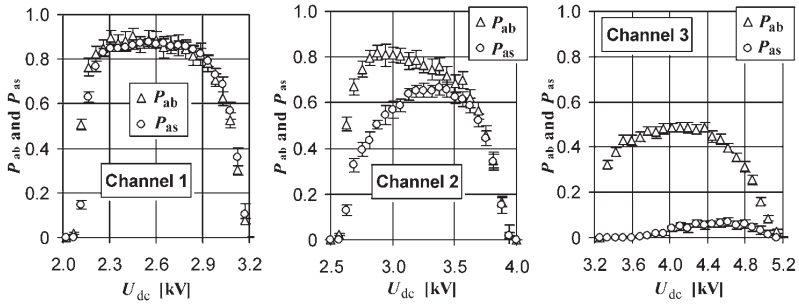

Figure 4. Rise probabilities of streamers depending on the dc voltage: $f = 1000$ Hz; $v = 1.4$ m s^{-1}; $\Phi = 3.04 \times 10^5$ s^{-1}. Channel 1, $U_{ac} = 430$ V; channel 2, $U_{ac} = 570$ V; channel 3, $U_{ac} = 890$ V.

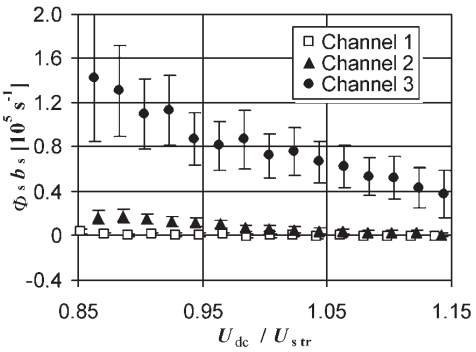

Figure 5. The product $\Phi_s b_s$ depending on the reduced dc voltage: $f = 1000$ Hz; $v = 1.4$ m s^{-1}; $\Phi = 3.04 \times 10^5$ s^{-1}. Channel 1, $U_{ac} = 430$ V; channel 2, $U_{ac} = 570$ V; channel 3, $U_{ac} = 890$ V.

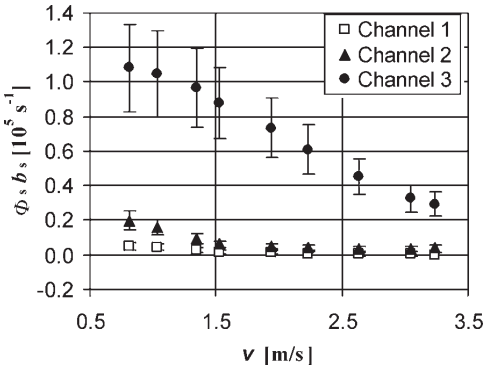

Figure 6. The product $\Phi_s b_s$ depending on the airflow velocity: $f = 1000$ Hz; $\Phi = 1.97 \times 10^5$ s^{-1}–4.54×10^5 s^{-1}. Channel 1, $U_{dc} = 2.41$ kV; $U_{ac} = 740$ V; channel 2, $U_{dc} = 3.13$ kV and $U_{ac} = 980$ V; channel 3, $U_{dc} = 4.27$ kV and $U_{ac} = 1520$ V.

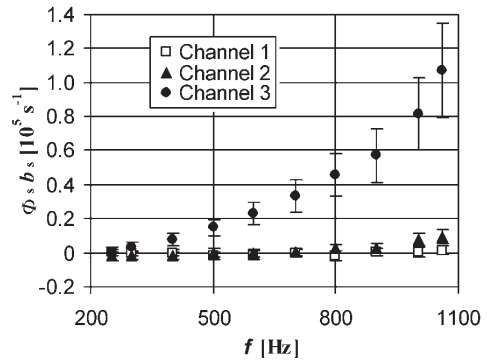

Figure 7. The product $\Phi_s b_s$ depending on the frequency of the ac voltage: $v = 1.4$ m s^{-1}; $\Phi = 3.04 \times 10^5$ s^{-1}. Channel 1, $U_{dc} = 2.41$ kV and $U_{ac} = 720$ V; channel 2, $U_{dc} = 3.13$ kV and $U_{ac} = 950$ V; channel 3, $U_{dc} = 4.28$ kV and $U_{ac} = 1490$ V.

next discharge and therefore they are unable to contribute to the after-effect.

The negative ions may be produced due to an ionizing radiation [14, 21, 22] of the previous streamer, which produces the electron–ion pairs also in the layer, L. Fast attachment of photoelectrons results in the formation of negative ions that are responsible for the after-effect because they reach the birth region of burst pulses one ac period later, during the time interval Δt_{bp}.

Figure 5 displays a quantitative characteristic of the after-effect, the effective ion flux, $\Phi_s b_s$, depending on the applied dc voltage, U_{dc}, reduced to the onset voltage of streamers in the corresponding channel. This flux is calculated according to formula (4). Under the combined voltage, the mean charge of streamers remains nearly unchanged by the dc voltage, because most streamers arise only slightly above the onset voltage, U_{str}. An increase in dc voltage causes an increase in z_0. Therefore, the number density of photoions decreases in the layer, L, and the after-effect of a streamer weakens.

Figure 6 demonstrates how the after-effect of the previous streamer depends on the airflow velocity, v. An increase in the airflow rate causes a more effective removal of the discharge products and a corresponding weakening of the after-effect of a streamer.

Figure 7 presents $\Phi_s b_s$ as a function of the frequency of the ac voltage. The time interval between discharges of subsequent ac cycles shortens with an increase in the frequency of the ac voltage. Consequently, less time is available for the removal of residual products. z_0 decreases and the number density of photoions in the layer, L, increases. As a result, the after-effect of a streamer enhances.

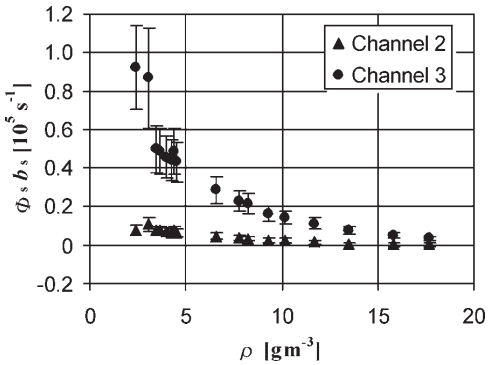

Figure 8. The product $\Phi_s b_s$ depending on the air humidity: $f = 1000$ Hz; $\Phi = 3.04 \times 10^5$ s^{-1}; $v = 1.4$ m s^{-1}. Channel 2, $U_{dc} = 3.07$ kV and $U_{ac} = 600$ V; channel 3, $U_{dc} = 4.19$ kV and $U_{ac} = 930$ V.

The effective flux of residual negative ions must be independent of the pre-ionization level maintained by the ionizer. Hence, an increase in the pre-ionization level reduces the relative contribution of the residual ions. The experiments confirm these considerations.

In our experiments where $U_{dc} \approx U_{str}$, the changes in peak value of the ac voltage, U_{ac}, had no influence on the intensity of the after-effect of a streamer.

Figure 8 demonstrates that the after-effect of a streamer weakens with an increase in the concentration of water vapour. Due to the water vapour in the air, absorption of the photoionizing radiation increases [14]. As a result, the number density of photoions increases near the streamer channel and decreases in the layer, L. The water vapour causes also a marked decrease in the length and the charge of a streamer [14], which in its turn reduces the number density of photoions. Moreover, in the moist air, the electron detachment from complex ions is less probable. The probability, b_s, of initiation of a burst pulse by a residual complex photoion decreases. As a result, the after-effect of a streamer will decrease in the moist air.

Considering figures 5-–8 one can see that the after-effect of a streamer weakens with a decrease in the point diameter. This happens mainly because the volume of the layer, L, decreases. The average length and power of a streamer also decrease with the point diameter. Both processes decrease the number of photoions in the layer, L, and the after-effect of a streamer weakens.

We calculated numerically the flux of ions, Φ_s, as if the ions were generated by the radiation of a streamer only, using the photoionization data obtained by Teich [21]. Teich measured the total number of ion pairs, Ψ, produced by photoionization in a 1 cm thick spherical layer (in the solid angle of 4π sr) at various distances from an avalanche per unit pressure and per one ionizing collision in the avalanche. In our case, the photoions responsible for the after-effect were generated by a streamer in a layer, L, located at a distance, z_0, from the point electrode. We had to take into account the fact that the streamer was a bulk source of radiation. As a simplification, we considered a streamer to be an unbranched single discharge channel developing instantaneously along

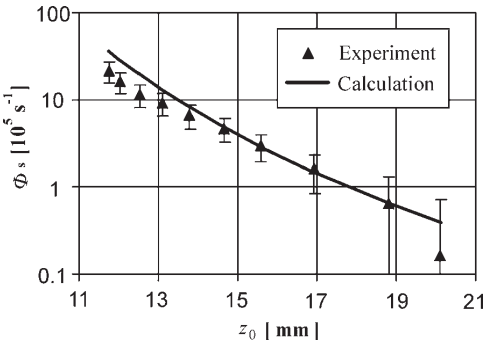

Figure 9. Flux of photoions, Φ_s, depending on z_0.

the gap axis up to the length, l. The local number of ionizing collisions in a channel element of length, dz, is proportional to the number of electrons there. The number of electrons in a discharge was found to be proportional to the intensity of the emitted light, I [23]. The distribution of the light intensity of a branched streamer, $I(z)$, along the gap axis was measured experimentally [24]. Knowing from the current measurements the total charge, Q, of the streamer, we calculate the unknown local number of ionizing collisions as

$$Q\left[e\int_0^l I(z)\,\mathrm{d}z\right]^{-1} I(z)\,\mathrm{d}z.$$

Here e denotes the elementary charge. For the ion flux, Φ_s, we write the integral in the form:

$$\Phi_s(z_0) \approx \frac{Qpv_i(0,z_0)}{4\pi e\int_0^l I(z)\,\mathrm{d}z}\int_0^l \left[I(z)\Theta(z)\Psi(pz_0 - pz)\right]\mathrm{d}z \tag{5}$$

where p is the pressure and $\Theta(z)$ is the solid angle under which the layer, L, is visible from an element of the streamer channel located at point z. Formula (5) is an approximate one because, in addition to the simplifications mentioned above, we disregard the real geometry of the layer, L, and the real distribution of ion mobilities.

Calculating Φ_s for different ac frequencies, we plot Φ_s as a function of the axial coordinate, z_0, of the layer, L. The line in figure 9 presents the calculated flux in channel 3. Measured flux is given by dots. All parameters are those indicated for figure 7. The value of the rise probability, b_s, needed for the calculation of Φ_s from $\Phi_s b_s$, we estimated (under the assumption that $b_s \approx b_0$) according to the algorithm proposed in paper [16]. In channel 3 ($d = 0.5$ mm) $b_s \approx 0.047$ for the ions of 0.3 s age.

The measured and calculated fluxes are in close agreement. On the one hand, this result demonstrates that the investigated after-effect of a streamer is originated by photoionization. On the other hand, it confirms that the method proposed in this paper is suitable for quantitative evaluation of the after-effect.

6. Conclusions

A method is developed to investigate the after-effect of a streamer on the rise of the following streamer. The method is based on the statistical analysis of sequences of streamers under the condition of the combined voltage (dc + ac). The negative ions left in the discharge gap by the previous streamer cause the after-effect. The method enables us to measure the flux of these ions. The analysis of the experimental results, as well as the two-dimensional numerical simulation of the ion drift in the air flux, reveal that the negative ions responsible for the after-effect are the products of photoionization. As the investigated device (streamer counter) is capable of operating as a detector of electronegative trace gases, the present results give a better understanding of the features peculiar to that device. The proposed detection method of the after-effect of streamers enables us, in each specific case, to select preferable parameters of the streamer counter so that the absence of the after-effect will be guaranteed.

Acknowledgment

The Estonian Science Foundations supported this work financially under Grant 3024.

References

[1] Aints M, Haljaste A, Kudu K and Plank T 1997 Repetition rate of streamers as a measure of content of electronegative additives in the air *J. Phys. D: Appl. Phys.* **30** 210–20

[2] Aints M, Haljaste A, Kudu K and Plank T 1996 Dependence of streamer corona characteristics on the concentration of electronegative trace gases in air *Proc. 5th Int. Symp. on High Pressure Low Temperature Plasma Chem. (Milovy)* pp 117–21

[3] Kudu K 1980 Some possible applications of a streamer counter *Proc. 6th Int. Conf. on Gas Discharges and Applications* Part 1 (Edinburgh: Heriot-Watt University Press) pp 275–8

[4] Waters R T 1978 *Spark Breakdown in Non-uniform Fields Electrical Breakdown of Gases* ed J M Meek and J D Craggs (Chichester: Wiley) pp 385–532

[5] Goldman M and Goldman A 1978 *Corona Discharges Gaseous Electronics. Electrical Discharges* vol 1, ed M N Hirsh and H J Oskam

[6] Gosho Y 1981 Enhancement of dc positive streamer corona in a point-plane gap in air due to addition of a small amount of an electronegative gas *J. Phys. D: Appl. Phys.* **14** 2035–46

[7] Gosho Y 1982 Considerable change in dc breakdown characteristics of positive-point–plane gaps due to varying concentrations of NO_X, CO_2 and H_2O in air and intensity of irradiation *J. Phys. D: Appl. Phys.* **15** 1217–25

[8] Andersson N E 1958 An investigation of the positive point streamer corona. Part I. The time distribution of the streamers *Arkiv Fysik* **13** 399–422

[9] Waters R T, Jones R E and Bulcock C J 1965 Influence of atmospheric ions on impulse corona discharge *Proc. IEE* **112** 1431–8

[10] Hepworth J K, Klewe R C and Tozer B A 1972 The effect of charged particles on impulse corona and breakdown in divergent field gaps *Proc. Int. Conf. Gas Discharges (London)* pp 227–9

[11] Gallimberti I 1979 The mechanism of the long spark formation *J. Physique* **40** C7 193–250

[12] Gosho Y and Harada A 1982 A new technique for detecting initial electrons by using Geiger counter region of positive corona *Proc. 7th Int. Conf. on Gas Discharges and Applications (London)* pp 193–5

[13] Gosho Y and Saeki M 1987 Triggering of dc positive corona by pulsed UV irradiation *J. Phys. D: Appl. Phys.* **20** 526–9

[14] Loeb L B 1965 *Electrical Coronas: Their Basic Physical Mechanisms* (Berkeley and Los Angeles: University of California Press)

[15] Miyoshi Y and Hosokawa T 1973 The formation of a positive corona in air *J. Phys. D: Appl. Phys.* **6** 730–3

[16] Plank T, Aints M and Haljaste A 1999 Investigation of rise probability of positive corona initiated by negative ions *Proc 24th Int. Conf. on Phenomena in Ionized Gases (Warsaw)* vol II, pp 145–6

[17] Bazelyan E M and Raizer J P 1998 *Spark Discharge* (Boca Raton, FL: CRC Press)

[18] Zhou P 1993 *Numerical Analysis of Electromagnetic Fields* (Berlin: Springer)

[19] Miller R W 1989 *Flow Measurement Engineering Handbook* 2nd edn (New York: McGraw-Hill)

[20] Dutton J A 1975 Survey of electron swarm data *J. Phys. Chem. Ref. Data* **4** 577-–856

[21] Teich T H 1967 Emission gasionisierender Strahlung aus Elektronlawinen *Z. Phys.* **199** 378–410

[22] Penney G W and Hummert G T 1970 Photoionization measurements in air, oxygen, and nitrogen *J. Appl. Phys.* **41** 572–7

[23] Raether H 1964 *Electron Avalanches and Breakdown in Gases* (London: Butterworths)

[24] Korge H, Kudu K and Laan M 1977 Development of dc corona pulses at atmospheric pressure *Proc 13th Int. Conf. on Phenomena in Ionized Gases (Berlin)* pp 451–2

III

Aints M Kudu K Haljaste A and Plank T
Origin of photoionizing radiation in corona discharges in air
J. Phys. D: Appl. Phys. (2001) **34** 905-8
http://www.iop.org/Journals/JPhysD

INSTITUTE OF PHYSICS PUBLISHING JOURNAL OF PHYSICS D: APPLIED PHYSICS
J. Phys. D: Appl. Phys. **34** (2001) 905–908 www.iop.org/Journals/jd PII: S0022-3727(01)20004-7

Origin of photoionizing radiation in corona discharges in air

M Aints, K Kudu, A Haljaste and T Plank

Institute of Experimental Physics and Technology, University of Tartu, 51010 Tartu, Estonia

Received 13 December 2000

Abstract
A hypothesis by Akishev *et al* (1999 *J. Phys. D: Appl. Phys.* **32** 2399–409), that the photoionizing radiation emitted by the positive corona discharge in air is soft x-rays generated by electron bombardment of the anode surface, is discussed. Absorption curves of the photoionizing radiation generated by positive and negative coronae in atmospheric air are compared. The coincidence of the shapes of these curves confirms the earlier, widely accepted opinion that the photoionizing radiation is emitted by gas molecules and atoms, which are excited via electron collision. Photographic detection of this photoionizing radiation performed by the method proposed by Akishev *et al* is found to be improbable, because of the very high attenuation of radiation by the light protecting envelope around the photographic film.

1. Introduction

It is generally recognized that the self-sustainment of a positive corona discharge in air is guaranteed by photoionization. The short-wave radiation generated by the discharge ionizes gas molecules, producing free electrons which trigger new electron avalanches [1–3]. It is widely accepted that this photoionizing radiation is emitted by gas molecules or atoms excited by electron collision. In air, the dominant processes leading to photoionization are believed to be as follows [4]:

(1) the excitation of nitrogen molecules to energies of 12.1–13.6 eV, with subsequent photoionization of oxygen molecules having an ionization potential of 12.1 eV;
(2) the dissociation of oxygen molecules with subsequent emission of photons with an energy above 12.1 eV by excited oxygen atoms must also be considered.

Electron collision processes leading to the excitation of nitrogen to energies above the ionization potential of the nitrogen molecule (13.6 eV) need comparatively high energies and therefore are believed to make a very small contribution to the production of photoelectrons in air discharges, although these processes are assumed to be dominant in pure nitrogen. The radiation emitted due to these processes has a very high absorption coefficient and will therefore interact with gas molecules within a very small region around the source.

Data about the above processes are mostly collected at low pressure. Phenomena at atmospheric and near-atmospheric pressures can be complicated by multiple collision processes and deactivation of excited states. Therefore, results obtained at low pressure should be used with caution for high-pressure discharges.

New results concerning the photoionizing radiation in a corona discharge were presented by Akishev *et al* [5–7]. They investigated, experimentally and theoretically, oscillations in the current and light from a positive glow corona in wire-cylinder and point-to-plane gaps in air [6, 7] and nitrogen [5]. They found that the oscillations arose due to the fast positive feedback via the photoionization of gas molecules. They suggested that the important ionizing agent in the experiments was soft x-ray radiation (bremsstrahlung), produced by collisions of electrons accelerated in a strong electric field near the anode against the anode surface [5]. To check this hypothesis, they carried out a simple experiment using point-to-plane electrode geometry but replacing the massive cathode by a metal mesh. 'Close behind this mesh a common x-ray spectroscopy film was placed, enclosed in dense black paper screening the film from visible and UV radiation' [5, 6]. This film was exposed for several hours to radiation generated in the positive corona and then developed. In the range of air pressures studied (∼1–80 Torr), a dark spot was observed on the photographic film around the axis of symmetry of the discharge. Therefore, they 'believe that bremsstrahlung x-ray radiation (with photon energy up to 100 eV) from the pin is the versatile and most important ionizing agent in a positive corona' [5].

Thus we are now faced with two very different views regarding the generation mechanism of photoionizing radiation in a corona discharge in air: (a) the radiation is emitted by gas atoms and molecules excited via electron collision; and (b) the

radiation is generated due to the electron bombardment of the anode surface. The aim of the present investigation is to find some experimental confirmation in favour of one or the other generation mechanism of photoionizing radiation.

2. Experimental details

2.1. Photographic investigation

We have tried to repeat the experiment performed by Akishev *et al* [5–7]. The discharge was initiated in a point-to-plane gap in atmospheric air at pressure $p = 80$ Torr. The point electrode was a hemispherically capped platinum wire, 1.5 mm in diameter. The opposite electrode was a plane metal mesh perpendicular to the point electrode at a distance of 2 mm from the point tip, just as described by Akishev *et al* [5, 6]. The diameter of the mesh wire was 0.15 mm and the wire spacing was 0.4 mm. The mesh was grounded. A positive potential was applied to the point electrode via a 100 MΩ series resistor. The discharge current was in the range of 10–50 μA. A flow of dry air of about 0.1 l min^{-1} was forced through the discharge gap to remove gaseous discharge products. The x-ray spectroscopy film KODAK MR 2000-1 was placed close behind the mesh. The film was enclosed in dense black paper to screen the film from visible and UV radiation. The film was exposed for several (up to ten) hours to the radiation generated in the corona, and was then developed. We did not find any dark spot on the film. We changed the film using all types of x-ray films available to us, and we changed the envelope material using thin paper and black plastic films of about 0.01 mm in thickness. Unlike the above-mentioned authors [5, 6], we never found any dark spots on the photographic films.

2.2. Absorption of corona radiation

2.2.1. Experimental set-up. The photoionizing radiation in our corona discharges was detected with the help of an adjacent discharge gap, here, in short, called the Geiger counter tube. This counter tube was made to respond to the radiation only through the ion pairs generated within the tube volume. A diagram of the experimental set-up is presented in figure 1.

The point electrode (1) of the corona gap (figure 1) was located on the axis of a metal tube which had an inner diameter of 20 mm. The end of the tube was closed with a metal plate facing the point electrode. The distance between the point electrode tip and the plate was 4 mm. The plate had a central hole 2 mm in diameter. The tube and the plate thus formed the opposite electrode of the discharge gap, and were connected to the ground via an ammeter. Another discharge gap similar to the first one, the 'Geiger tube', was used as a counter of photoelectrons and photoions. The gaps faced each other along a common axis. The point electrode (2) of the Geiger tube was a 2 mm tungsten wire with a conic tip, placed axially in a tube (the counter body) with an inner diameter of 10 mm. The distance between the tip of point electrode (2) and the end-plate of the counter body was 4 mm. The end-plate had a central orifice 2 mm in diameter. The edges of the orifice were smoothed. The body of the counter was grounded, and the high voltage of +5.4 kV was applied to the point electrode via a series resistor of 22 MΩ. If a charged particle (electron or negative ion) was generated in the active space of

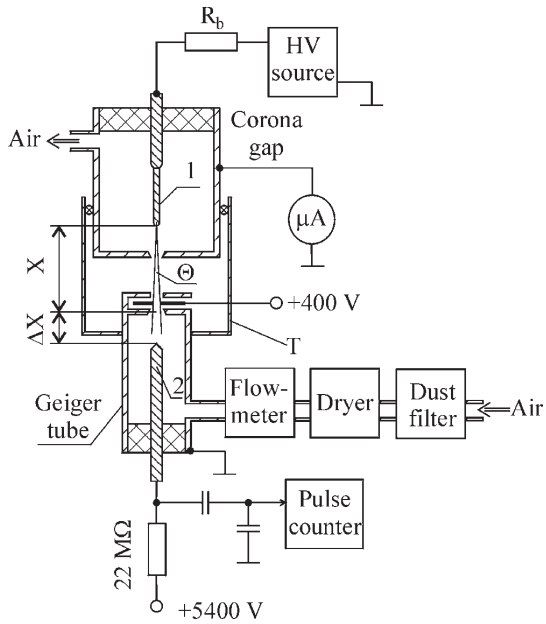

Figure 1. Schematic diagram of the experimental set-up.

the Geiger tube an incomplete breakdown occurred, and the ensuing electrical pulse was counted by a pulse counter. The dead time τ of the Geiger counter was 0.3 ms. An additional screening plate electrode with a 1.5 mm orifice in the centre was aligned parallel to the end-plate of the Geiger tube and put on +400 V. The distance between this screening electrode and the end-plate of the Geiger tube was 0.5 mm. Together with the airflow, the electric field from the additional electrode prevented an injection of negative ions from the outside into the Geiger tube. In addition, it screened the edges of the entrance orifice of the Geiger tube from radiation to avoid the generation of electrons via the photoeffect. Another plate at zero potential with an opening in the centre was located above the screening electrode. The corona gap and the Geiger tube were connected by means of a tube (T). The distance between the corona gap and the Geiger tube was changeable. Filtered dry air was forced through the Geiger tube and the corona gap. The airflow rate was 0.5 l min^{-1}. The airflow removed discharge products from the gaps and prevented the injection of particles from the outside into the Geiger tube.

We calculated the combined force caused by the electric field and air stream on the negative ions in the region of the entrance orifice of the Geiger tube, and determined the position of the surface where the axial component of this force was zero. The space between this surface and the point electrode (2) is the active space of the Geiger counter. Its extent along the common axis is denoted by ΔX. According to our calculations $\Delta X = 4.6$ mm. The distance from the above-mentioned surface to the point electrode (1) of the corona gap is denoted by X in figure 1, and equals the path length the photons must travel before being detected.

The counter responded neither to the UV radiation of a low-pressure mercury lamp nor to the ions created with the help of an α-active source in the space outside and near the

entrance orifice. The background of the counter was less than 0.2 pulses per second. The counter had no effect on the corona discharge. Neither the corona current nor the repetition rate and amplitude of the corona pulses changed when voltages were applied to the counter.

2.2.2. Results of measurements. Measurements were carried out at atmospheric pressure in laboratory air dried by silica gel. The counting rate was recorded as a function of distance X. Counter pulses were recorded during a time interval of 10 s at each distance X. The counting rate was in the range of 1–2500 s^{-1}. We used hemispherically capped Pt, W and Al points as corona point electrode (1). The diameters of the corona points were 0.05 and 1.0 mm for every material used. The polarity of the voltage applied to the corona point was changed and the discharge current was varied. In the case of a positive corona there was a steady glow, but in the case of a negative corona Trichel pulses appeared with a repetition rate of 20–-50 kHz depending on the current and the electrode diameter. An example of the results of these measurements is presented in figure 2 as a $\Psi(pX)$ plot, where p is the gas pressure and Ψ is the number of photoions generated in a layer of unit thickness at distance X from the radiation source, per ionizing collision in the discharge, at unit pressure:

$$\Psi = \frac{eN}{(1 - N\tau)\,\Theta i p \Delta X \eta}.$$

Here, e is the elementary charge, N is the counting rate, Θ is the solid angle determined by distance X and the diameter of the opening of the screening electrode of the Geiger tube (see figure 1), i is the mean current of the corona discharge, and η is the efficiency of the Geiger counter. The term $(1 - N\tau)$ takes into account the dead time of the counter. The number of photoions generated by the corona radiation in the active space of the Geiger tube is

$$n = \frac{N}{(1 - N\tau)\eta}.$$

When choosing $\eta = 0.03$ our values of Ψ became close to those presented in earlier papers [8, 9]. The relationship between n and N is more complicated for the pulse corona in the general case. However, under our experimental conditions, the repetition rate of Trichel pulses $F \gg \frac{1}{\tau}$ and $\eta \ll 1$, and thus the above relationship between N and n is valid.

Our measurements show that Ψ does not depend on the mean current i of the corona discharge. This result is in agreement with the results of other authors [8, 9].

In figure 2, it can be seen that the values of Ψ coincide within the limits of uncertainty for Pt and Al point electrodes as well as for positive and negative polarities. Values of Ψ obtained for other tested electrodes also laid on the presented curve within the limits of uncertainty.

2.3. Absorption of ionizing radiation in thin film materials

We placed various thin films between the Geiger tube and the corona source. The distance X between the corona electrode and the Geiger tube was 6 mm. Readings of the counter were recorded both in the presence and in the absence of the film. Samples of various thicknesses d made from various materials were used: dense black paper ($d = 0.12$ mm); thin capacitor paper ($d = 0.01$ mm); aluminium ($d = 0.01$ mm); polyethylene ($d = 0.01$ mm); Teflon ($d = 0.01$ mm); glass ($d = 0.001$ mm); quartz ($d = 0.001$ mm); and nitro-cellulose ($d = 0.001$ mm). In the presence of the films, the readings of the counter were always close to the background. The attenuation of the radiation caused by a film was at least 10^5 in all cases. The result depended neither on corona electrode material and diameter nor on corona current intensity and polarity.

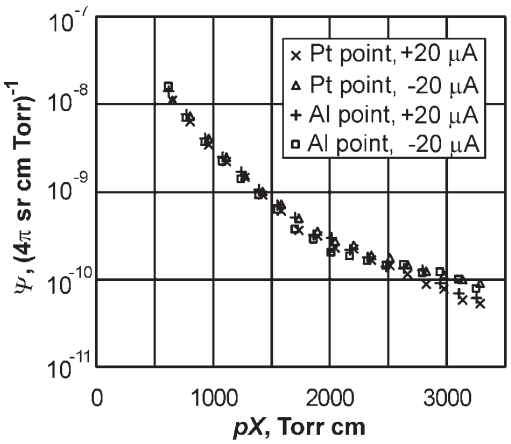

Figure 2. Absorption curves of corona radiation. The diameter of the corona point electrode is 1 mm; $p = 775$ Torr.

3. Discussion

3.1. Absorption characteristics

If photoionizing radiation is produced by collisions of electrons with the anode surface, at least two characteristic effects should appear.

(1) The intensity of photoionizing radiation should depend on the material of the anode, and should be higher for metal of a greater atomic weight.
(2) Generation of the bremsstrahlung is impossible in negative coronae, because of the very low energy of electrons hitting the plane, low-field anode. Therefore, the spectral characteristics of photoionizing radiation, and thus the shape of the curves Ψ versus pX, should be different for positive and negative coronae. The radiation intensity should be much higher for positive coronae.

Figure 2 shows that the shapes of the Ψ versus pX curves do not depend on the material of the corona electrodes. There is, however, a small systematic difference between values of Ψ for positive and negative coronae. The radiation intensity of a negative corona seems to be about 10–50% higher. However, this difference is less than the experimental uncertainty. This difference may be caused by the difference in the spatial structure of positive and negative coronae. Thus we may conclude that there are no significant changes in the generation mechanism of photoionizing radiation when the corona polarity or the material of the corona electrodes are changed.

3.2. Photographic detection

Unfortunately, neither the type of the photographic film nor the envelope material have been described by Akishev *et al* [5, 6]. Therefore, we are not sure whether we have repeated exactly the experiment described there, and this may be the reason for a difference between our results and the results published in [5, 6].

However, it is astonishing that the imprint of the mesh is not seen in the photographs published in [5, 6]. This should appear on films exposed to x-rays in the apparatus described in [5, 6].

Our measurements show that the attenuation of photoionizing radiation by paper of a thickness of 0.01 mm is at least 10^5 or more. A very high absorption of radiation by the envelope of the photographic film is the most probable reason why we did not discover any dark spot on our films exposed to the corona radiation. Therefore, photographic detection of the corona radiation by a film enclosed in 'dense black paper' seems to be impossible, unless the coronae studied by Akishev *et al* in some way produced electrons of much higher energies and much harder x-rays than ours.

4. Conclusions

A method for detecting photoionizing radiation based on an internal gas discharge (Geiger) counter is developed. The production of photoions by negative coronae is recorded in air at atmospheric pressure and compared for the first time with that of positive coronae. Our conclusion is that the photoionizing radiation generated by a corona discharge is mainly emitted by gas molecules or atoms. The radiation caused by electron bombardment of the anode surface constitutes so small a fraction of the total radiation that it is impossible to distinguish it from the total radiation with our experimental method.

Evidently, the processes leading to the dark spots on the films obtained by Akishev *et al* need further explanation.

Acknowledgments

This work was supported by the Estonian Science Foundation under grant no. 4518. The authors would like to thank Professor R S Sigmond for his interest and helpful comments concerning this paper.

References

[1] Loeb L B 1965 *Electrical Coronas: Their Basic Physical Mechanisms* (Berkeley: University of California Press)
[2] Raether H 1964 *Electron Avalanches and Breakdown in Gases* (London: Butterworths)
[3] Meek J M and Craggs J D (eds) *Electrical Breakdown of Gases* (Chichester: Wiley)
[4] Badaloni S and Gallimberti I 1972 Basic data of air discharges *UPee–72/05* (Padova University)
[5] Akishev Yu S, Grushin M E, Deryugin A A, Napartovich A P, Pankin M V and Trushkin N I 1999 Self-oscillations of a positive corona in nitrogen *J. Phys. D: Appl. Phys.* **32** 2399–409
[6] Akishev Yu S, Grushin M E, Deryugin A A, Napartovich A P, Pankin M V and Trushkin N I 1999 Integral and local characteristics of an extended positive corona in the regime of non-linear oscillations: experiment *Plasma Phys. Rep.* **25** 867–76
[7] Akishev Yu S, Grushin M E, Deryugin A A, Napartovich A P, Pankin M V and Trushkin N I 1999 Integral and local characteristics of an extended positive corona in the regime of non-linear oscillations: theory *Plasma Phys. Rep.* **25** 877–81
[8] Teich T H 1967 Emission gasionisierender Strahlung aus Elektronlawinen *Z. Phys.* **199** 378–410
[9] Penney G W and Hummert G T 1970 Photoionization measurements in air, oxygen, and nitrogen *J. Appl. Phys.* **41** 572–7

IV

Aints M Haljaste A Kudu K and Plank T
Corona based detector of electronegative trace gases
Meas. Sci. Technol. (2001)**12** 557-65
http://www.iop.org/Journals/MST

INSTITUTE OF PHYSICS PUBLISHING MEASUREMENT SCIENCE AND TECHNOLOGY
Meas. Sci. Technol. **12** (2001) 557–565 www.iop.org/Journals/mt PII: S0957-0233(01)16309-5

Corona based detector of electronegative trace gases

M Aints, A Haljaste, K Kudu and T Plank

Institute of Experimental Physics and Technology, University of Tartu, Tähe 4, 51010 Tartu, Estonia

Received 11 August 2000, accepted for publication 13 February 2001

Abstract
The repetition rate of streamers of a positive corona depends strongly on the concentration of electronegative trace gases in the air. On the basis of this dependence, one can build a simple and cheap detector of trace gases—a streamer counter. However, the earlier models of the counter are unable to distinguish the strongly electronegative trace gases from additional H_2O or CO_2 in air. In the present paper, the operation principle of the streamer counter is analysed and a new model of detector together with the method of data processing is elaborated. As a principal technical innovation in the new model of the detector, several discharge gaps are operated simultaneously. These discharge gaps (detector channels) differ from each other in the diameter of the hemispherically capped point electrode. Another technical improvement is the online measurement and processing of data. It is shown experimentally that the relative increase in the formation probability of a streamer with an increase in the concentration of an electronegative admixture is different for different channels as well as for different admixtures. Using these differences, it is possible to distinguish between different admixtures. If the admixture is identified, the evaluation of its concentration is possible from the measured formation probability of a streamer.

Keywords: corona streamers, burst pulses, detector of electronegative trace gases, air, water vapour, carbon dioxide, iodine, sulphur hexafluoride, ozone, NO_x

1. Introduction

It is well known that corona discharges show high sensitivity to many electronegative trace gases and aerosols [1, 2]. For example, the repetition rate of Trichel pulses (in negative corona) increases with an increase in the concentration of an electronegative admixture in the main gas. Sigmond *et al* [3], Sigmond [4] and Lågstad [5] investigated this dependence with the purpose of elaborating a detector of an electronegative admixture in argon and in air. The investigations revealed that using the repetition rate and duration of Trichel pulses, the detection limit for SF_6 in argon was 0.1 ppm [3]. For SF_6 in air, the sensitivity was considerably lower and there were serious problems with the stability of the negative corona.

The voltage range of the onset streamers of a positive dc corona and their repetition rate depend on the geometry of the discharge gap as well as on the properties of the filling gas (pressure, temperature, preionization level, velocity of the gas flux and the chemical composition of the gas) [1, 2]. Andersson and Hertz [6] made the first known attempt to use the repetition rate of dc corona streamers in practice. Measurement of the concentration of water vapour in air was their objective.

A modified technique to estimate the concentration of water vapour or halogens in air was developed by Kudu [7], who suggested a simultaneous application of a dc voltage and an ac voltage to the gap. The main advantage of this kind of combined voltage is that the combined voltage enables us to reduce dramatically variations in the repetition rate of streamers caused by variations in pressure and temperature of the ambient air.

In our earlier investigation [8] we found that in air the repetition rate of streamers increased with the concentration of admixtures such as H_2O, CO_2, O_3, HNO_3, HCl, H_2SO_4, H_3PO_4, $CHCl_3$, C_6H_6, NH_4OH, CH_3COOH, $C_{10}H_{16}O$, HCHO, I_2 and Cl_2. Especially high sensitivity was observed in the case of halogens. For example, a detectable change in repetition rate of streamers took place at fractional concentration of iodine $C_{I_2} = 1$ ppb. It was concluded that

streamer counters could be used as simple and cheap detectors of electronegative trace gases. However, the earlier models of the streamer counters, which used only one discharge gap, were unable to distinguish between electronegative admixtures.

In the present investigation, we establish how the formation probability of a streamer depends on the tip radius of a point electrode in the case of different admixtures. We show that using several discharge gaps simultaneously it is possible to create a corona based detector capable of distinguishing between H_2O, CO_2 and strongly electronegative trace gases.

2. Operation principle of the streamer counter at combined voltage

The basic element of a streamer counter is a discharge gap with a hemispherically capped point electrode. The positive dc voltage and the ac voltage are applied to the point electrode. Values of dc and ac voltages are chosen in such proportions that the discharge extinguishes with each negative half-cycle and arises again during each positive half-cycle of the ac voltage. Air entering the discharge gap contains negative ions created before with the help of a special ionizer. The flux of those negative ions is intense enough to ensure the discharge inception during every ac cycle. When the instantaneous value of the applied voltage U exceeds the onset potential of burst pulses U_{bp}, then the burst pulse can be initiated with a certain probability due to the decomposition of the negative ions (electron detachment). This probability depends on the intensity of the ion flux, the nature of ions, and the time interval Δt during which the voltage U lies between the onset voltage of burst pulses U_{bp} and the onset voltage of streamers U_{str}. The appearance of a burst pulse during Δt eliminates the formation of a streamer during the same ac cycle [8]. If the burst pulse is not initiated during the time interval Δt, then the discharge starts with a streamer during this ac cycle. Both a burst pulse and a streamer develop into a steady glow with voltage increase. The steady glow burns during this cycle while the voltage exceeds the onset value of the discharge. During negative half cycles there is no discharge in the gap. A discharge arises again as a burst pulse or a streamer during the next positive half cycle. There arises no more than one streamer per cycle. The magnitude of the streamer current exceeds that of other corona pulses by a factor of about 50 and thus the streamers can be easily detected by a special interface. The probability Q that a streamer arises during an ac cycle (formation probability of a streamer) is given by the formula [8]

$$Q = \exp(-\Delta t \Phi_T b). \tag{1}$$

Here Φ_T is the stationary flux of negative ions reaching the active zone of the point electrode. b denotes the mean (averaged over the voltage interval $U_{bp} \leqslant U < U_{str}$ and over the active zone of the point electrode) probability of initiation of a burst pulse by a single negative ion. The value of b depends on the nature of the ions. Δt can be calculated from values of the dc voltage U_{dc}, ac voltage U_{ac}, frequency f of the ac voltage and values of U_{bp} and U_{str}. If Φ_T is a known quantity, e.g. controlled by the ionizer, then b can be determined from the measured $Q = n/f$ (here n is the number of streamers per second). *Vice versa*, if b is known then Φ_T can be determined.

In the general case, not all of the ions entering the discharge gap reach the active zone of the point electrode. We denote the measured flux of ions at the inlet of the electrode system with Φ, and the ratio Φ_T/Φ by g. The factor g depends on the mobility of the ions and on the configuration of the discharge gap.

Actually the flux of ions consists of different ion species, which have different values of b and g. Thus equation (1) should be rewritten in the form

$$Q = \exp[-\Delta t \Phi(\varphi_1 g_1 b_1 + \varphi_2 g_2 b_2 + \cdots + \varphi_j g_j b_j + \cdots + \varphi_m g_m b_m)]. \tag{2}$$

Here φ_j is the fractional flux of ions of a certain nature, which is defined as the ratio of the flux Φ_j of ions of that nature to the flux Φ. Factor g_j ($0 \leqslant g_j \leqslant 1$) characterizes the possibility that a j-type ion will reach the active zone. b_j ($0 \leqslant b_j \leqslant 1$) denotes the mean probability for a j-type ion in the active zone to initiate a burst pulse. Under the influence of an admixture the values of φ_j change, causing changes in the formation probability of a streamer.

The probability b_j for a certain ion to initiate a burst pulse depends on the decomposition probability of the ion, which in turn depends strongly on the electric field strength (at constant gas number density). The maximum field strength on the axis of the discharge gap is the stronger the smaller is the radius of curvature of the point tip. According to numerical calculation, in our discharge gaps (see next section) the maximum field strength $E_{max} = 250$ kV cm^{-1} if the point diameter $d = 0.13$ mm, and $E_{max} = 120$ kV cm^{-1} if $d = 0.5$ mm, provided that $U = U_{str}$. Thus it can be supposed that the probability b of initiating a burst pulse by a negative ion depends on the tip radius of the point electrode and, furthermore, the dependence of b on the tip radius is different for different kinds of ion. Using m point electrodes (channels) with different tip curvatures we obtain a set of linear equations

$$\begin{cases} \ln Q_1 = -\Delta t_1 \Phi(a_{1,1}\varphi_1 + a_{1,2}\varphi_2 + \cdots + a_{1,j}\varphi_j + \cdots + a_{1,m}\varphi_m) \\ \ln Q_2 = -\Delta t_2 \Phi(a_{2,1}\varphi_1 + a_{2,2}\varphi_2 + \cdots + a_{2,j}\varphi_j + \cdots + a_{2,m}\varphi_m) \\ \cdots \\ \ln Q_i = -\Delta t_i \Phi(a_{i,1}\varphi_1 + a_{i,2}\varphi_2 + \cdots + a_{i,j}\varphi_j + \cdots + a_{i,m}\varphi_m) \\ \cdots \\ \ln Q_m = -\Delta t_m \Phi(a_{m,1}\varphi_1 + a_{m,2}\varphi_2 + \cdots + a_{m,j}\varphi_j + \cdots + a_{m,m}\varphi_m). \end{cases} \tag{3}$$

Here index i indicates the channel number and index j the type of ion. $Q_1, Q_2, \ldots, Q_m$ are streamer formation probabilities measured in different channels. $a_{i,j}$ denotes the product $b_{i,j} g_{i,j}$.

If the numerical values of $a_{i,j}$ are known, then solving this set of equations yields the values of φ_j. In that way we obtain a distribution of the ion flux by values of $a_{i,j}$, that is, a spectrum of ions by $a_{i,j}$. The spectrum shape depends on gas composition. Once the spectrum is known, some conclusions about gas composition are possible.

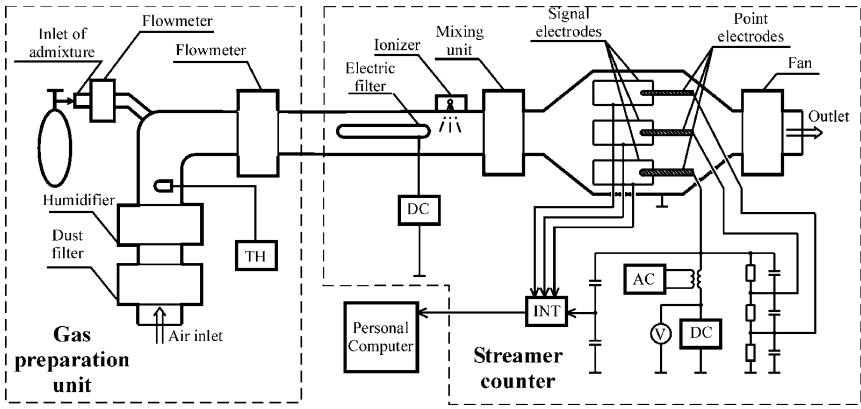

Figure 1. Experimental set-up.

Table 1. Onset potentials (at normal pressure and temperature 31 °C).

Channel number, i	d (mm)	U_{bp} (kV)	U_{str} (kV)	U_g (kV)
1	0.13	2.33	2.39	2.73
2	0.25	2.90	2.99	3.29
3	0.50	3.87	4.01	4.29

Table 2. Applied voltages and Δt for point electrodes used.

Channel number, i	d (mm)	U_{dc} (kV)	U_{ac} (kV) (peak value)	Δt_i (μs)
1	0.13	2.55	0.76	25.5
2	0.25	3.31	1.01	32.2
3	0.5	4.52	1.55	30.4

3. Experimental device

The sketch of the streamer counter and that of the gas preparation unit are shown in figure 1.

3.1. The streamer counter

An electric filter removed the ions from air entering the streamer counter. An ionizer created thereafter a controlled number of ions and the air stream, formed by the fan, carried them to the point electrodes. Three hemispherically capped platinum cylinders with diameters $d = 0.13, 0.25$ and 0.50 mm served as the point electrodes. The coaxial signal electrodes had an inner diameter of 28 mm. High dc and ac voltages were applied simultaneously to the point electrodes. The voltages were set so that the instantaneous value of the resultant voltage U ran sequentially through the voltage regions of different corona modes: burst pulses ($U_{bp} \leqslant U < U_{str}$), streamers ($U_{str} \leqslant U < U_g$) and steady glow ($U \geqslant U_g$). Here U_g denotes the onset potential of the glow corona. Values of the onset potentials for the discharge gap configurations used are presented in table 1.

The streamer counter included an interface (INT) that formed rectangular pulses from current pulses of streamers and rectangular clock pulses from the ac voltage. A personal computer recorded sequences of those pulses from all discharge gaps, calculated thereafter the formation probability of a streamer for every channel and presented the detector response graphically in the form of a four-bar (pseudo-) spectrum of ions.

3.2. The gas preparation unit

The experiments were carried out in laboratory air under normal pressure and a temperature of 31 °C. The entering air passed a dust filter. A desired level of humidity was adjusted by evaporation of distilled water in a humidifier and measured by a digital thermo-hygrometer TH. CO_2 and SF_6 were introduced into the air stream from a cylinder. Concentration of the admixture in the discharge gap was calculated from readings of flowmeters. Iodine admixture was obtained by blowing air through a vessel whose inner walls were covered with crystals of iodine. Air, saturated with iodine vapour, was diluted in the proportion of 1:1000 and introduced as a controlled flow into the inlet of the electronegative admixture of the experimental device. O_3 was produced with the help of a barrier discharge ozonizer using oxygen as feeding gas. O_3+NO_x was produced with the help of the same ozonizer using dry air as feeding gas.

4. Results of measurements

Results of measurements are presented in figures 2–4, where the streamer formation probability Q is plotted against the fractional concentration C of different admixtures. The number of streamers was counted during $\tau = 30$ seconds at each measuring point while the frequency f of the ac voltage was 500 Hz. Q is the number of streamers counted during τ and divided by $f\tau$. The air flow velocity in discharge gaps was 3.6 m s^{-1}. The ion flux Φ determined by the cross section of signal electrodes was 6.2×10^6 s^{-1} in each channel. Ions reaching discharge gaps had an age of approximately 0.12 s under the above conditions. Voltages applied to the point electrodes are given in table 2.

As one can see in figures 2–4, Q has generally the highest value in channel 1 and the lowest in channel 3. This is partly caused by the difference in ion fluxes reaching the active zone in the different channels. The number of ions reaching the active zone during the time interval Δt is the smaller the finer is the point electrode. According to equation (2), the decreases

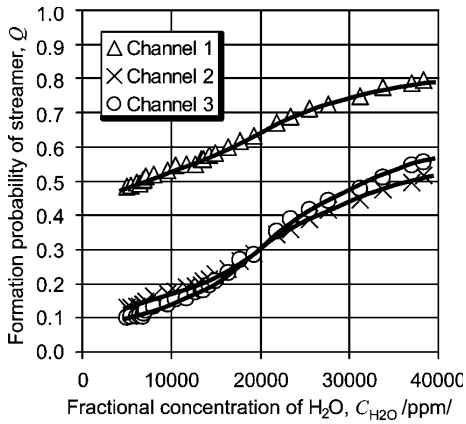

Figure 2. Dependence of streamer formation probability on the fractional concentration of water vapour C_{H_2O}.

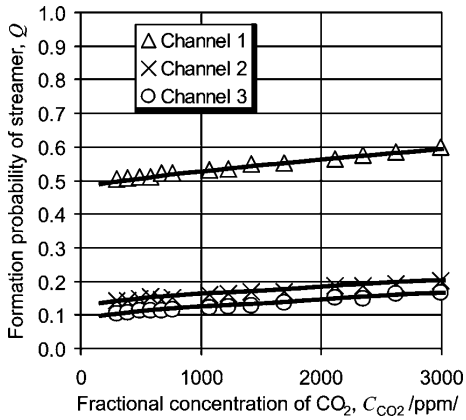

Figure 3. Dependence of streamer formation probability on the fractional concentration of CO_2 C_{CO_2}. Fractional concentration of H_2O was 6500 ppm.

in factors g_j increase the formation probability Q of streamers. Consequently, the finer is the point electrode the higher is Q.

One can see in figures 2–4 that Q increases with fractional concentration of all admixtures used, in all channels. Under the influence of electronegative admixture the number of ions with high probability of initiating burst pulses decreases due to conversion reactions, and the number of ions with lower probability to initiate burst pulses increases. According to equation (2), these changes in ion flux composition result in changes of Q upon introduction of an electronegative admixture.

The relative increase in Q with fractional concentration of admixture is different in different channels in the case of a definite admixture. For instance, look at figure 2, where the H_2O curves for channels 2 and 3 are even intersecting. This is in accordance with our hypothesis that the initiation probability b of a burst pulse depends on the point diameter differently for different ion species. To use this difference for evaluation of an ion spectrum, the device must be calibrated. In other words, the coefficients $a_{i,j}$ of the equations (3) should be determined.

Table 3. Values of energy ε_x released or absorbed in different conversion reactions [9].

x	Reaction	ε_x (eV)
0	$O_2 \leftrightarrows O_2^-$	0.22
1	$O_2^- \leftrightarrows O_2^-(H_2O)$	0.46
2	$O_2^-(H_2O) \leftrightarrows O_2^-(H_2O)_2$	0.28
3	$O_2^-(H_2O)_2 \leftrightarrows O_2^-(H_2O)_3$	0.18
4	$O_2^-(H_2O)_3 \leftrightarrows O_2^-(H_2O)_4$	0.106
5	$O_2^-(H_2O)_4 \leftrightarrows O_2^-(H_2O)_5$	0.056

5. $a_{i,j}$ in the case of water vapour

We determine the values of $a_{i,j}$ using the known ion composition of clean humid air. The most populous ions in clean humid air are the ions of $O_2^-(H_2O)_x$, with $x = 2, \ldots, 5$ [9, 10]. Allen [9] has presented formulae for calculation of the stationary number densities of these ions depending on the humidity of air:

$$\left.\begin{aligned} \frac{[O_2^-(H_2O)_x]}{[e]} &= \frac{\nu_x}{\nu_x^*} \cdot \cdots \cdot \frac{\nu_0}{\nu_0^*}[H_2O]^x[O_2] \\ [e] + \sum_x [O_2^-(H_2O)_x] &= \text{const} \end{aligned}\right\} \tag{4}$$

where

$$\frac{\nu_x}{\nu_x^*} = \frac{1}{[M]} \exp\left(\frac{\varepsilon_x}{kT}\right).$$

Here $[O_2^-(H_2O)_x]$ is the number density of complex ions. x denotes the number of water molecules in a complex ion, [e] is the number density of free electrons and $[H_2O]$ and $[O_2]$ are number densities of water vapour and oxygen, respectively. ε_x is the released or absorbed energy, k is the Boltzmann constant and T is the absolute temperature of air. ν_x and ν_x^* are the rate constants of the reversible reaction

$$O_2^-(H_2O)_{x-1} + H_2O + M \underset{\nu_x^*}{\overset{\nu_x}{\longrightarrow \longleftarrow}} O_2^-(H_2O)_x + M + \varepsilon_x.$$

M is a third body (a nitrogen or another oxygen molecule) with concentration [M]. Values of ε_x of some reactions are given in table 3.

Formulae for fractional concentration of the ions $O_2^-(H_2O)_x$ come out of equations (4):

$$\begin{aligned} \varphi_x^*(h) &= \frac{[O_2^-(H_2O)_x]}{[e] + \sum_x [O_2^-(H_2O)_x]} \\ &= s\,h^x \exp\left(\frac{1}{kT}\sum_{w=0}^{x}\varepsilon_w\right) \\ &\quad \times \left[1 + s\sum_{v=0}^{5}\left(h^v \exp\left(\frac{1}{kT}\sum_{w=0}^{v}\varepsilon_w\right)\right)\right]^{-1} \end{aligned} \tag{5}$$

where h is the fractional concentration of H_2O and s is that of oxygen.

According to our model, $\ln(Q)$ is proportional to the linear combination of fluxes of different ions (see equation (3)). As a first approximation, we suppose that in clean humid air only the ions of $O_2^-(H_2O)_x$ are present. Fractional fluxes of these ions are equal to fractional concentrations φ_x^*. Using the curve fitting method, coefficients $a'_{i,x}$

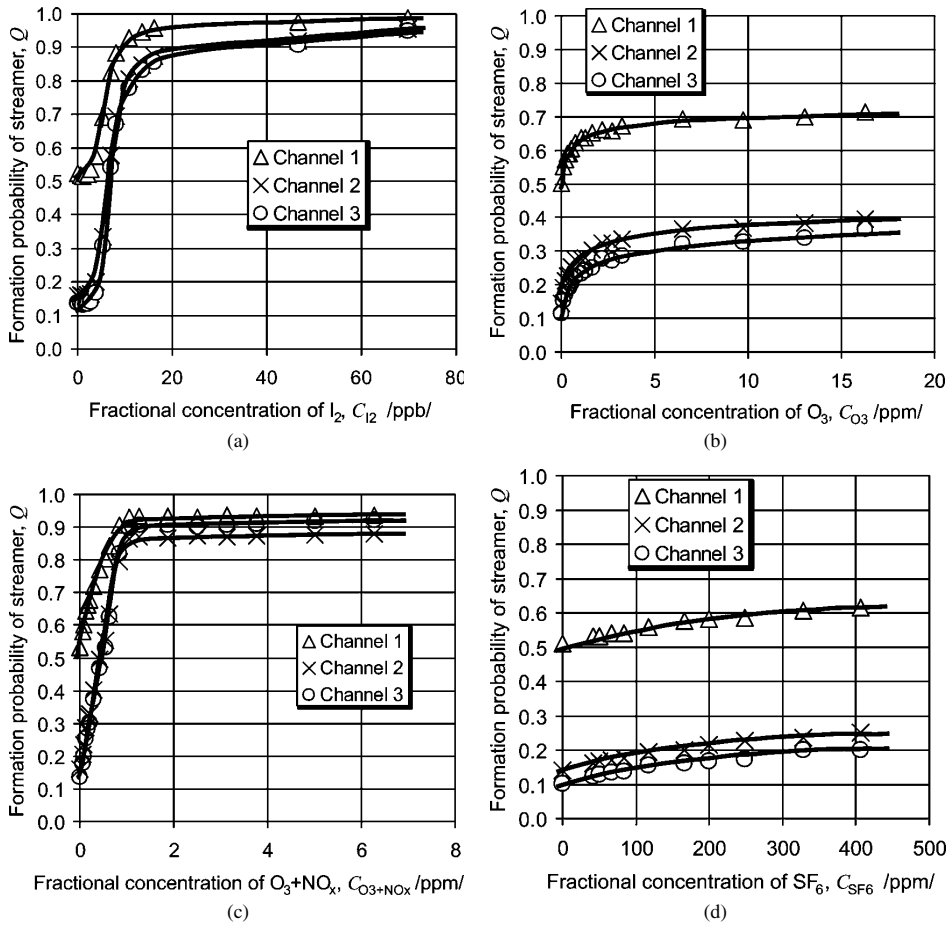

Figure 4. Dependence of streamer formation probability on the fractional concentration C of different strongly electronegative trace gases. Fractional concentration of H_2O was 8800, 8400, 9100 and 5100 ppm for graphs (a)–(d), respectively.

were found such that curves $f_i(h) = \sum_x a'_{i,x}\varphi^*_x(h)$ fitted experimental points on $-(\Delta t\Phi)^{-1}\ln(Q(h))$ versus h plots, for all three channels. Here the subscript $i = 1, 2, 3$ denotes the serial number of a channel. It turned out that only the ions $O_2^-(H_2O)_x$ with $x = 2, \ldots, 5$ had to be taken into account. Under our experimental conditions, where $h = 5000, \ldots, 38\,000$ ppm, the fractional concentrations of $O_2^-(H_2O)$ and O_2^- were too small to have an effect on the shape of the curves $f_i(h) = \sum_x a'_{i,x}\varphi^*_x(h)$. The obtained values of $a'_{i,x}$ are presented here in the first three rows of the matrix **A**:

$$\mathbf{A} = \begin{pmatrix} 7.90\times10^{-3} & 5.47\times10^{-3} & 5.16\times10^{-4} & 2.18\times10^{-6} \\ 2.85\times10^{-2} & 1.01\times10^{-2} & 2.29\times10^{-3} & 8.43\times10^{-6} \\ 3.96\times10^{-2} & 1.17\times10^{-2} & 1.05\times10^{-3} & 5.13\times10^{-6} \\ 1 & 1 & 1 & 1 \end{pmatrix} \tag{6}$$

The first row corresponds to channel 1, the second to channel 2, the third to channel 3. The first column consists of coefficients $a'_{i,2}$, the second of coefficients $a'_{i,3}$, the third of coefficients $a'_{i,4}$ and the fourth of coefficients $a'_{i,5}$. Values of $a'_{i,x}$ decrease with increase in x, while the relative decrease is the most rapid in channel 3 ($i = 3$). Values of $a'_{i,5}$ are practically zero.

A solvable set of linear equations (3) must be equal in number of equations to the number of unknowns. Our experimental device had three channels. Thus we can write the above set in terms of three equations. The number of ion species taken into account above was four. Constancy of the sum of fractional ion fluxes yields the additional condition $\sum_j \varphi_j = 1$. Coefficients of the latter are presented in the fourth row of the matrix **A**.

By solving the equation

$$\mathbf{A}\cdot\boldsymbol{\varphi} = \boldsymbol{q} \tag{7}$$

for $\boldsymbol{\varphi}$, where

$$\boldsymbol{\varphi} = \begin{pmatrix} \varphi_1 \\ \varphi_2 \\ \varphi_3 \\ \varphi_4 \end{pmatrix} \quad \text{and} \quad \boldsymbol{q} = \begin{pmatrix} -(\Delta t_1\Phi)^{-1}\ln Q_1 \\ -(\Delta t_2\Phi)^{-1}\ln Q_2 \\ -(\Delta t_3\Phi)^{-1}\ln Q_3 \\ 1 \end{pmatrix}$$

the four components of the detector response $\boldsymbol{\varphi}$ can be determined. Each component is characterized by certain values of $a_{i,j}$. The response component with subscript 1 corresponds to the ions which have the greatest probability to initiate a burst pulse, the component with subscript 4 to the ions with the smallest probability, close to zero.

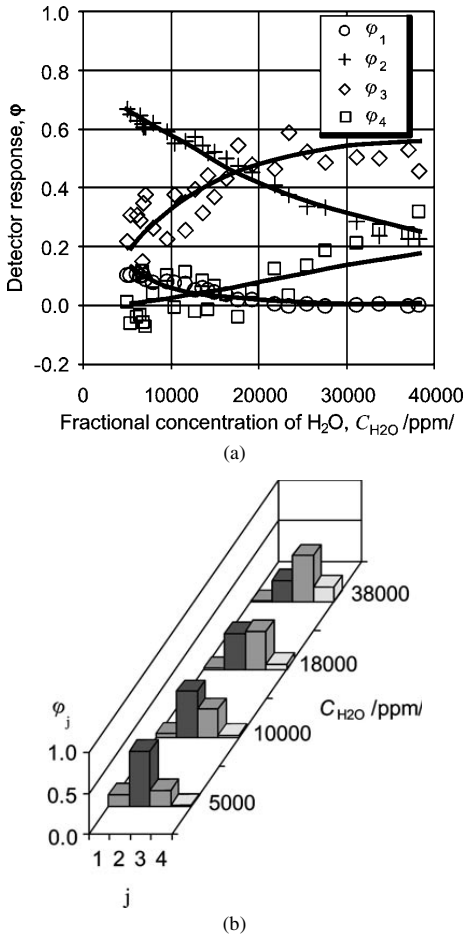

Figure 5. Response of the detector versus concentration of H_2O.

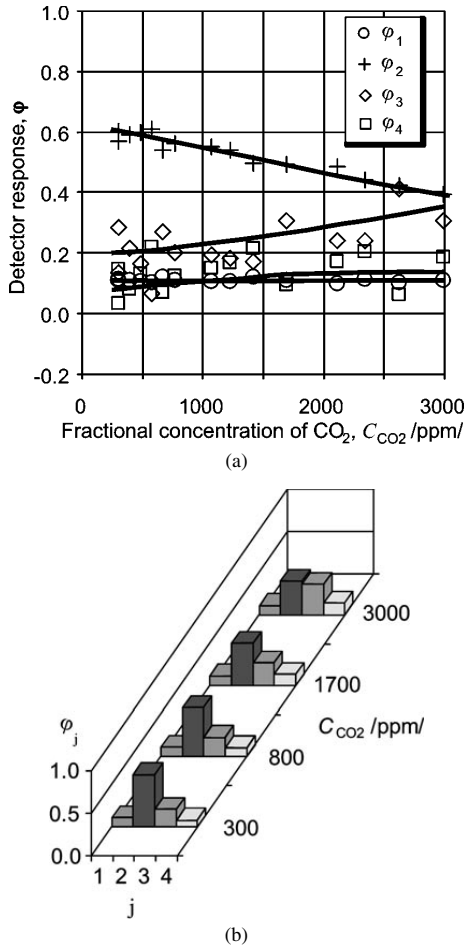

Figure 6. Response of the detector versus concentration of CO_2.

6. Results of calculation

The detector response φ was calculated using equation (7), matrix (6) and experimental data presented in figures 2–4. The results are presented in figures 5(a)–10(a) as plots of φ_j versus fractional concentration of the additives. The same results are presented in figures 5(b)–10(b) as histograms (bar charts) for some fractional concentrations C of the additives. These histograms will be named spectra below.

Curves of H_2O (figure 5(a)) represent the functions (5) because the matrix **A** is determined with the help of these functions. The spectrum specific for humid clean air has one peak, which moves towards smaller values of a (higher values of j) with increase in concentration of H_2O, according to the expression (5). This spectrum can be considered as an actual one in so far as the expression (5) describes correctly the ion composition of the clean humid air.

The negative ion composition depends strongly on the sort of the electronegative admixture added to air, and values of coefficients $a_{i,j}$ depend on the sort of negative ion. In the general case, some different trace gases are present in air, and the number m of ion species with different values of a may be great enough. If m is greater than $n + 1$, where n is the number of channels, then the actual spectrum of ions by a cannot be resolved, because the number of unknowns is greater than the number of equations available. Nevertheless, we can solve an $(n + 1)$-order set (7). As a result, we obtain a solution (that is, the device response) different from the actual spectrum of the ions. The number of components of that response (four in our case) is different from the number of components in the actual spectrum, and the values $a_{i,j}$ chosen for the matrix elements of the n-channel device may differ from those of the actual spectrum. Though $m \leqslant n + 1$, a discrepancy between the response and the actual spectrum also appears when the species of ions under detection are different from those used for calibration of the detector (coefficients $a_{i,j}$ of ions under detection are different from values of matrix elements used for calculation of the response). Despite these discrepancies, the device response in the form of an $(n + 1)$-bar spectrum is useful, because it enables us to distinguish between admixtures more easily than can be done on the basis of formation probabilities of a streamer. To accentuate the possible differences between the detector response and

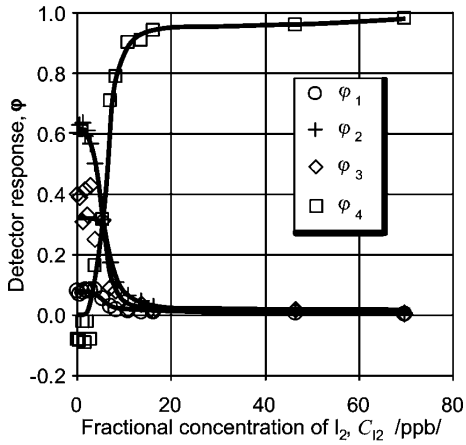

(a)

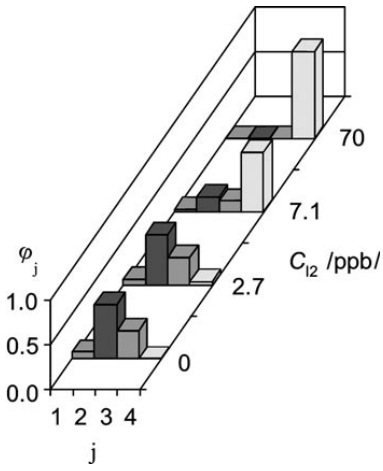

(b)

Figure 7. Response of the detector versus concentration of I_2.

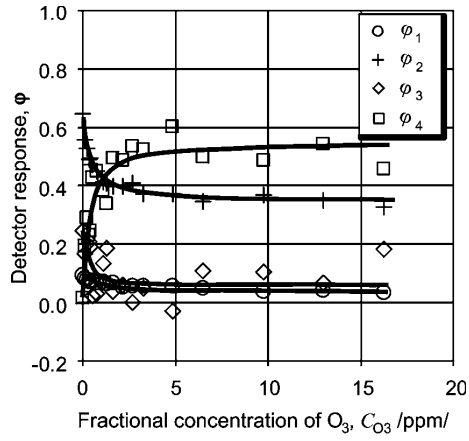

(a)

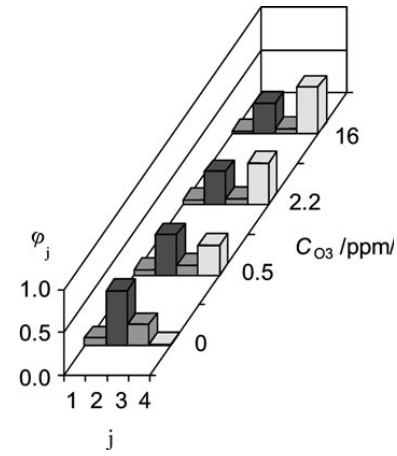

(b)

Figure 8. Response of the detector versus concentration of O_3.

the actual spectrum of ions, the detector response will be named a pseudospectrum below when the response to the electronegative admixtures is discussed.

Under the influence of CO_2, φ_1 and φ_4 stay practically unchanged whereas φ_3 increases and φ_2 decreases with increase in concentration of CO_2 (figure 6). However, the initial relationship among the components of φ, $\varphi_2 > \varphi_3 > \varphi_1 \approx \varphi_4$, remains unchanged over the investigated range of concentrations of CO_2.

Strongly electronegative trace gases I_2, O_3 or $O_3 + NO_x$ cause quite similar changes in the pseudospectrum (figures 7–9). The values of φ_1, φ_2 and φ_3 decrease and that of φ_4 increases with increase in concentration of electronegative admixture. If the concentration of the admixture reaches a certain critical value for the given admixture, then changes in the pseudospectrum cease. The pseudospectrum acquires a stationary shape with one peak in the case of I_2 or $O_3 + NO_x$ and two peaks in the case of O_3, while the highest peak belongs to φ_4. In the case of O_3, a peak of φ_2, specific for clean air of low humidity, remains observable as well. The stationary responses are specific for each admixture:

$$\varphi_{I_2} = \begin{pmatrix} 0.004 \\ 0.008 \\ 0.005 \\ 0.983 \end{pmatrix} \qquad \varphi_{O_3+NO_x} = \begin{pmatrix} 0 \\ 0.091 \\ 0.107 \\ 0.802 \end{pmatrix}$$

$$\varphi_{O_3} = \begin{pmatrix} 0.036 \\ 0.355 \\ 0.063 \\ 0.546 \end{pmatrix}.$$

In the case of I_2 the ratio of components is $\varphi_4 > \varphi_3 \approx \varphi_2 \approx \varphi_1$. In the case of $O_3 + NO_x$ we have $\varphi_4 > \varphi_3 \approx \varphi_2 > \varphi_1$. In the case of O_3 the ratio of components is $\varphi_4 > \varphi_2 > \varphi_3 \approx \varphi_1$.

The influence of SF_6 on the shape of the pseudospectrum (figure 10) is similar to that of small concentrations of other strongly electronegative gases I_2, O_3 and $O_3 + NO_x$. However, to obtain the same effect, the concentration of SF_6 must be over 500 times higher than that of O_3, for example.

As can be seen from figures 7–9, the component φ_4, which corresponds to the ions with practically zero probability of initiating burst pulses, begins to dominate in the presence of I_2, O_3 or $O_3 + NO_x$ in air. φ_4 acquires the highest value

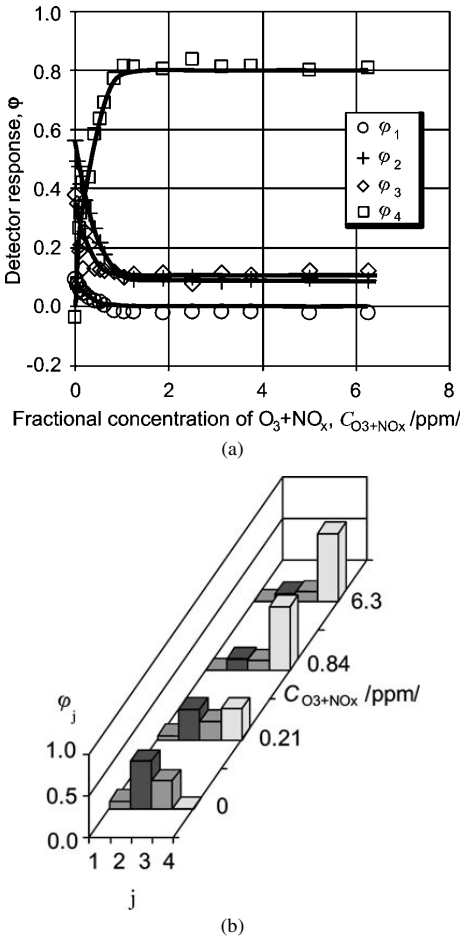

Figure 9. Response of the detector versus concentration of $O_3 + NO_x$.

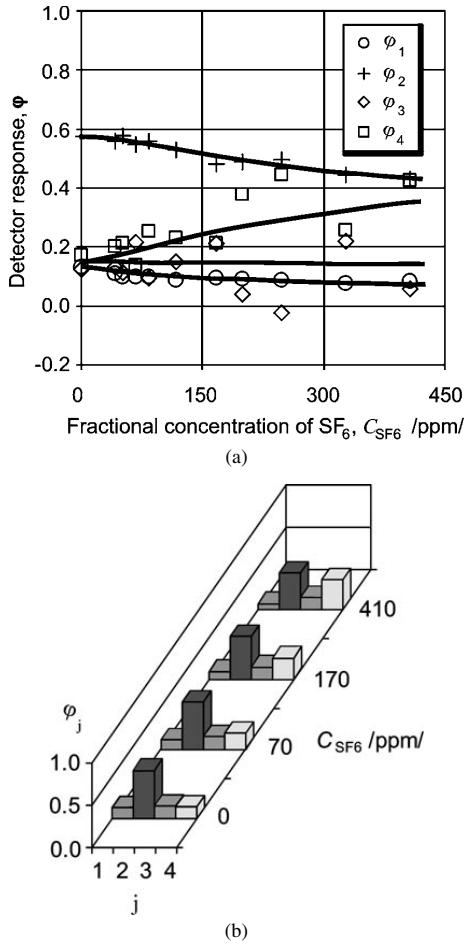

Figure 10. Response of the detector versus concentration of SF_6.

among the components of φ. Under the influence of SF_6 (figure 10) or H_2O (figure 5), φ_4 increases as well but here the components φ_2 or φ_3 have the highest value. In the case of CO_2, φ_4 remains unchanged (figure 6). Therefore it is possible to determine the presence of some strongly electronegative trace gases (I_2, O_3, O_3+NO_x, SF_6) in air on the basis of the four-bar pseudospectrum obtained with the help of a three-channel streamer counter. Furthermore, analysing relations between components of φ, it is possible to distinguish between I_2, O_3 and $O_3 + NO_x$, for example, provided that the concentrations of trace gases exceed the critical ones. Once the admixture is identified, its concentration can be determined on the basis of formation probability of a streamer versus admixture concentration curves (like those presented in figures 2–4). Accurate measurements of concentrations are possible, if only one additional gas (H_2O, CO_2, I_2, O_3, $O_3 + NO_x$, SF_6) is present in air.

To increase the selectivity of the detector the number of channels (electrodes) can be stepped up, but as one can see the scattering of points around the smoothed curves in figures 5–10 is relatively great compared to that in figures 2–4. This results from the fact that relative changes in Q caused by a particular admixture are quite similar in different channels. Therefore, the accuracy of determining φ decreases rapidly with increase in the number of channels. In any case, determination of optimal number of channels and channel geometry need further investigation.

Another thing in need of improvement is the determination of the matrix **A**. We have used the matrix **A** obtained by changing the concentration of H_2O. Application of this matrix to other admixtures gives a pseudospectrum. Differences between the pseudospectrum and the actual one depend on the values of the elements of matrix **A**. Another matrix **A**, obtained by changing the concentration of some other admixture, might lead to the pseudospectra of another shape. What kind of matrix is the best one needs further investigation. However, the detector responses in the form of four-bar pseudospectra like those presented above seem to be quite appropriate for the present task—to distinguish strongly electronegative trace gases from additional H_2O and CO_2 in air.

7. Conclusions

It can be concluded that a three-channel streamer counter can be used as a detector of electronegative trace gases in

air with the capability to distinguish at least four strongly electronegative trace gases from additional H_2O or CO_2 in air. Once the admixture is identified, its concentration can be determined on the basis of formation probability of a streamer versus admixture concentration plots. The optimal number of channels, as well as the configuration of discharge gaps (electrodes), needs further investigation. Accurate measurements of concentration are possible, if only one additional gas is present in air. In situations where several admixtures are present at the same time, the applicability of the detector needs further investigation.

Acknowledgments

This work was supported by the Estonian Science Foundation under grant No 3024, and the EU Copernicus grant CIPA-CT94-0186.

References

[1] Sigmond R S and Goldman M 1983 Corona discharge physics and applications *Electrical Breakdown and Discharges in Gases* ed E E Kunhard and L H Luessen (New York: Plenum) pp 1–64

[2] Loeb L B 1965 *Electrical Coronas: Their Basic Physical Mechanisms* (Berkeley, CA: University of California Press)

[3] Sigmond R S, Goldman A, Goldman M, Laan M, Bjones B and Olsen I H 1993 Detection of electronegative trace gases by corona discharges *Proc. 11th Int. Symp. on Plasma Chemistry (Loughborough)* vol 4, ed J E Harry, pp 1315–20

[4] Sigmond R S 1995 Corona physics and diagnostics *Proc. 22th Int. Conf. on Phenomena in Ionized Gases (Hoboken, NJ)* invited papers, pp 332–45

[5] Lågstad I H 1997 Corona detectors and the positive glow corona discharge *PhD Thesis* Norwegian University of Science and Technology, Trondheim

[6] Andersson N E and Hertz C H 1955 Positive Spitzenentladung als Hygrometer geringer Trägheit *Z. Ang. Phys.* **7** 361–6

[7] Kudu K 1980 Some possible applications of a streamer counter *Proc. 6th Int. Conf. on Gas Discharges and Applications* (Edinburgh: Heriot-Watt University Press) part 1, pp 275–8

[8] Aints M, Haljaste A, Kudu K and Plank T 1997 Repetition rate of streamers as a measure of content of electronegative additives in air *J. Phys. D: Appl. Phys.* **30** 210–20

[9] Allen N L 1985 The effect of humidity on positive corona discharges in air *Proc. 17th Int. Conf. on Phenomena in Ionized Gases (Budapest)* invited papers, pp 62–72

[10] Gallimberti I 1979 The mechanism of the long spark formation *Proc. 14th Int. Conf. on Phenomena in Ionized Gases (Grenoble)* invited papers, pp 193–250

V

Plank T Aints M and Haljaste A
Investigation of rise probability of positive corona initiated by negative ions
Proc. 24th Int. Conf. on Phenomena in Ionized Gases (1999) **II** 145-6

Investigation of Rise Probability of Positive Corona Initiated by Negative Ions

T. Plank, M. Aints, A. Haljaste
Institute of Experimental Physics and Technology, University of Tartu, Tähe 4, 51010 Tartu, ESTONIA

Abstract

The rise probabilities of burst pulses and streamers of positive corona, initiated by flux of negative ions, are investigated experimentally. It is shown that rise probability of a corona pulse may be affected by the previous discharge that creates an additional number of initiating negative ions. A method to determine this additional ion flux is proposed.

1. Introduction

Aints et al. [1, 2] have investigated the repetition rate of corona streamers in air when corona gap was fed simultaneously by positive DC and AC voltage. An external ionizer was used to initiate the discharge. If the preionization level was high enough so that discharge arose at every AC cycle, then

1) the appearance of a burst pulse during Δt_{bp} eliminated the rise of a streamer during this AC cycle (Δt_{bp} is the time interval during which the resultant voltage U lies between the onset potential of burst pulses U_{bp} and the onset potential of streamers U_{str});
2) if the burst pulse was not initiated during the time interval Δt_{bp}, the streamer arose at this AC cycle.

According to these results an equation was derived which gives the probability P that a streamer arises during an AC cycle:

$$P = \exp\left(-\Phi \cdot P_{bp} \cdot \Delta t_{bp}\right). \qquad (1)$$

Here Φ is a stationary stochastic flux of negative ions reaching the active zone of the point electrode and P_{bp} is the probability to initiate a burst pulse by a single negative ion. P_{bp} depends on the point curvature and nature of ions. According to Eq. (1) it is possible to determine P_{bp} if Φ and Δt_{bp} are known. A detection method of trace gases in air based on Eq. (1) was proposed in [2]. The aim of the present investigation is to verify experimentally the validity of Eq. (1).

2. Experimental set-up

The sketch of the experimental set-up is shown in Fig. 1.

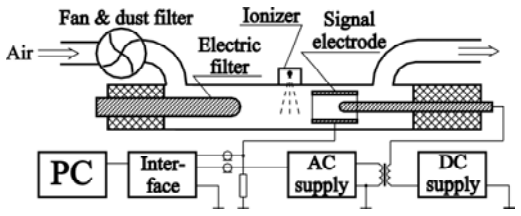

Figure 1. Experimental set-up.

The air under test is forced with a fan through a dust filter. The ions are neutralized by an electric filter. Fixed number of ions is thereafter created by an ionizer and carried by air stream to the platinum point electrode. Three hemispherically capped electrodes with diameter d = 0.13; 0.25 and 0.50 mm are used as the point electrodes. The coaxial signal electrode has diameter 28 mm. High DC and AC voltages are applied simultaneously to the point electrode. The voltages are set so that instantaneous value of the resultant voltage U runs sequentially through the voltage regions of different corona modes: burst pulses ($U_{bp} \le U < U_{str}$), streamers ($U_{str} \le U < U_g$) and steady glow ($U \ge U_g$). Here U_g denotes the onset potential of glow corona. Magnitude of the streamer current exceeds the magnitude of other corona pulses about ten times and thus streamers can be easily detected by a special interface. Sequences of streamers are recorded by PC synchronously with AC voltage. Present experiments are carried out in dry air under normal pressure, temperature 33°C and relative humidity less than 4 %.

3. Experimental results

Statistical analysis shows that P may be different for AC cycles with and without streamer during foregoing AC cycle. Therefore two streamer rise probabilities P will be used:

- with P_{ab} we denote the streamer rise probability for AC cycle that is preceded by AC cycle without any streamer;
- with P_{as} we denote the streamer rise probability providing that there was a streamer during the foregoing cycle.

In Fig. 2a the streamer rise probability P_{ab} versus flux of negative ions Φ_i is plotted in the semilogarithmic scale.

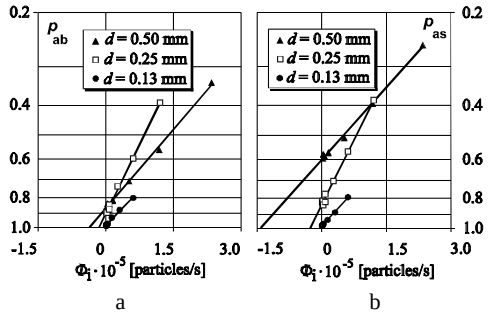

Figure 2. Rise probabilities of streamers depending on the flux of negative ions Φ_i. f = 1000 Hz; v = 3.3 m/s.
▲ : U_{DC} = 4.38 kV; U_{AC} = 1410 V; Δt_{bp} = 14.9 µs.
□ : U_{DC} = 3.20 kV; U_{AC} = 900 V; Δt_{bp} = 14.7 µs.
● : U_{DC} = 2.46 kV; U_{AC} = 680 V; Δt_{bp} = 10.4 µs.

Here the flux Φ_i is the number of negative ions per second produced by the ionizer and reaching the active zone of the point electrode. Φ_i is calculated proceeding from ionizer efficiency, air flow rate and numerically calculated trajectories of ions in electric field. The same dependence for P_{as} is presented in Fig. 2b. In figure captions v denotes the air flow velocity at the axis of the discharge gap, U_{DC} the DC voltage, U_{AC} the AC voltage amplitude, and f the AC frequency. One can see that experimental points fall on straight lines in both figures. These lines are not going through the axes origin ($P = 1$; $\Phi_i = 0$). The intersection points of trendlines with Φ_i-axis are farther from 0 in case of P_{as} than in the case of P_{ab}. They are the farther from 0 the bigger the point diameter is. The similar curves like presented in Fig. 2 are recorded under the same conditions for different frequencies of AC voltage. The intersection points of trendlines with abscissa are determined. The distances Φ_0 from 0 to intersection points are presented in Fig. 3. One can see that Φ_0 increases with AC frequency.

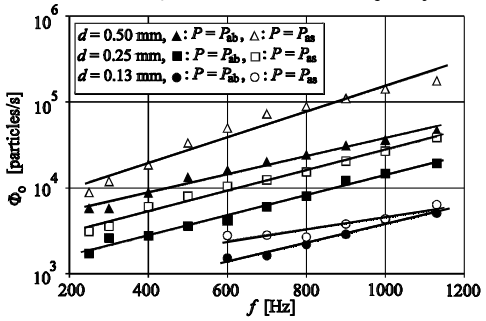

Figure 3. Φ_0 depending on AC frequency.

4. Discussion

According to Eq. (1) the plots $P_{as} = f(\Phi_i)$ and $P_{ab} = f(\Phi_i)$ should represent straight lines in the semilogarithmic scale. These lines should go through the point ($P = 1$; $\Phi_i = 0$). From Fig. 2 one can see that experimental points fall really on the straight lines, but they do not go through the point ($P = 1$; $\Phi_i = 0$).

Penney and Hummert [3] have shown that corona discharge produces photoionizing radiation proportional to the discharge current. They measured the number of photoions as a function of air pressure and distance from the point electrode. According to calculations based on [3] not all photoions are removed from our discharge gap before new discharge starts at next AC cycle. The number of remaining ions is comparable with the number of ions produced by the ionizer. Therefore the experimental fact that the straight lines in Fig. 2 are not going through the point ($P = 1$; $\Phi_i = 0$) can be explained by presence of additional negative ions. These ions are produced by photoionizing radiation of the discharge during the foregoing cycle. The flux of these ions Φ_0 can be determined elongating the straight lines to the crossing with the abscissa.

If we take into account only these AC cycles that are preceded by the cycle with the same type of discharge, keep constant air flow velocity, DC voltage, amplitude and frequency of AC voltage, then the average number of additional negative ions Φ_0 reaching the active zone of the point electrode during Δt_{bp} should be constant. Thus the total flux $\Phi = \Phi_i + \Phi_0$ can be considered stationary and the assumptions of Eq. (1) are satisfied.

From Fig. 3 one can see that Φ_0 increases with AC frequency. The increase is understandable because the higher is the AC frequency the shorter is the removal time of additional ions before discharge rise at next AC cycle. Φ_0 can be much higher than Φ_i. Therefore the after-effect of discharge cannot be neglected. Fig. 2 and 3 show that Φ_0 increases with point diameter. Φ_0 after AC cycle with a streamer is higher than Φ_0 after AC cycle with burst pulses. This result accords with data presented in paper [3] as the discharge current increases with point diameter and mean current of streamers is higher than that of burst pulses [4].

For average probability of one negative ion to initiate the burst pulse under conditions mentioned in section 2 and using $\Phi = \Phi_i + \Phi_0$ in Eq. (1) we have got at $f = 250$ Hz: $P_{bp} = 0.172(30)$ for $d = 0.50$ mm; $P_{bp} = 0.254(36)$ for $d = 0.25$ mm and $P_{bp} = 0.293(51)$ for $d = 0.13$ mm.

5. Conclusions

The main results can be summarized as follows:

1. The possible additional flux of negative ions Φ_0 caused by previous discharge must be taken into account in experiments concerning the corona rise probability.
2. Φ_0 can be determined from semilog $P = f(\Phi_i)$ curves.
3. Φ_0 increases with discharge current and AC frequency, and may be much higher than the flux produced by ionizer.
4. The average probability to initiate the burst pulse by one negative ion under our experimental conditions is determined for three different point electrodes.

Acknowledgements

This work was financially supported by the EU COPERNICUS project CIPA-CT94-0186 and by the Estonian Science Foundation under Grant 3024.

References

[1] M. Aints, A. Haljaste, K. Kudu, T. Plank: J. Phys. D: Appl. Phys., 30 (1997) 210-220

[2] M. Aints, A. Haljaste, K. Kudu, T. Plank: *5th Int. Symp. High Pressure Low Temperature Plasma Chem.* (1996) *117-121*

[3] G. W. Penney, G. T. Hummert: J. Appl. Phys., 41 (1970) 572-577

[4] R. T. Waters, T. E. Rickard and W. B. Stark: *IEE Int. Conf. Gas Discharges* (1972) *188-190*

VI

Aints M Haljaste A Kudu K and Plank T
Dependence of streamer corona characteristics on the concentration of electronegative trace gases in air
Proc. 5th Int. Symp. on High Pressure Low Temperature Plasma Chem. (1996) 117-21

DEPENDENCE OF STREAMER CORONA CHARACTERISTICS ON THE CONCENTRATION OF ELECTRONEGATIVE TRACE GASES IN AIR

M. Aints, A. Haljaste, K. Kudu, and T. Plank

Institute of Experimental Physics and Technology, University of Tartu,
Tähe 4, EE2400 Tartu, ESTONIA

Introduction

The repetition rate of streamers of positive corona depends on the air humidity as well as on the presence of small amounts of electronegative trace gases. This dependence was used by Andersson and Hertz [1] to create a humidity meter, and by Kudu to develop the detector of halogens [2]. Kudu [2] suggested a new idea - to feed the corona gap simultaneously by DC voltage and AC voltage of 50 Hz. If the so called mixed voltage is supplied to the corona gap, then the repetition rate of streamers is comparatively insensitive to the variations of DC voltage and air pressure. This enables to simplify the design of corona based detector of electronegative trace gases. This detector is named streamer counter below.

In the present paper the principle of operation of streamer counter is discussed. Some new ideas are suggested how to make the device somewhat selective with respect to the trace gas properties.

Experimental device

The sketch of the experimental device is shown in Fig. 1.Air under analysis is sucked with a fan through a tube 10 mm in bore ("body" of the counter in Fig. 1). Electric filter neutralizes inhausted ions. The electric filter is followed by an ionizer. Ions created by the ionizer are carried by air stream to the point electrode (platinum wire 0.25 mm in diameter with hemispherical cap) on the opposite end of the tube. Negative ions decompose with great probability in strong electric field near the point tip. Detached electrons initiate avalanches which can develop into different corona modes (burst

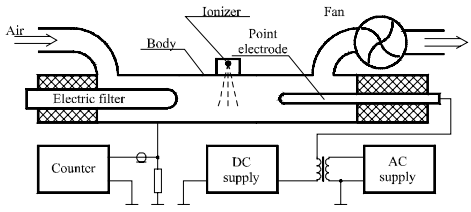

Figure 1. Principle chart of a streamer counter.

pulse, streamer or steady glow) depending on the instantaneous value of applied voltage and other conditions. Amplitude value of the streamer current pulse exceeds about two orders of magnitude the amplitudes of other corona pulses and could be thus easily recorded by the counter. DC and AC voltages are applied to the point electrode simultaneously.

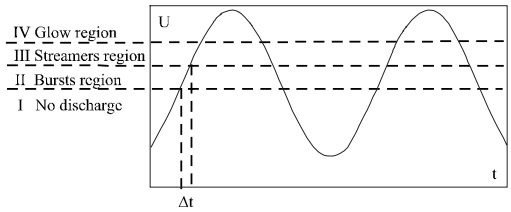

Figure 2. Voltage at the point electrode.

The voltages are set so that instantaneous value of the mixed voltage runs sequentially through the voltage regions of the above mentioned corona modes during every cycle (Fig. 2). Oscillograms of corona current show that if a burst pulse develops during Δt in voltage region II (see Fig. 2), then streamer does not appear during the same cycle, as a rule. In this case the burst pulse develops into a steady glow without streamers. The steady glow burns while the voltage exceeds the onset value of the discharge during this cycle. If a burst pulse does not appear during the time interval Δt, when voltage runs through the region II, then a streamer appears in regions III or IV. The streamer is followed by the steady corona. No more than one streamer per cycle was observed. The probability for streamer development during a certain cycle depends strongly on the concentration of negative ions and their nature.

Discussion

If appearance of a burst pulse during Δt excludes the development of a streamer during the same cycle of AC voltage, then the rise probability of a streamer is

$$Q = \exp[-\Delta t(\lambda_1 p_1 + \lambda_2 p_2 + ... + \lambda_n p_n)].$$

Here λ_1, λ_2, ..., λ_n are the numbers of ions of different nature reaching immediate vicinity of the point electrode during unit of time. $\lambda_1 + \lambda_2 + ... + \lambda_n = \lambda_0$, where λ_0 is the total number of those negative ions. p_1, p_2, ..., p_n are the rise probabilities of burst pulses originated by negative ions of different nature. Subscripts indicate the nature of ions. The probability $Q = N/f$, where N is the number of streamers per second and f is the frequency of AC voltage, can be measured experimentally. The value of λ_0 is determined by the intensity of the ion source and thus λ_0 is the known quantity. Δt can be calculated proceeding from values of voltages and AC frequency. Thus, for measured Q one can calculate the mean rise probability of a burst pulse

$\bar{p} = \frac{\lambda \cdot p_1 + \lambda_2 \cdot p_2 + \cdots + \lambda_n \cdot p_{n1}}{\lambda_0} = -\frac{\ln Q}{\Delta t \cdot \lambda_0}$. Or vice versa, if $\bar{p}$ is the known quantity, the number of ions can be calculated from these measurements. The effect of electronegative admixture on the Q is due to conversion reactions of ions. In the presence of a strongly electronegative admixture the number of ions specified by low probability to initiate a burst-pulse increases. The number of ions specified by high probability decreases accordingly. Thus, the mean rise probability of burst pulses decreases and that of streamers Q increases. This explains the principle of operation of streamer counter as a detector of trace gases. According to our measurements in air the minimal detectable changes in concentration of some admixtures are as follows: I_2 - 1 ppb, Cl_2 - 10 ppb, O_3 - 0.4 ppm, CO_2 - 1000 ppm, H_2O - 1000 ppm.

Streamer counter as a detector of trace gases has a disadvantage - the lack of selectivity. No information can be obtained from counting characteristics about the nature of the trace gas causing a change in repetition rate of streamers. We suggested that a possibility to discriminate between different admixtures can be obtained, if several parallel point electrodes with different tip curvatures are used in the counter simultaneously. Probabilities $p_{i,j}$ must be fairly different both for the different point electrode *i* and for different admixture *j*. Difference between values of $p_{i,j}$ for different admixtures is due to the difference between their electron affinities, molecule masses and their structure. Mainly those quantities determine the value of the probability of detachment as the function of electric field strength. The electric field strength corresponding to Δt is different for point electrodes with different tip curvatures. Due to this difference the probabilities $p_{i,j}$ are different for different point electrodes. Using a streamer counter with *m* parallel point electrodes a system of equations with *m* equations can be stated:

$$\begin{cases} \ln Q_1 = -\Delta t(p_{11}\lambda_1 + p_{12}\lambda_2 + \ldots + p_{1n}\lambda_n) \\ \ln Q_2 = -\Delta t(p_{21}\lambda_1 + p_{22}\lambda_2 + \ldots + p_{2n}\lambda_n) \\ . \\ . \\ \ln Q_m = -\Delta t(p_{m1}\lambda_1 + p_{m2}\lambda_2 + \ldots + p_{mn}\lambda_n) \end{cases} \quad (1)$$

Eq. (1) allow to find the values of $\lambda_1, \lambda_2, \ldots, \lambda_n$.

A discharge tube containing three point electrodes with diameters of d = 0.25, 0.5 and 1.0 mm was built to test this hypothesis. All three electrodes were fed from the same voltage supply by the RC voltage divider. For each electrode the value of DC voltage was adjusted close to the onset potential of streamers. The peak value of AC voltage constituted about 0.2 of the value of DC voltage. The frequency of AC voltage was 100 Hz, air velocity was 0.5 m/s and ion flux

$\lambda_0 = 0.4 \cdot 10^6$ 1/s. Air humidity and concentration of CO_2 were varied during experiments. Obtained experimental values of $\overline{p}$ are presented in Table 1 for different point electrodes and air compositions. As one can see, the values of $\overline{p}$ for different point electrodes differ significantly. The ratios $\overline{p}_1 / \overline{p}_2$ and $\overline{p}_2 / \overline{p}_3$ depend strongly on air composition. Using these data it is possible to determine the number of three kinds of ions specified by known probabilities $p_{i,j}$. Actually the number of ions of different kind is much greater than three.

TABLE 1

	Concentration of CO_2 and H_2O in the air (t = 19°C, p = 768 Torr)		$\overline{p}_i$		
	C_{H2O} [ppm]	C_{CO2} [ppm]	i = 1 (d = 0.25 mm)	i = 2 (d = 0.5 mm)	i = 3 (d = 1.0 mm)
a	5800	300	$1.90 \cdot 10^{-3}$	$3.93 \cdot 10^{-3}$	$10.9 \cdot 10^{-3}$
b	11000	300	$0.44 \cdot 10^{-3}$	$1.14 \cdot 10^{-3}$	$7.26 \cdot 10^{-3}$
c	18300	300	$0.40 \cdot 10^{-3}$	$1.10 \cdot 10^{-3}$	$1.30 \cdot 10^{-3}$
d	5800	8200	$0.71 \cdot 10^{-3}$	$1.01 \cdot 10^{-3}$	$4.19 \cdot 10^{-3}$

TABLE 2

$$p = \begin{bmatrix} 5.0 & 0.5 & 0.05 \\ 9.87 & 1.22 & 0.433 \\ 17.5 & 12.9 & 0.008 \end{bmatrix} \cdot 10^{-3}$$

The spectrum of ions (ions distribution depending on the initiation probability of burst pulses) can be considered as continuous. Using three electrodes a step-like distribution curve of three steps can be determined instead of continuous one. Here the probabilities $p_{i,j}$ must be considered as mean probabilities for ions of given group to initiate a burst pulse at given point electrode. To solve the system of equations (1) with $m = 3$, $n = 3$ with respect to λ_j values of $p_{i,j}$ must be determined. We set values of $p_{i,j}$ ($0 < p_{i,j} < 1$) around the values of $\overline{p}_i$ in such a way that solutions of Eq. (1) would satisfy the restrictions

$$\sum_{j=1}^{3} \lambda_j = \lambda_0 , \qquad 0 < \lambda_j < \lambda_0 \qquad (2)$$

simultaneously for three gas compounds. Values of λ_j satisfying Eq. (1) and restrictions (2), are presented in Fig. 3a, b, c. The ranges of possible variations of λ are striped. One possible

matrix of *p* satisfying Eq. (1) and (2) is presented in Table 2. Using this matrix the spectrum of ions for the case d (air with small addition of CO_2) was calculated. This spectrum is presented in Fig. 3d. As one can see, the number of ions with lower probability to initiate burst pulse increases with the concentration of H_2O or CO_2 in air. Shapes of spectrums corresponding to different admixtures differ significantly.

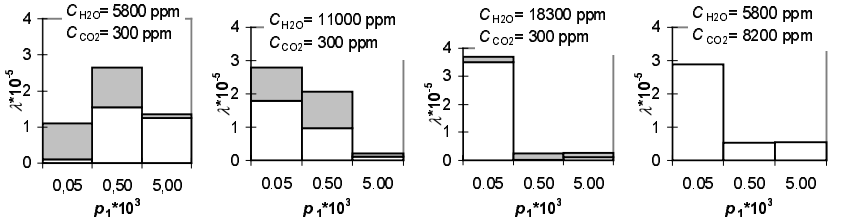

Figure 3. Spectra of ions at different air composition.

Conclusions

Using properties of streamer corona a detector of trace gases can be designed for air or other gases. The selectivity of the device can be improved increasing the number of electrodes of different tip curvatures. The rise probability of burst pulse is related to the electron affinity of the additive. Special experiments are necessary to determine this relation. If this relation is find out, the distribution of ions according to their affinities can be determined by the streamer counter. Using a multielectrode counter simultaneously with an ion mobility spectrometer, the selectivity of combined device can be improved significantly.

References

1. Andersson N. E. and Hertz C. H. 1955 Positive Spitzenentladung als Hygrometer geringer Trägheit. *Z. angew. Phys.* **7**, *S. 361-6*
2. Kudu K. Some possible applications of a streamer counter. *Proc. 6th Int. Conf on Gas Discharges (Edinburgh, 1980) Pt. 1, p. 275-8*

VII

Plank T Aints M Haljaste A ja Kudu K
Segapinge koroonalahendus saastegaaside detektorina
EFS aastaraamat 2000 (2001) 40-50

SEGAPINGE KOROONALAHENDUS SAASTEGAASIDE DETEKTORINA

Toomas Plank, Märt Aints, Ants Haljaste ja Kalju Kudu
Tartu Ülikool

1. Sissejuhatus

Gaaslahenduse uurijatele on hästi teada, et atmosfääriõhus on mitmesugused koroonavormid tundlikud paljude lisandgaaside ja aerosoolide suhtes. Käesoleval ajal uuritakse mitmetes laborites võimalusi, kuidas koroonalahenduse baasil konstrueerida keskkonnamonitooringuks sobivaid saastegaaside detektoreid. Uuringuid stimuleerivate momentidena tõstetakse esile koroonaseadmete kompaktsust, mobiilsust, töökindlust, odavust, lihtsat sidestatavust personaalarvutiga, radioaktiivsete ionisaatorite puudumist ja sellest tulenevat keskkonnasõbralikkust. Uuritakse nii positiivse kui ka negatiivse koroona kasutusvõimalusi.

Käesoleva ettekande eesmärgiks on tutvustada üht positiivsel koroonal põhinevat detektorit ning näidata, kuidas on võimalik parandada tema tehnilisi näitajaid. Detektori tööpõhimõtete paremaks mõistmiseks kirjeldame esmalt uuritavas detektoris esinevaid koroonavorme.

2. Koroona positiivse potentsiaaliga teravikul

Rakendades elektroodidele alalispinge, tekivad positiivse potentsiaaliga teraviku tipu lähedal teatud pingest U_{bp} alates purskeimpulsid. Visuaalselt kujutavad purskeimpulsid endast väikese võimsusega valgussähvatusi mis tekivad teravikulähedases õhukeses õhukihis (joonis 1a). Purskeimpulsis järg-

neb primaarsele elektronlaviinile mitusada väiksema võimsusega sekundaarlaviini. Teraviku potentsiaali kasvades saavad purskeimpulsid tekkida järjest kaugemal teraviku tipust, sekundaarlaviinide arv kasvab ja ajavahemik purskeimpulsside vahel väheneb. Teatavast pingest U_g alates pole üksikud purskeimpulsid enam üksteisest eristatavad ja moodustavad teraviku pinda helendava õhukese kihina katva pideva koroona (joonis 1b).

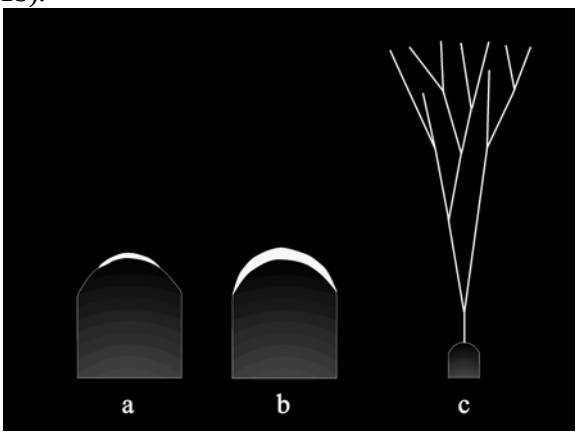

Joon. 1. Positiivse koroona lahendusvormid: a) purskeimpulss; b) pidev koroona; c) algstriimer.

Kui elektroodidevaheline pinge on suurem kui U_{str}, siis on võimalik veel teise koroonavormi – algstriimeri – teke allpool pidev koroona läve U_g. Striimer kujutab endast väga kiiresti teravikust eemalduvat helenduvat plasmakerakest. Teravikust kaugemal võib moodustuda mitu väiksemat kera – striimer hargneb. Visuaalselt meenutab nende kerade teekond puuoksa (joonis 1c). Striimer põhjustab elektroodi toiteahelas vooluimpulsi mis on purskeimpulsi vooluimpulsist mitukümmend korda võimsam (joonis 2). Striimeriga kaasneb purskeimpulss, millele tavaliselt järgneb purskeimpulsside jada. Järgmine striimer saab tekkida siis, kui eelmisest impulsist jäänud positiivsete ioonide ruumlaeng teraviku tipu lähedal

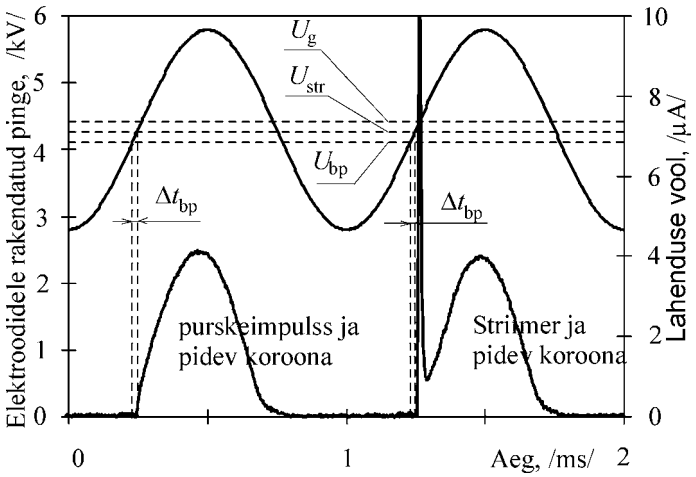

Joon. 2. Elektroodidele rakendatud segapinge ostsillogramm (ülemine) ja lahenduse voolu ostsillogramm (alumine). Δt_{bp} tähistab ajavahemikku, mil pinge on vahemikus [U_{bp},U_{str}).

on hajunud. Ruumlaengu olemasolu tõttu lakkab puhta alalispinge tingimustes algstriimerite teke kui rakendatud pinge tõsta kõrgemale pideva koroona lävest U_g.

Rakendades elektroodidele ajas perioodiliselt muutuva pinge, nn. segapinge (alalispinge + vahelduvpinge) nii et teravik oleks positiivse potentsiaaliga (joonis 2), saavutame olukorra kus lahendusvorm on määratud lahendust algatava osakese (negatiivse iooni) saabumise hetkele vastava pingega U:

- Kui $U_{bp} \le U < U_{str}$, tekib purskeimpulss (joonis 2). Purskeimpulssidest maha jääv ruumlaeng takistab striimeri tekkimist sellel segapinge perioodil. Pinge tõustes kõrgemale kui U_g kasvavad purskeimpulsid üle pidevaks koroonaks. Pinge langemisel alla U_{bp} lahendus kustub ja tekib võimalus teraviku lähedase ruumala puhastamiseks positiivsete ioonide ruumlaengust.
- Kui $U \ge U_{str}$, siis tekib striimer (joonis 2). Segapinge tingimustes saab striimer tekkida ka pideva koroona lävest U_g kõrgemal pingel, kui madalamal pingel pole lahendust tekkinud. Igale striimerile järgneb samasugune pidev koroona, nagu purskeimpulsilegi. Pideva koroona poolt tekitatud ruumlaeng välistab teise striimeri tekkimise segapinge

selle perioodi vältel. Segapinge järgmise perioodi alguseks on suurem osa ruumlaengust eemaldatud ja on olemas kindel tõenäosus kas purskeimpulsi või striimeri tekkeks negatiivse iooni saabumisel.

3. Striimerite kordussageduse kasutamine saastegaaside detekteerimiseks

Striimerite kordussagedus sõltub elektroodidele rakendatud pingest, gaasi voolukiirusest ja ioonide kontsentratsioonist lahendusvahemikus, samuti gaasi keemilisest koostisest, rõhust ja temperatuurist. Ajalooliselt olid Andersson ja Hertz esimesed kes kasutasid seda sõltuvust õhuniiskuse mõõtmiseks [1]. Kudu soovitas lisada alalispingele 50 Hz-se sagedusega vahelduvpinge, kuna nii õnnestub elimineerida striimerite kordussageduse sõltuvus gaasi rõhu ja temperatuuri ning elektroodidele rakendatud alalispinge väikestest muutustest [2]. Samas töös kasutati striimerkoroonat esmakordselt halogeenide detekteerimiseks õhus. Segapinge koroonalahendusel põhinevat saastegaaside detektorit nimetame allpool striimerloenduriks.

4. Striimerloenduri ehitus

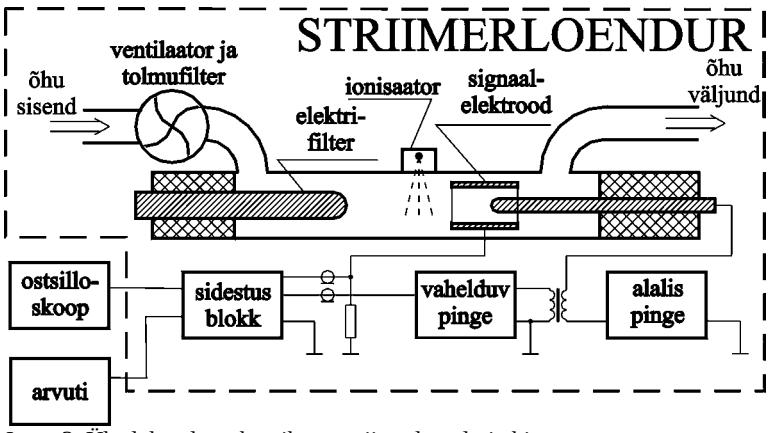

Joon. 3. Ühe lahendusvahemikuga striimerloenduri ehitus.

Ühe lahendusvahemikuga striimerloenduri ehitus on näidatud joonisel 3. Uuritav õhk suunatakse ventilaatori abil läbi tolmu-

ja elektrifiltrite. Elektrifilter eemaldab õhust kerged ioonid. Elektrifiltri järel paiknev ionisaator tekitab kontrollitava koguse ioone, mille õhuvool kannab poolsfäärilise tipuga teravikelektroodini. Elektroodidele rakendatakse üheaegselt alalispinge ja vahelduvpinge nii et teravik oleks positiivse potentsiaaliga. Alalispinge U_{DC} väärtus valitakse ligikaudu võrdne algstriimerite lävepingega U_{str}. Vahelduvpinge amplituudiks U_{AC} valitakse $U_{AC} \approx 0.3\, U_{DC}$. Andmeid striimerite poolt signaalelektroodil indutseeritud vooluimpulsside kordussageduse ja tekkefaasi kohta registreeritakse ning töödeldakse personaalarvutiga. Vajadusel võib vooluimpulsse uurida ostsilloskoopiliselt.

5. Striimerloenduri tööpõhimõte

Algstriimeri tekkimise tõenäosus segapingel avaldub valemiga [3]:

$$p = \exp(-\Delta t_{bp} b \Phi)\,, \qquad (1)$$

kus b tähistab tõenäosust millega üks negatiivne ioon algatab purskeimpulsi (pingevahemikus $U_{bp} \le U < U_{str}$). Φ on teraviku tippu jõudvate negatiivsete ioonide voog. Φ võib koosneda kuni kolmest komponendist: ionisaatori poolt tekitatud ioonide voost $g\Phi_0$, eelneva striimeri poolt lahendusvahemikku maha jäetud ioonide voost $g\Phi_{str}$ ja eelmise perioodi pideva koroona poolt lahendusvahemikku maha jäetud ioonide voost $g\Phi_g$ [4]. Kaks viimatinimetatud voogu esindavad eelneva lahenduse järelmõju. Kordaja g iseloomustab teraviku tippu jõudvate ioonide osakaalu lahendusvahemikku jõudvate/jäävate ioonide koguvoost.

Koroonalahenduse uurijatele on lahenduse järelmõju nähtus ammu teada. Sellele vaatamata pole tänaseni välja töötatud sobivaid meetodeid lahenduse järelmõju intensiivsuse mõõtmiseks. Käesoleva töö raames töötati välja meetod nii pideva koroona [5] kui ka striimeri [4] järelmõju mõõtmiseks. Meetodi aluseks on võrrand (1), millest saab avaldada pideva koroona ja striimeri efektiivse järelmõju suuruse, vastavalt $bg\Phi_g$ ja

$bg\Phi_s$:

$$bg\Phi_g = \frac{-1}{\Delta t_{bp}} \ln(p_{ab}) - bg\Phi_0 ,$$

$$bg\Phi_s = \frac{1}{\Delta t_{bp}} \ln(\frac{p_{ab}}{p_{as}}) .$$

Siin p_{ab} tähistab striimeri tekkimise tõenäosust pärast sellist segapinge perioodi, kus lahendus algas purskeimpulsiga, ja p_{as} tähistab striimeri tekkimise tõenäosust pärast sellist segapinge perioodi, kus lahendus algas striimeriga. Parameetri b hindamise metoodika on publitseeritud [5], parameetrit g saab hinnata modelleerides elektrivälja jaotust lahendusvahemikus.

Lahenduse järelmõju uurimine näitas, et nii striimeri kui ka pideva koroona järelmõju kahaneb koos õhu voolukiiruse v kasvu ja/või vahelduvpinge sageduse f kahanemisega. Vahelduvpinge amplituudi U_{AC} muutus striimeri järelmõju ei mõjuta, pideva koroona järelmõju kasvab koos U_{AC} kasvuga. Alalispinge U_{DC} kasvades striimeri järelmõju väheneb, pideva koroona järelmõju aga veidi kasvab. Osutus, et striimerloenduri tööparameetreid (U_{DC}, U_{AC}, vahelduvpinge sagedus f, gaasivoolu kiirus v, Φ_0) valides on võimalik saavutada olukord, kus $\Phi_{str} \approx \Phi_g \approx 0$ [4]. Eelmise lahenduse järelmõju puudumine lihtsustab mõõtmistulemuste interpreteerimist: ioonide vood Φ_0, Φ_g, Φ_{str} koosnevad erineva vanusega ioonidest, seetõttu võivad olla erinevad ka ioonide kooslused nendes voogudes ja purskeimpulsi algatamise tõenäosused b.

Kui teravikule saabuv ioonivoog koosneb n sorti ioonidest, peame võrrandit (1) täiustama:

$$p = \exp(-\Delta t_{bp} \Phi_0 \sum_{i=1}^{n} b_i g_i \varphi_i) \qquad (2)$$

Siin tähistab φ_i i-ndat sorti ioonide osakaalu ionisaatori poolt tekitatud ioonide voos Φ_0; g_i ja b_i tähistavad vastavalt i-nda iooni teraviku lähedale sattumise tõenäosust ja selle iooni poolt purskeimpulsi algatamise tõenäosust.

Elektronegatiivsete lisandite mõju striimeri tekkimise tõenäosusele p tuleneb konversioonireaktsioonidest, mis vähendavad nende ioonide osakaalu, mille küljest purskeimpulsi

algatamiseks vajaliku algelektroni irdumise tõenäosus teravikulähedases väljas on suur. Samal ajal kasvab nende ioonide osakaal, millest elektroni irdumine on väga väikese tõenäosusega. Selle tulemusena elektronegatiivse lisandi kontsentratsiooni kasvades purskeimpulsi algatamise keskmine tõenäosus *b* väheneb ja striimeri tekkimise tõenäosus *p* suureneb.

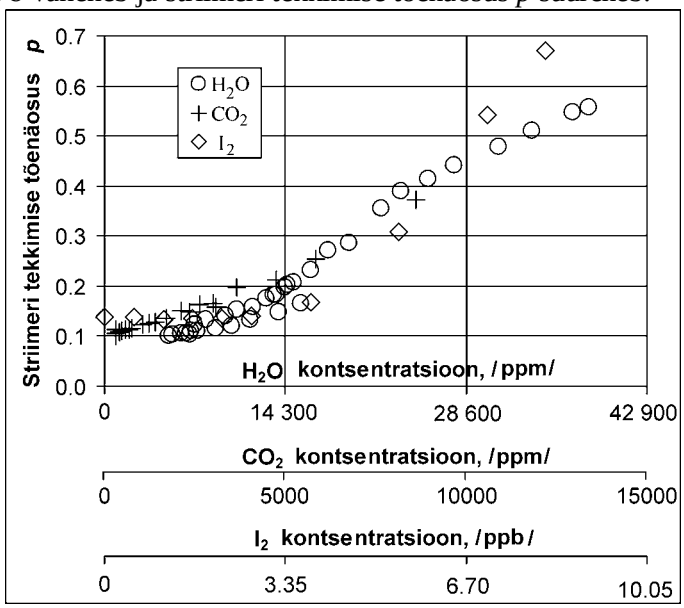

Joon. 4 Striimeri tekkimise tõenäosus sõltuvalt kas veeauru, süsihappegaasi või joodi kontsentratsioonist õhus.

Joonisel 4 on esitatud striimeri tekkimise tõenäosus 0,5 mm diameetriga teravikelektroodil sõltuvalt veeauru, süsihappegaasi ja joodi kontsentratsioonist õhus. Jooniselt näeme, et striimeri tekkimise tõenäosus kasvab veeauru, süsihappegaasi või joodi kontsentratsiooni suurenemisel õhus. Seega saab striimerloendurit edukalt kasutada lisandgaasi kontsentratsiooni mõõtmiseks õhus, eeldusel et eelnevalt on teada, milline lisand striimeri tekkimise tõenäosust mõjutab. Kahjuks ei ole ainult ühe lahendusvahemikuga striimerloenduri näidu alusel võimalik öelda, kas õhus on tõusnud veeauru või mõne saastegaasi kontsentratsioon.

6. Mitme lahendusvahemikuga striimerloendur

Purskeimpulsi algatamise tõenäosus b_i sõltub teravikelektroodi lähedase elektrivälja jaotusest [6]. Valides m erineva kõverusraadiusega teravikelektroodi saame valemi (2) asemel võrrandisüsteemi:

$$\begin{cases} p_1 = \exp(-\Delta t_{bp_1} \Phi_0 \sum_{i=1}^{n} b_{i,1} g_{i,1} \varphi_i) \\ p_2 = \exp(-\Delta t_{bp_2} \Phi_0 \sum_{i=1}^{n} b_{i,2} g_{i,2} \varphi_i) \\ \ldots \\ p_m = \exp(-\Delta t_{bp_m} \Phi_0 \sum_{i=1}^{n} b_{i,m} g_{i,m} \varphi_i) \end{cases} \quad (3)$$

Täiendavaks tingimuseks on $\sum_{i=1}^{n} \varphi_i = 1$.

Teades g_i ja b_i väärtusi, saame selle võrrandisüsteemi lahendamisel leida ioonide spektri purskeimpulsi algatamise tõenäosuse järgi. Saadud spektrid võimaldavad hinnata, milliseid lisandeid või lisandirühmi uuritav õhk sisaldab [6].

Idee realiseerisime striimerloenduris, mis sisaldas kolm lahendusvahemikku erimõõtmeliste teravikelektroodidega (diameetrid d = 0.13, 0.25 ja 0.50 mm).

Joonisel 5 on esitatud kolme lahendusvahemikuga striimerloenduriga registreeritud ioonide spektrid. Spektrite saamisel kasutatud korrutise $g_i b_i$ väärtused meie teravike puhul on esitatud tabelis:

	i			
d (mm)	1	2	3	4
0,13	$7{,}90\times10^{-3}$	$5{,}47\times10^{-3}$	$5{,}16\times10^{-4}$	$2{,}18\times10^{-6}$
0,25	$2{,}85\times10^{-2}$	$1{,}01\times10^{-2}$	$2{,}29\times10^{-3}$	$8{,}43\times10^{-6}$
0,50	$3{,}96\times10^{-2}$	$1{,}17\times10^{-2}$	$1{,}05\times10^{-3}$	$5{,}13\times10^{-6}$

Joonisel 5 esitatud spektrite argumendiks on indeks i, mis määrab ära tõenäosused, millistega i-ndasse gruppi kuuluvad

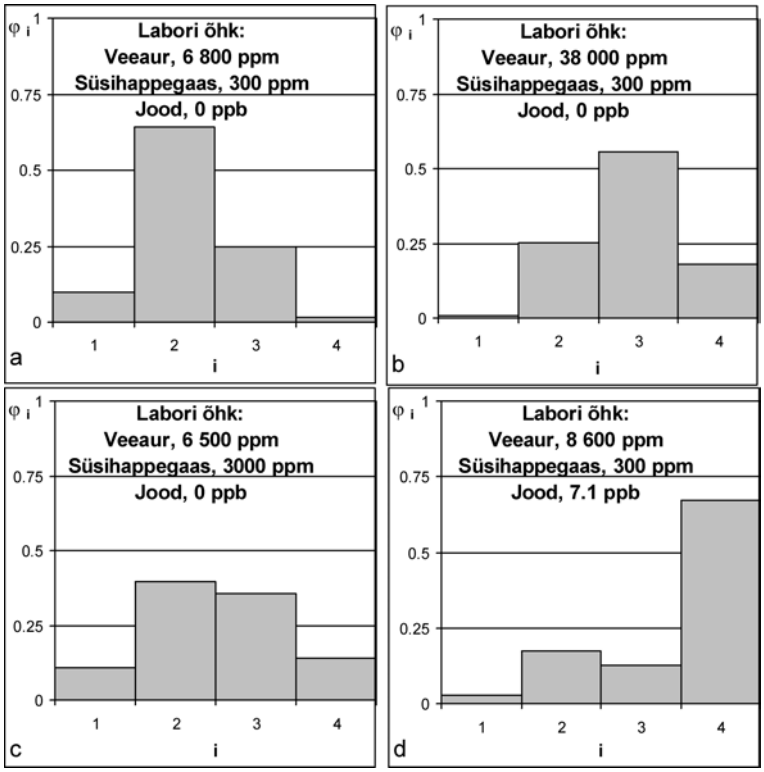

Joon. 5. Kolme lahendusvahemikuga striimerloenduriga registreeritud ioonide spektrid: a) "tavaline" labori õhk; b) H_2O mõju; c) CO_2 mõju; d) I_2 mõju.

ioonid algatavad purskeimpulsse striimerloenduri elektroodidel (vt. tabelit). Jooniselt näeme, et kolme lahendusvahemikuga striimerloenduriga registreeritud spektrid võimaldavad öelda, kas striimerite arvu kasv on tingitud veeauru, süsihappegaasi või joodi lisamisest labori õhule.

Tegelik ioonisortide arv õhus on kindlasti suurem kui 4. Sel juhul kuulub igasse kolme lahendusvahemikuga loenduriga eristatud ioonirühma mitut sorti ioone, millede keskmine purskeimpulsi algatamise tõenäosus on $b_{i,j}$, kus indeks j on elektroodi järjenumber. Soovides striimerloenduri lahutusvõimet parandada, tuleks loenduris kasutada rohkem lahendusvahemikke. Seejuures tuleb uute lahendusvahemike geomeetria valida niisugune, et teravikelektroodi lähedase välja tugevus ja mittehomogeensuse aste striimeri lävepingel oleks oluliselt

erinevad juba olemasolevate vahemike elektrivälja vastavatest näitajatest.

7. Põhitulemused

Käesoleva töö põhitulemused on järgmised:

- On koostatud striimerloenduris asetleidvate protsesside matemaatiline kirjeldus, mis annab seose striimerite kordussageduse ja loenduri tööparameetrite ning purskeimpulsi algatamise tõenäosuse vahel.
- On välja töötatud meetod lahenduse järelmõju kvantitatiivseks määramiseks striimerite jadade statistilise analüüsi põhjal. Meetod võimaldab määrata loenduri tööparameetrite optimaalsed väärtused, aga on ka laiemalt huvi pakkuv koroonalahenduse füüsika ja rakenduste alal.
- Eksperimentaalselt on määratud striimerloenduri loenduskiiruse sõltuvus mitmesuguste lisandainete kontsentratsioonist.
- Eksperimentaalselt on näidatud, et mitme lahendusvahemikuga striimerloendur kui lisandgaasi detektor võimaldab määrata lisandi tüüpi.

8. Kirjandus

1. Andersson N. E. and Hertz C. H. 1955 Positive Spitzenentladung als Hygrometer geringer Trägheit, *Z. Ang. Phys.* **7** 361-6
2. Kudu, K. 1980 Some possible applications of a streamer counter. *Proc. 6th Int. Conf. on Gas Discharges and Applications* (Edinburgh: Heriot-Watt University Press) Part 1 pp 275-8
3. Aints, M., Haljaste, A., Kudu, K. and Plank, T 1997 Repetition rate of streamers as a measure of content of electronegative additives in the air *J. Phys. D: Appl. Phys.* **30** 210-20
4. Plank, T., Haljaste, A. and Aints, M. 2000 The after-effect of streamers of positive corona under combined voltage *J. Phys. D: Appl. Phys.* **33** 2791-2797
5. Plank, T., Aints, M. and Haljaste, A. 1999 Investigation of rise probability of positive corona initiated by negative ions *Proc 24th Int. Conf. on Phenomena in Ionized Gases* (Warsaw) vol II, pp 145-6

6. Aints, M., Haljaste, A., Kudu, K. and Plank, T. 1996 Dependence of streamer corona characteristics on the concentration of electronegative trace gases in air *Proc. 5th Int. Symp. on High Pressure Low Temperature Plasma Chem.* (Milovy) pp 117-21

CURRICULUM VITAE

Toomas Plank

Citizenship:	Estonian
Date of birth:	April 27, 1971
Personal status:	Single
Address:	University of Tartu, Institute of experimental physics and technology, Tähe 4, Tartu 51010, Estonia
Phone:	+(372) 51 51599
Fax:	+(372) 7 375858
E-mail:	tomas@ut.ee

Education

1978–1979	Tartu Secondary School No 5
1980–1989	Tartu Secondary School No 14 (graduated with gold medal)
1989–1993	University of Tartu, Faculty of Physics and Chemistry, graduated 1993 *cum laude* in field of electronics
1993–1995	University of Tartu, master student, MSc in physics, graduated 1995 in field of optics and spectroscopy,
1995–2000	University of Tartu, PhD student

Special courses

1995, 1997	L'Ecole Superieur d'Electricité, Gif-sur-Yvette, France, scholar of French government

Employment

1996–present	University of Tartu, FKEF assistant
1996–1997	University of Tartu, FKEF senior engineer
1998	Health Protection Service of Tartu, computer consultant

Research

His scientific interests in physics lie in the field of positive– and negative corona discharge, ion mobility spectrometry and ozone synthesis in HF discharges.

His scientific interests in medical science lie in medical statistics.

Has 9 scientific publications.

ELULUGU

Toomas Plank

Kodakondsus:	Eesti
Sünniaeg:	27. aprill 1971
Perekonnaseis:	Vallaline
Aadress:	Tartu Ülikool, eksperimentaalfüüsika ja tehnoloogia instituut, Tähe 4, Tartu 51010, Eesti
Telefon:	+(372) 51 51599
Fax:	+(372) 7 375858
E-post:	tomas@ut.ee

Hariduskäik

1978–1979	Tartu 5. Keskkool
1980–1989	Tartu 14. Keskkool (lõpetas kuldmedaliga)
1989–1993	Tartu Ülikool, Füüsika-keemia teaduskond, lõpetas 1993 kiitusega elektroonika erialal
1993–1995	Tartu Ülikool, magistrantuur, MSc füüsikas, optika ja spektroskoopia erialal omistatud 1995
1995–2000	Tartu Ülikool, doktorantuur

Erialane enesetäiendamine

1995, 1997	Kõrgem Elektrikool, Gif-sur-Yvette, Prantsusmaa, Prantsuse valitsuse stipendiaat

Teenistuskäik

1996–tänaseni	Tartu Ülikool, FKEF assistent
1996–1997	Tartu Ülikool, FKEF vaneminsener
1998	Tartu Tervisekaitsetalitus, (lepinguline) arvutikonsultant

Teadustegevus

Teaduslikud huvid füüsikas on seotud positiivse– ja negatiivse koroonalahendusega, liikuvusspektromeetriaga ja osooni sünteesiga kõrgsageduslahenduses.

Teaduslikud huvid arstiteaduses on seotud meditsiinistatistikaga.

On avaldanud 9 teaduspublikatsiooni.

LIST OF PUBLICATIONS BY THE AUTHOR

1. Aints M Haljaste A and Plank T 1993 Ozone Electrosynthesis in the HF Discharge. *4th Int. Symp. on High Pressure Low Temperature Plasma Chem.* (Bratislava) 25-30
2. Aints M Haljaste A Kudu K and Plank T 1996 Dependence of streamer corona characteristics on the concentration of electronegative trace gases in air *Proc. 5th Int. Symp. on High Pressure Low Temperature Plasma Chem.* (Milovy) 117-21
3. Aints M Haljaste A Kudu K and Plank T 1997 Repetition rate of streamers as a measure of content of electronegative additives in the air *J. Phys. D: Appl. Phys*. **30** 210-20
4. Plank T Aints M and Haljaste A 1999 Investigation of rise probability of positive corona initiated by negative ions *Proc 24th Int. Conf. on Phenomena in Ionized Gases* (Warsaw) **II** 145-6
5. Plank T Haljaste A and Aints M 2000 The after-effect of streamers of positive corona under combined voltage *J. Phys. D: Appl. Phys*. **33** 2791-7
6. Aints M Kudu K Haljaste A and Plank T 2001 Origin of photoionizing radiation in corona discharges in air *J. Phys. D: Appl. Phys*. **34** 905-8
7. Aints M Haljaste A Kudu K and Plank T 2001 Corona based detector of electronegative trace gases *Meas. Sci. Technol.* **12** 557-65
8. Plank T Aints M Haljaste A ja Kudu K 2001 Segapinge koroonalahendus saastegaaside detektorina *EFS aastaraamat 2000* **XI** 40-50
9. Uusküla A Plank T Lassus A and Bingham J 2001 Sexually transmitted infections in Estonia – syndromic management of urethritis in a European country? *International Journal of STD and AIDS* **12** 493-8